EVOLVING EPHEMERAL CHANNELS: CHARACTERIZING SHIFTING FLOW DYNAMICS AND THEIR HYDROLOGIC IMPACT IN SEMI-ARID ENVIRONMENTS

by

LEA JERRY DAVIDSON

(Under the Direction of Adam M. Milewski)

ABSTRACT

Though present in all climatic environments, non-perennial channels are a dominant hydrologic feature of semi-arid regions. At present, projected warming trends are anticipated to shift climate patterns within arid regions, increasing maximum temperatures and decreasing precipitation volume. In combination, these changes have the potential to alter the flow patterns of many presently perennial river systems, decreasing their discharge and resulting in infrequent, seasonal, or cyclic periods of flow cessation. This evolution from perennial to ephemeral systems will likely have important effects on regional hydrologic processes and water management. This dissertation explores the varied impact of this transition in semi-arid regions both domestically and in Morocco, applying a combination of statistics, remote sensing, and field work to better characterize shifting flow dynamics and their impact on regional groundwater recharge.

(1) Significant trends in stream drying are observed within semi-arid regions of CONUS. From 1980 to present, the timing of wet season moisture was identified as a primary control on the novel stream intermittency observed as developing across the region.

Projected shifts in regional precipitation underscore the expected expansion of non-perennial stream flow into higher elevation, perennial systems.

(2) Characterization of intermittent flow patterns remain a challenge in data-scarce regions, which lack sufficient gaging. Linear Discriminant Function Analysis is demonstrated to effectively predict channel flow in a shallow, turbid, and flashy ephemeral system in central Morocco. From 1984 to 2022, flow frequency was observed to decrease. The spatial and temporal distribution of flow however, which was maintained in the channel upstream and during the wet season, support potential channel infiltration and groundwater recharge despite this reduction.

(3) Infiltration through ephemeral channels is a primary form of aquifer recharge in arid regions. In central Morocco, subsurface temperature probes were deployed to characterize surface flow events and their connection to infiltration. Across two ephemeral channels in disparate recharge zones, infiltration was concentrated within the upstream channel reach, and increased in velocity with greater depth in the subsurface. Improved characterization of channel flow patterns informs our understanding of potential transmission loss, crucial for accurate estimates of groundwater recharge in semi-arid environments.

INDEX WORDS: HYDROGEOLOGY, ARID ZONE HYDROLOGY, REMOTE SENSING, NON-PERENNIAL CHANNELS, TRANSMISSION LOSS, GROUNDWATER RECHARGE, DISCRIMINANT FUNCTION ANALYSIS

EVOLVING EPHEMERAL CHANNELS: CHARACTERIZING SHIFTING FLOW DYNAMICS AND THEIR HYDROLOGIC IMPACT IN SEMI-ARID ENVIRONMENTS

by

LEA JERRY DAVIDSON

B.A., Macalester College, 2018

A Dissertation Submitted to the Graduate Faculty of The University of Georgia in Partial Fulfillment of the Requirements for the Degree

DOCTOR OF PHILOSOPHY

ATHENS, GEORGIA

2024

EVOLVING EPHEMERAL CHANNELS: CHARACTERIZING SHIFTING FLOW DYNAMICS AND THEIR HYDROLOGIC IMPACT IN SEMI-ARID ENVIRONMENTS

by

LEA JERRY DAVIDSON

Major Professor:	Adam M. Milewski
Committee:	Charlotte Garing
	Wondwosen Seyoum
	Todd C. Rassmussen

Electronic Version Approved:

Ron Walcott
Vice Provost for Graduate Education and Dean of the Graduate School
The University of Georgia
December 2024

DEDICATION

To my Grandpa Tom, one of the brightest burning in a long row of candles. Thank you for your love, laughter, and endless stories. In part, this dissertation is possible because of the web of family before me that deeply believed in the value of education, whether afforded to them or not, and who worked and wished hard for that success for their children. All of my love.

ACKNOWLEDGEMENTS

Thank you to all who have helped prepare me for the path. Despite its inherent challenges, the closing of this chapter is bittersweet. I have loved the opportunities to think, experience, and grow over the past four and a half years. When I began my PhD, I viewed it as a mountain to climb, that with methodical and deliberate work I could deliver myself to the other side relatively unaffected. Yet now, looking back, I can see the true depth of change. I am grateful for this experience and all that it has taught me, largely about hydrogeology and science, but also about myself.

Thank you to my advisor, Dr. Adam Milewski, for the constant belief, encouragement, grounding advice and assurance of doubts. Whenever I was feeling lost or that it was all unraveling, meeting with you always helped restore my belief in it all. I feel incredibly grateful for the numerous experiences to travel for field work, experiences which further clarified my desire to work internationally and my curiosity about the world. Thank you for helping to shape me into the scientist that I am today, your unwavering guidance and commitment to my success was foundational in the realization of this work. I truly can't imagine completing my PhD under different guidance.

Outside of my advisor, this dissertation was made possible by a large network of individuals, both in Athens and abroad, who encouraged my excitement for research and helped spark ever evolving questions. To my committee members, your advice and guidance has been paramount to the success of this work, thank you. Additional thanks to my many professors over the course of this dissertation, who introduced me to new areas of geology, ways of thinking, and

deeper questioning. To Dr. Charlotte Garing, thank you for both your professional and personal support over these past years. I specifically appreciate your sharp eye for detail, and your guidance has been meaningful. Thank you to all the WRRS lab members, both past and present, for the solidarity, laughter, and support.

To my family, specifically my parents Tim and Krista Davidson, brother and sister-in law Anders and Caroline Davidson, and partner Johnny Mueller, your love throughout this process has been grounding. I largely attribute my love of science, writing, and nature to my parents, who made all of that possible through a childhood spent outdoors together in eastern Washington. Thank you for the hikes, but also for reading to me constantly. Thank you to Johnny, for constantly holding down the fort, talking me down, and reminding me what's really important. To our pets, Birdie and Alfie, thank you for the love and concern through it all.

Thank you to everyone who walked with me at any point on this journey, I hope that our paths cross again.

TABLE OF CONTENTS

Page

LIST OF TABLES

Page

LIST OF FIGURES

Page

CHAPTER 1

INTRODUCTION

Non-perennial channels, or rivers which experience periods of flow cessation or discontinuity, are a naturally occurring hydrologic feature present across all climate regimes. By some estimates, such intermittent systems encompass greater than one third of all global river length (Datry et al., 2014; Messager et al., 2021). Non-perennial channels span a broad spectrum of environments, with flow disruption ranging from intra-seasonal to inter-annual. A number of sub-categories are loosely applied to differentiate temporal and spatial variability in flow, however both their definition within the literature and physical characteristics occur on a continuum (Busch et al., 2020). A key subset within the broad umbrella of intermittent systems are ephemeral channels, or rivers which flow only in response to hydrologic inputs (McMahon and Nathan, 2021). Ephemeral systems are recognized as predominantly dry, losing or disconnected streams which lack groundwater input to support baseflow (Busch et al., 2020). Channels may be separated from the water table by an unsaturated zone, through which surface water infiltrates during periods of flow. These systems experience wetting and drying cycles in response to local precipitation, snowmelt, or artificial hydrologic inputs such as reservoir releases. Moisture inputs are largely seasonal, and their timing and duration primarily control surface flow within the channel (Fakir et al., 2021).

Though present in variable climates, ephemeral channels are the most common hydrologic feature in arid and semi-arid systems (Milewski et al., 2015; Hammond et al., 2021; Messager et al., 2021). This is in part due to the limited precipitation inputs which classify these

environments as drylands (Beck et al., 2018). Although ber of variables have been identified as controlling stream intermittency, climate factors (precipitation, ET, and temperature) are widely considered the primary drivers (Costigan et al., 2016; Hammond et al., 2021; Zipper et al., 2021). Physical features such as channel elevation, slope, geomorphology, and near-surface geology additionally play a important roles in regulating the development and extent of ephemeral flow patterns (Costigan et al., 2016; Hammond et al., 2021; Zipper et al., 2021). Within arid basins, ephemeral channels are found across a continuum from the mountain front to basin plain (Bouimouass et al., 2024). High elevation mountain fronts frequently support intermittent channel flow, driven by rapid surface runoff and the underlying geology (Bouimouass et al., 2024). On basin plains, ephemeral channels develop in response to sporadic hydrologic inputs, elevated evapotranspiration, and infiltration into near-surface sediments (Scamardo and Wohl, 2024). The loss of stream discharge to sediment infiltration is a phenomenon known as transmission loss, as stream flow declines with distance downstream (McMahon and Nathan, 2021). The rate, depth of infiltration, and initial sediment saturation control whether water will be reevaporated or contribute to groundwater recharge (Fakir et al., 2021). Within arid environments, this form of direct recharge through ephemeral channels is considered the primary source of aquifer recharge (Shentsis and Rosenthal, 2003; Levick et al., 2008; Shanafield and Cook, 2014). Surface and groundwater interaction via transmission loss further facilitates crucial nutrient transport and biogeochemical cycling, characteristic of intermittent systems (Stubbington et al., 2020; Zimmer et al., 2022).

Despite their ubiquity, physical, economic, and social barriers have all contributed to the limited study of intermittent channels. Ephemeral systems have historically been categorized as distinct from perennial streams, in part due to lack of monitoring. Ephemeral channels are less

suited to traditional gaging due to large sediment pulses during flood events (Constantz and Thomas, 1997; Zimmer et al., 2020, 2022). Systems with sustained zero-flow periods are further deprioritized for hydrologic monitoring infrastructure, particularly in low-income nations that comprise approximately 90% of arid land globally (UNEMG, 2011; Zimmer et al., 2022). This lack of gaging has created a data gap for many ephemeral systems, particularly outside of North America.

With warming climate, arid regions are projected to experience broad shifts toward reduced precipitation and elevated temperature (Scheff and Frierson, 2012; Ficklin et al., 2016; Beck et al., 2018). This has the potential to facilitate the expansion of intermittent flow regimes in previously perennial systems (Jaeger et al., 2014; Costigan et al., 2016; Schilling et al., 2021; Sauquet et al., 2021; Kelly and Bruckerhoff, 2024). Though this process will likely occur on a continuum, as systems experience decreasingly sporadic periods of intermittency in line with climate extremes, it remains poorly characterized. At present, there is limited understanding of the potential spatial and temporal extent of these shifts, or how this alteration may impact current and future estimates of groundwater recharge. Key questions remain regarding the variables which control and facilitate ephemeral channel development, and how to sustainably manage systems projected to experience a shift from perennial to intermittent flow.

This dissertation broadly explores stream disconnection, the spatial and temporal development of intermittent systems, and its overall impact on hydrologic processes. It specifically focuses on the expansion of intermittent flow regimes in semi-arid environments at varying scales. This research works to address three key challenges within the field of intermittent flow regimes, (1) improved understanding of the variables which drive spatial and temporal expansion of ephemeral channels, (2) characterization of intermittent flow patterns in

data-scarce environments, and (3) quantifying the contribution of ephemeral flow to groundwater recharge through transmission losses in disparate recharge environments.

This dissertation begins at the broadest continental scale in chapter two, exploring which variables control the spatial and temporal expansion of intermittent channels across semi-arid regions of the United States. This work specifically utilizes the extensive gage network and monitoring history of USGS stream gages, paired with 33 climatic, physical, and anthropogenic variables, to better understand primary controls on patterns of stream intermittency. This work further characterized present trends in stream discharge, and trends in the frequency and duration of dry periods within a subset of intermittent channels. Broad trends point to the drying of perennial streams and the expansion of dry periods in intermittent systems. It additionally identified the importance of the timing of wet season moisture, both precipitation and soil moisture, as a dominant control on developing intermittency across the region.

The third chapter focuses in from the continental to the basin scale, and shifts from gaged to ungaged systems. Specifically, it works to characterize intermittent flow patterns in a minimally gaged ephemeral channel in central Morocco, through the development of a novel methodology for water pixel classification. This methodology was further applied to historic satellite images to identify shifts in temporal and spatial flow patterns across the system. Broadly, frequency of stream flow within the channel was found to be in decline, both spatially, moving from the upstream to the downstream reaches, and temporally across the observation period. Despite these reductions, flow patterns were observed to be maintained across the wet season. In tandem, this signifies the potential of sustained levels of aquifer recharge, despite overall reductions in flow within the channel. Additionally, it highlights both the accuracy and

utility of discriminant function analysis in ephemeral channel investigation through satellite imagery.

The fourth chapter further explores channel intermittency within ungaged systems in central Morocco, but shifts its focus from the basin to field scale. Specifically, it explores the connection between intermittent stream flow and the spatial variability of potential recharge via transmission loss, across two disparate recharge zones. Installation of temperature monitoring probes within the subsurface of two ephemeral channels was utilized as a proxy for infiltration during periods of surface flow. Broad observations highlight that both spatial and temporal variability in potential infiltration have favorable implications for groundwater recharge, as it promotes the antecedent sediment moisture conditions necessary support deeper infiltration.

Across drylands, the projected impact of warming climate has the potential to further exacerbate the transition of presently perennial streams to intermittent channels. Advancements in our understanding of intermittent channel flow patterns have the potential to alter estimates of present groundwater storage, particularly in data-limited environments. Improved projections have direct implications for increased sustainable water management, both domestically and abroad.

1.1 References

Beck, H.E., Zimmermann, N.E., McVicar, T.R., Vergopolan, N., Berg, A., and Wood, E.F., 2018, Present and future Köppen-Geiger climate classification maps at 1-km resolution: Scientific Data, v. 5, p. 180214, doi:10.1038/sdata.2018.214.

Bouimouass, H., Tweed, S., Marc, V., Fakir, Y., Sahraoui, H., and Leblanc, M., 2024, The importance of mountain-block recharge in semiarid basins: An insight from the High-Atlas, Morocco: Journal of Hydrology, v. 631, p. 130818, doi:10.1016/j.jhydrol.2024.130818.

Busch, M.H. et al., 2020, What's in a Name? Patterns, Trends, and Suggestions for Defining Non-Perennial Rivers and Streams: Water, v. 12, p. 1980, doi:10.3390/w12071980.

Constantz, J., and Thomas, C.L., 1997, Stream bed temperature profiles as indicators of percolation characteristics beneath arroyos in the Middle Rio Grande Basin, USA: Hydrological Processes, v. 11, p. 1621–1634, doi:10.1002/(SICI)1099-1085(19971015)11:12<1621:AID-HYP493>3.0.CO;2-X.

Costigan, K.H., Jaeger, K.L., Goss, C.W., Fritz, K.M., and Goebel, P.C., 2016, Understanding controls on flow permanence in intermittent rivers to aid ecological research: integrating meteorology, geology and land cover: Integrating Science to Understand Flow Intermittence: Ecohydrology, v. 9, p. 1141–1153, doi:10.1002/eco.1712.

Datry, T., Larned, S.T., and Tockner, K., 2014, Intermittent Rivers: A Challenge for Freshwater Ecology: BioScience, v. 64, p. 229–235, doi:10.1093/biosci/bit027.

Fakir, Y., Bouimouass, H., and Constantz, J., 2021, Seasonality in Intermittent Streamflow Losses Beneath a Semiarid Mediterranean Wadi: Water Resources Research, v. 57, doi:10.1029/2021WR029743.

Ficklin, D.L., Robeson, S.M., and Knouft, J.H., 2016, Impacts of recent climate change on trends in baseflow and stormflow in United States watersheds: Geophysical Research Letters, v. 43, p. 5079–5088, doi:10.1002/2016GL069121.

Hammond, J.C. et al., 2021, Spatial Patterns and Drivers of Nonperennial Flow Regimes in the Contiguous United States: Geophysical Research Letters, v. 48, doi:10.1029/2020GL090794.

Jaeger, K.L., Olden, J.D., and Pelland, N.A., 2014, Climate change poised to threaten hydrologic connectivity and endemic fishes in dryland streams: Proceedings of the National Academy of Sciences of the United States of America, v. 111, p. 13894–13899, doi:10.1073/pnas.1320890111.

Kelly, B.T., and Bruckerhoff, L.A., 2024, Dry, drier, driest: Differentiating flow patterns across a gradient of intermittency: River Research and Applications, v. n/a, doi:10.1002/rra.4289.

Levick, L. et al., 2008, The Ecological and Hydrological Significance of Ephemeral and Intermittent Streams in the Arid and Semi-arid American Southwest: U.S. Environmental Protection Agency and USDA/ARS Southwest Watershed Research Center, doi:EPA/600/R-08/134, ARS/233046.

McMahon, T.A., and Nathan, R.J., 2021, Baseflow and transmission loss: A review: WIREs Water, v. 8, p. e1527, doi:10.1002/wat2.1527.

Messager, M.L., Lehner, B., Cockburn, C., Lamouroux, N., Pella, H., Snelder, T., Tockner, K., Trautmann, T., Watt, C., and Datry, T., 2021, Global prevalence of non-perennial rivers and streams: Nature, v. 594, p. 391–397, doi:10.1038/s41586-021-03565-5.

Milewski, A., Elkadiri, R., and Durham, M., 2015, Assessment and Comparison of TMPA Satellite Precipitation Products in Varying Climatic and Topographic Regimes in Morocco: Remote Sensing, v. 7, p. 5697–5717, doi:10.3390/rs70505697.

Sauquet, E., Shanafield, M., Hammond, J.C., Sefton, C., Leigh, C., and Datry, T., 2021, Classification and trends in intermittent river flow regimes in Australia, northwestern Europe and USA: A global perspective: Journal of Hydrology, v. 597, p. 126170, doi:10.1016/j.jhydrol.2021.126170.

Scamardo, J.E., and Wohl, E., 2024, Recognizing the ephemeral stream floodplain: Identification and importance of flood zones in drylands: Earth Surface Processes and Landforms, v. 49, p. 210–235, doi:10.1002/esp.5754.

Scheff, J., and Frierson, D.M.W., 2012, Robust future precipitation declines in CMIP5 largely reflect the poleward expansion of model subtropical dry zones: Geophysical Research Letters, v. 39, doi:10.1029/2012GL052910.

Schilling, O.S., Cook, P.G., Grierson, P.F., Dogramaci, S., and Simmons, C.T., 2021, Controls on Interactions Between Surface Water, Groundwater, and Riverine Vegetation Along Intermittent Rivers and Ephemeral Streams in Arid Regions: Water Resources Research, v. 57, p. e2020WR028429, doi:10.1029/2020WR028429.

Shanafield, M., and Cook, P.G., 2014, Transmission losses, infiltration and groundwater recharge through ephemeral and intermittent streambeds: A review of applied methods: Journal of Hydrology, v. 511, p. 518–529, doi:10.1016/j.jhydrol.2014.01.068.

Shentsis, I., and Rosenthal, E., 2003, Recharge of aquifers by flood events in an arid region: Hydrological Processes, v. 17, p. 695–712, doi:10.1002/hyp.1160.

Stubbington, R., Acreman, M., Acuña, V., Boon, P.J., Boulton, A.J., England, J., Gilvear, D., Sykes, T., and Wood, P.J., 2020, Ecosystem services of temporary streams differ between wet and dry phases in regions with contrasting climates and economies (A. J. Castro, Ed.): People and Nature, v. 2, p. 660–677, doi:10.1002/pan3.10113.

UNEMG, 2011, Global Drylands: A UN System-Wide Response: Environment Management Group of the United Nations, Geneva.

Zimmer, M.A. et al., 2020, Zero or not? Causes and consequences of zero-flow stream gage readings: WIREs Water, v. 7, doi:10.1002/wat2.1436.

Zimmer, M.A., Burgin, A.J., Kaiser, K., and Hosen, J., 2022, The unknown biogeochemical impacts of drying rivers and streams: Nature Communications, v. 13, p. 7213, doi:10.1038/s41467-022-34903-4.

Zipper, S.C. et al., 2021, Pervasive changes in stream intermittency across the United States: Environmental Research Letters, v. 16, p. 084033, doi:10.1088/1748-9326/ac14ec.

CHAPTER 2

PREDICTING SHIFTS TOWARD INTERMITTENCY IN VULNERABLE STREAMS ACROSS THE CONTINENTAL UNITED STATES

Davidson, L.J. and Milewski, A.M. Submitted to Water Resources Research, October 10th, 2024.

2.1 Chapter Abstract

Broad trends point to the slow drying of streams, with increasing maximum temperatures and altered precipitation fueling declines in discharge across the Western United States. Sustained reductions in streamflow have the potential to drive the evolution of non-perennial channels, yet this process remains poorly characterized, with limited understanding of the variables which control stream vulnerability to intermittency or the spatial and temporal extent of these shifts. This research identifies trends toward novel intermittency across semi-arid CONUS, within 483 stream gages from 1980 to 2024. Greater than half of all gages demonstrated reductions in discharge and increases in the frequency and duration of flow cessation. The timing of wet season moisture, specifically December and January precipitation, were identified as primary controls on developing intermittency. With forecasted reductions in total precipitation across CONUS, intermittent flow regimes are projected to expand further into previously perennial basins, as well as exacerbate drying in vulnerable channels.

2.2 Introduction

River systems are a principal indicator of changing climate, in which they both convey and are transmuted by altered patterns of precipitation and land surface temperature. Stream networks across the landscape capture local and regional shifts in historic climate and communicate these changes through variations in streamflow. Across the contiguous United States (CONUS), broad trends point to declines in stream discharge, particularly in the Southwest (Lins and Slack, 2005; Ficklin et al., 2016; Dudley et al., 2020; Dethier et al., 2020; Hammond et al., 2021, 2022; Zipper et al., 2022). Drying rivers are, in part, a response to a steady reduction in total precipitation across dryland zones (Ting et al., 2018; Seager et al.).

Trends in elevated land surface temperature and water cycle intensity further augment these declines by increasing evapotranspiration and reducing stored soil moisture and surface water (Ting et al., 2018; Zowam et al., 2023; U.S. Environmental Protection Agency, 2024; Seager et al.). These climate patterns mirror broader global trends, in which dryland regions are projected to shift toward increased aridity, altering local and regional river systems in the process (Scheff and Frierson, 2012; Beck et al., 2018; U.S. Environmental Protection Agency, 2024; Seager et al.).

Semi-arid regions encompass one-quarter of CONUS, with 42% concentrated in the Western U.S. (Beck et al., 2018). Streamflow in dryland river systems is distinctly seasonal; in line with precipitation, lowest flows are observed during the summer dry season, with the highest discharge during the wetter winter (Lins and Slack, 2005; Goodrich et al., 2018; Ting et al., 2018; Seager et al.). In the absence of consistent precipitation, perennial baseflow is sustained by groundwater discharge and headwater snowmelt (Levick et al., 2008; Gleeson et al., 2020; Chen et al., 2022). For semi-arid streams with already limited discharge, reduced precipitation inputs have the potential to drive drying to the point of periodic disconnection and the development of intermittent flow regimes (Jaeger et al., 2014; Costigan et al., 2016; Schilling et al., 2021; Sauquet et al., 2021; Kelly and Bruckerhoff, 2024). Though non-perennial and ephemeral streams are a significant and naturally occurring component of the global river network, their number is only expected to grow with increased aridity (Datry et al., 2014; Costigan et al., 2016; Messager et al., 2021). Limited attention has focused on present trends in the evolution of intermittent flow regimes or their projected future distribution, particularly in dryland streams with the greatest vulnerability to reduced stream permanence (Levick et al., 2008; Zimmer et al., 2022). Understanding and quantifying the factors which predispose a stream to shift from

perennial to intermittent flow is crucial for sustainable management, but complicated by interactions between numerous physical, climatic, and anthropogenic controls (Costigan et al., 2016; Jaeger et al., 2018; Schilling et al., 2021; Hammond et al., 2021, 2022; Zipper et al., 2021). Aridity has been strongly linked to increased flow disruption; however, the dominant influence of this signal has the potential to obscure the impact of other relevant variables in multi-climate studies (Eng et al., 2016; Peña-Gallardo et al., 2019; Hammond et al., 2021; Zipper et al., 2021).

Currently, the majority of river systems in the Western U.S. are managed under the assumption of the perennial availability of flow, with water users reliant on surface water to sustain agriculture through seasonally variable precipitation (Kampf et al., 2021; Zipper et al., 2022; Ketchum et al., 2023). Failure to appropriately predict and account for developing stream intermittency has the potential to exacerbate stream drying and disconnection (O'Connor et al., 2014; Ketchum et al., 2023). The anticipated alteration of historic flow patterns requires a shift from passive to proactive management of developing ephemerality, to ensure a future of sustainable water availability (Kovach et al., 2019).

This research explores the evolution of novel stream intermittency and the primary variables driving shifts in historic flow patterns. We conducted a large-scale analysis of developing intermittent flow regimes across 483 stream gages located in semi-arid zones of CONUS, for a minimum 30-year period spanning 1980 to 2024. Each gage was evaluated for trends in seasonal discharge, with gages identified as non-perennial assessed for the seasonal distribution and duration of zero-flow days. Physical, hydrologic, climatic, and anthropogenic variables were further compiled for each gage, with relationships evaluated via Principal Component Analysis (PCA) and combined with Discriminant Function Analysis (DFA) for flow

differentiation and prediction. The goals of our analyses were, (1) characterize the current patterns and distribution of seasonal non-perennial flow across streams in semi-arid CONUS, (2) identify the dominant variables driving perennial vs. intermittent stream flow in semi-arid systems, and (3) predict a streams vulnerability to the development of flow intermittency in basins with limited gaging.

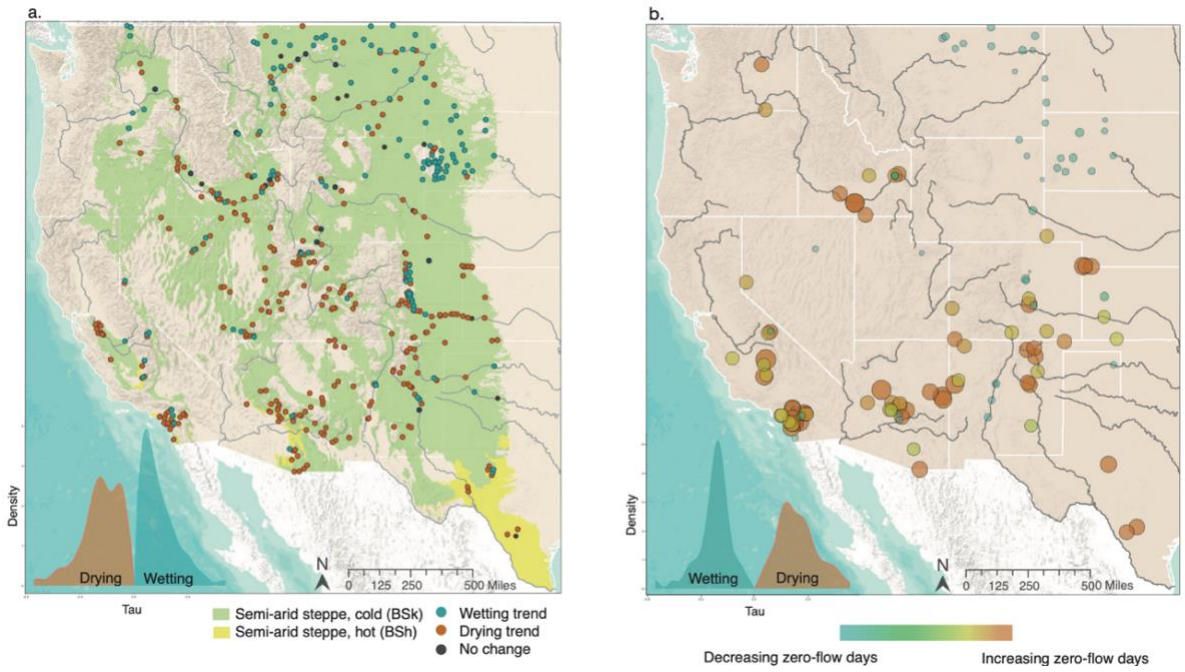

Figure 2-1. Drying streams across semi-arid CONUS.

(a) Seasonal discharge trends reveal statistically significant decreases in stream discharge, particularly across the Southwest. (b) Streams with intermittent flow patterns are expanding further, with 60.2% of stream gages experiencing an increase in the frequency of a completely dry channel. Here, gage size signals increasing or decreasing strength of trend.

2.3 Methods

This section describes the sourcing, organization, and analysis of both U.S. Geologic Survey (USGS) stream gages and related variables. The goal of this analysis was to explore existing and developing patterns of non-perennial flow across 483 USGS stream gages in semi-arid zones of the CONUS from 1980 to 2024. Specially, daily discharge measurements at each gage were aggregated seasonally and analyzed for seasonal trends in discharge, days with zero-stream flow, and length of zero-flow periods. For each gage, we worked to aggregate 33 unique variables related to stream intermittency for exploration via linear discriminant function analysis (LDA). The resulting linear function was further used to predict flow intermittency in 448 USGS stream gages with insufficient data history, as well as identify the primary variables which predispose a stream section to non-perennial flow. A detailed description of the data sourcing and methodology follows.

Gage Selection

Stream gages located within semi-arid regions of CONUS were the primary focus of this study, as dryland systems with both seasonal and limited precipitation have increased vulnerability to periodic flow cessation (Levick et al., 2008; Boulton et al., 2017). Semi-arid zones were defined by the Köppen-Geiger climate classification, which differentiate semi-arid steppe into subgroups based on mean annual air temperature (BSh and BSk) (Beck et al., 2018).

Active stream gage data was sourced from the USGS National Water Information System (NWIS) database (U.S. Geological Survey, 2001). USGS stream gages located within these defined semi-arid regions were filtered and further evaluated for sufficient daily discharge using R statistical software (v4.1.1) and the dataRetrieval R package (v2.7.12) (R Core Team, 2011;

DeCicco, 2024). Gages which lacked consistent daily discharge values for a continuous 30-year period between 1980 and 2024 were excluded, resulting in 483 gages with a sufficient data history for statistical analysis. Gages excluded for insufficient discharge data were filtered by unique subbasins (USGS defined 8-digit hydrologic unit), to produce a secondary dataset of 448 stream gages with unknown intermittency patterns (U.S. Geological Survey and U.S. Department of Agriculture, Natural Resources Conservation Service, 2013).

Trend Analysis

Seasonal Mann-Kendall trend analysis was applied to stream gages in the primary dataset to identify seasonal trends in discharge and historic patterns of intermittent streamflow. In addition to seasonal trends in stream discharge (increasing, decreasing, or no change), we explored two hydrologic signatures linked to intermittency: zero-flow occurrence and zero-flow duration (Zipper et al., 2021). Specifically, seasonal zero-flow occurrence estimates the trend in frequency of 'no flow' days during both seasons, with an increasing trend indicating a drier system with more periods of zero-flow. Seasonal zero-flow duration estimates the trend in the length of a no flow period (the number of consecutive days without streamflow) over the same seasonal breakdown, with an increasing trend indicative of longer stretches in which the gage reads zero. For CONUS, we broadly define the wet season as October through March, and the dry season as April through September (Ting et al., 2018; Seager et al.). Seasonal zero-flow occurrence was further used to classify each gage as either intermittent or perennial based on the presence of zero-flow days (234 and 249 gages, respectively).

Mann-Kendall trend analysis is a non-parametric statistical test used to estimate statistically significant trends in time-series data (Mann, 1945; Kendall, 1948; Meals et al.,

2011). In seasonal Mann-Kendall analysis, the trend for each season is calculated individually before being combined. This method is ideal for hydrologic data, which generally displays seasonal patterns related to precipitation and groundwater abstraction (Hirsch et al., 1982; Meals et al., 2011). Seasonal discharge data was delineated monthly, while zero-flow occurrence and duration were calculated based on aggregated values within the broadly defined dry and wet seasons for North America (Ting et al., 2018). Statistical analysis was performed using the R package Kendall (v.2.2.1) (McLeod, 2022). It is important to note, that a gage reading of zero, though intended to signal flow cessation, may in fact represent equipment error, flow reversal, or management diversion (Zimmer et al., 2020). To address this, preference was given to stream gage data checked for accuracy by the reporting agency.

Variable Selection and Data Collection

Diverse physical, climatic, and anthropogenic variables have been identified in previous studies as potentially significant controls on flow intermittency (Costigan et al., 2015; Boulton et al., 2017; Schilling et al., 2021; Hammond et al., 2021; Zipper et al., 2021). Thirty-three variables were selected for analysis and synthesized for each gage in both the primary and secondary datasets, resulting 30,723 measurements across 931 gages. Variable details and sources are outlined below (Table 2-1).

Table 2-1. Variable Data Source and Availability.

*Variables with an asterisk were log transformed prior to analysis to normalize their distribution, required for the statistical analysis.

Variables	Data Description	Spatial Resolution
Contributing Drainage Area[1]	Sourced from the USGS NWIS dataset, USGS defined contributing drainage area (sq. miles). A minority of stream gages lacked this metric, and USGS designated watershed areas (HUC 10) were used as a substitute.	30 m
Dams*[2,3]	USDOT National Inventory of Dams dataset. The state of Texas was supplemented with an inventory of state regulated dams (TCEQ). Dam counts were aggregated for each gage sub-basin (HUC 8)	NA
Elevation[1]	USGS derived gage elevation (ft), from USGS NWIS dataset. Values were supplemented by elevation from USGS 1-arc second DEM.	30 m
Evapotranspiration (ET)[4]	Elnashar et al. (2021) multi-product and satellite aggregated global ET dataset. ET was averaged monthly from 2010–2019, with average ET calculated for each gage sub-basin (HUC 8).	0.1°
Irrigated Area*[5]	Landsat based irrigation dataset (LANID) for CONUS (2018–2020). Percent irrigated area was aggregated for each gage sub-basin (HUC 8).	30 m
Land Cover[6]	NLCD MRLC land cover classification for CONUS (2021). Dominant land cover type (percentage of total area) within gage sub-basin (HUC 8) was extracted.	30 m
Maximum Land Surface Temperature (LST)[7]	Zhang et al. (2021) NASA MODIS (Terra/Aqua) generated dataset. LST averaged monthly from 2010–2019, with units converted to °F. Maximum LST within each gage sub-basin (HUC 8) was extracted.	0.1°
Precipitation*[8]	PRISM average monthly 30-year normal precipitation dataset (CONUS). Values were averaged across each gage sub-basin (HUC 8).	800 m

Soil Hydrologic Group[9]	U.S. Soil Hydrologic Group (SSURGO) water infiltration classification. Dominant soil hydrologic group (percentage of total area) within gage sub-basin (HUC 8) was extracted.	30 m
Soil Moisture (SM)*[10,11]	Jiang et al. (2022) multi-product and satellite generated dataset, downscaled by Zowam and Milewski (2024). SM was averaged monthly from 2010–2019, and further averaged across each gage sub-basin (HUC 8).	0.1°
Slope[12]	Average slope across each gage sub-basin (HUC 8), derived from USGS 1-arc second DEM.	30 m

Notes: [1]U.S. Geological Survey, 2001; [2]U.S. Dept. of Transportation, 2013; [3]Texas Commission on Environmental Quality; [4]Elnashar et al., 2021; [5]Martin et al., 2023; [6]Dewitz and U.S. Geological Survey, 2021; [7]Zhang et al., 2021; [8]PRISM Climate Group, 2014; [9]NRCS Database; [10]Jiang et al., 2022; [11]Zowam & Milewski, 2024; [12]1U.S. Geological Survey, 2022.

Discriminant Function Analysis (DFA) and Principal Component Analysis (PCA)

We applied Discriminant Function Analysis (DFA) to identify variables with the strongest relationship to channel intermittency, and to generate a linear function for prediction of non-perennial flow in systems with a limited gaging history (Appendix Chapter 2, Figure 1). Linear DFA is a statistical method used to sort continuous data into known categorical groups (here, intermittent, or perennial channels) through the generation of a linear function built on provided variables (Davis, 2002). Stream gages with sufficient time series data were used as a training dataset, with the predictive accuracy of the linear DFA evaluated by whether its classifications matched known group membership (79.50% predictive accuracy) (Maindonald and Braun, 2003). Prior to analysis, a subset of variables were log transformed to normalize their data distribution. Z-scores were further calculated for all variables to standardize data for comparison. Validation was performed through jackknife resampling which produces a secondary predictive accuracy, free of resubstitution error (74.33% predictive accuracy) (Maindonald and Braun, 2003). We then applied our DFA linear function to the secondary gage

dataset with insufficient time-series data, to predict gage vulnerability to intermittent flow. DFA statistical analysis and data processing was performed in R using the MASS R package (v7.3–60) (Venables and Ripley, 2002).

Principle Component Analysis (PCA) was additionally applied to explore variable relationships and corroborate observations from DFA analysis. PCA is a statistical analysis used to reduce the dimensionality of a dataset, particularly ideal for situations with many variables (Lever et al., 2017). This method organizes data by reorienting axes based on decreasing variance (Lever et al., 2017). PCA was performed on stream gages with sufficient time series data, generating four principal components which explained 78.1% of the data variance. A correlation biplot was additionally generated to visualize the spatial relationships between variables (Appendix Chapter 2, Figure 2).

2.4 Results

Stream gages distributed across semi-arid regions of CONUS reveal significant patterns of drying. From 1980 to 2024, 63.1% of stream gages demonstrated statistically significant seasonal trends in decreased discharge. Across the 483 gages analyzed, less than one-third (29.4%) experienced increases in seasonal discharge, while 7.5% of gages exhibited no statistically significant change. Though drying streams are distributed across all semi-arid regions of CONUS, they are most concentrated within the Southwest; gages with increased discharge were focused within the Northern Great Plains (Figure 2-1a.). Seasonal discharge trends were further explored for two signatures of stream intermittency: zero-flow occurrence and zero-flow duration. Seasonal zero-flow occurrence analyzes the quantity of zero discharge days per season, while seasonal zero-flow duration explores the consecutive length of daily zero-flow gage readings. Statistically significant trends in zero-flow occurrence were observed in 118

stream gages from 1980 to 2024, with 60.2% experiencing an increase in the number of no-flow days per season (Figure 2-1b.). Of the 117 gages with statistically significant trends in duration of zero-flow period, 59.8% shifted seasonally toward longer periods without stream discharge ($p < 0.05$). Stream gages undergoing a seasonal expansion in the frequency and length of zero-flow periods paralleled the spatial distribution of streams experiencing decreased seasonal discharge. Periods of zero-flow occurrence were used to classify stream gages as either intermittent or perennial stream sections. Regardless of current intermittency status, stream gages are largely becoming drier; 65.5% of perennial and 60.7% of intermittent gages demonstrate seasonal and statistically significant reductions in flow. This implies the likely expansion of the number of stream sections shifting toward patterns of intermittent flow across semi-arid regions of CONUS.

In conjunction with this projected shift, dominant drivers of flow intermittency were identified in exclusively dryland zones (Table 2-1). Broadly, variables related to wet season moisture had the greatest influence on differentiating perennial from intermittent stream flow (Figure 2-2). During October through March, the timing of precipitation and soil moisture variables at distinct points within the wet season primarily drove group separation. Dominant variables contributing to the distinction between perennial and intermittent systems were identified through Discriminant Function Analysis (DFA). Average December precipitation had the overall greatest influence on distinguishing between stream types. Specifically, average December precipitation and average soil moisture for both January and March were identified as the greatest controlling variables for intermittent streams. Average precipitation for January and November, paired with average February soil moisture, demonstrated the greatest impact on perennial flow (Appendix Chapter 2, Figure 1). Considering the timing of these variables, our results imply that the concentration and maintenance of moisture at the end of the wet season is

largely what separates an intermittent from perennial system. Soil moisture is closely tied to precipitation in the month preceding, a relationship highlighted by the grouping of November precipitation–December soil moisture and December precipitation–January soil moisture (Sehler et al., 2019) (Appendix Chapter 2, Table 2). The relevance of November precipitation further suggests that an early onset of soil moisture influences the overall storage of a hydrologic system for the entire wet season, reducing a systems vulnerability to flow disruption in the drier summer months. The role of moisture seasonality was further validated through Principal Component Analysis (PCA), which established an inverse relationship between wet season precipitation and dry season soil moisture (Appendix Chapter 2, Figure 2). Correlation between decreased wet season soil moisture and increased elevation was observed, suggesting the role of snowpack in higher elevation gages to sustain perennial flow during the lower precipitation dry season. Excluding climate variables, which demonstrate the greatest overall contribution to the DFA's group differentiation, several physical variables exerted a secondary influence on intermittency. Specifically, the contributing drainage area of each gage, and the dominance of both Shrub/Scrub land cover and slow infiltration soils (class C) within each sub-basin were identified as non-climate related controls with influence on group differentiation (Appendix Chapter 2, Figure 3).

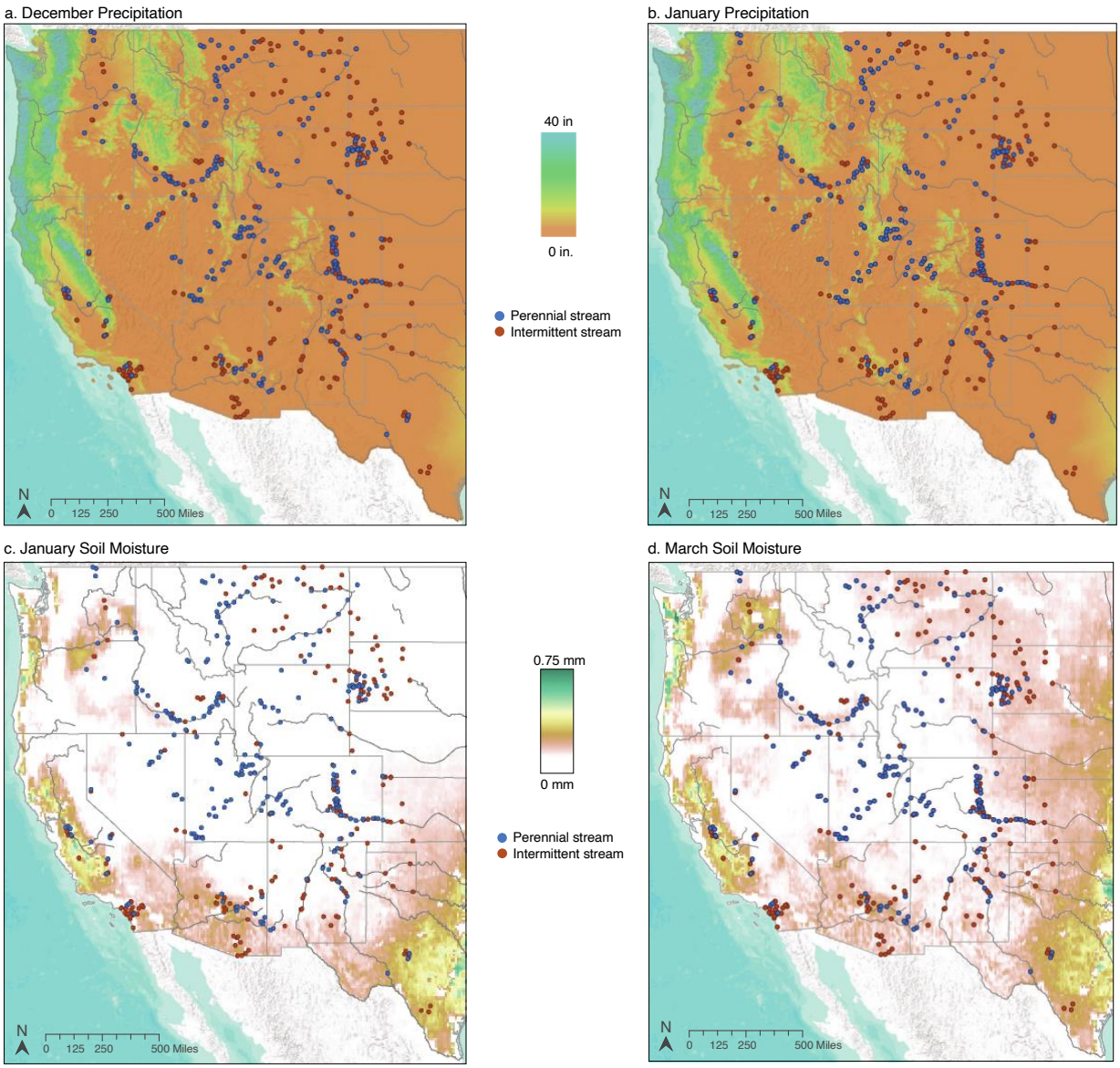

Figure 2-2. Timing of wet season moisture controls developing intermittency. Average December precipitation exerts the most significant control on non-perennial flow. Sustained moisture inputs late in the wet season are correlated to strong distinctions between channels which flow perennially and those which dry up.

Broad shifts towards decreased stream discharge and increased non-perennial flow highlight the necessity of efficient characterization for stream management and conservation. Across stream gages located in semi-arid regions of CONUS which lack sufficient data history for trend analysis, we applied the previous DFA characterization to predict non-perennial flow and identify gage vulnerability to stream intermittency. Of the 448 gages with insufficient discharge data, 49.6% were predicted to experience intermittent flow patterns (Figure 2-3). Gages predicted to be intermittent were uniformly spatially distributed across semi-arid CONUS, with minor concentration in the Southwest and Southern Great Plains. The exception was the upper Rocky Mountain region (Utah, Wyoming, Colorado), in which the majority of gages were predicted to be in perennially flowing systems. Projected shifts in water cycle intensity, however, highlight the potential for an even greater expansion of intermittency into these regions, with broad swaths of the Central and Southwest U.S. predicted to experience declines in precipitation with stable evapotranspiration (Figure 2-3a). (Zowam et al., 2023). This scenario could likely exacerbate projected stream drying, increasing both the distribution and acute severity within individual streams.

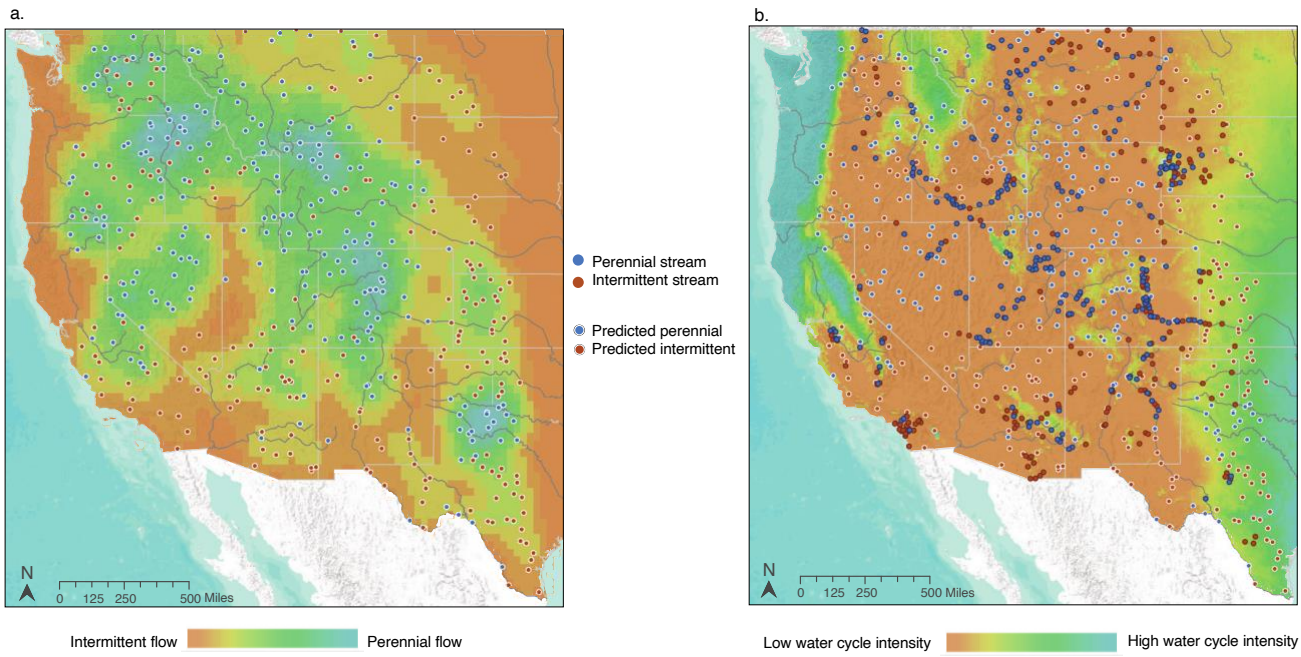

Figure 2-3. Stream intermittency is projected to expand. (a) Across semi-arid CONUS, 49.6% of gages with an insufficient data history were predicted to be vulnerable to the development of stream intermittency. (b) Changing climate patterns, particularly reductions in precipitation paired with stable ET, highlight the potential expansion of non-perennial flow into historically perennial stream reaches.

2.5 Discussion and Conclusions

Changing climate patterns across dryland CONUS are rapidly altering river flows, with increasing trends toward drying and expansion of intermittency. Stream gages are documenting both an elevated frequency of zero-flow periods and progressively longer temporal stretches before water returns. The timing and distribution of moisture, particularly within the winter wet season, is identified as the primary control on non-perennial flow. Higher precipitation in the latter half of the wet season, December and January, is expected to translate to elevated soil

moisture and overall increased water storage within a hydrologic system (Small, 2005). Accumulation of moisture, particularly at the cessation of the wet season, likely helps to sustain discharge throughout the advancing dry season.

Our results further identified the relevance of early onset wet season precipitation for channel intermittency. The initial rains in November generally mark a transition to the wet season, bringing with them not only moisture inputs, which may reactivate a non-flowing or low-discharge channel, but ushering in a drop in temperature and reduced evapotranspiration. Soil moisture content plays a significant role in arid systems, where antecedent sediment moisture is necessary for sustained infiltration to the water table (Fakir et al., 2021). Early wet season precipitation thus can drive increased percolation and overall greater seasonal recharge, through both focused recharge via the stream channel and diffuse recharge across the landscape (Small, 2005). This has the potential to raise the height of the water table and increase groundwater discharge into streams, supporting perennial baseflow.

Our results further underscore the impact of bracketed seasonal moisture on the development of channel intermittency, via both precipitation and soil moisture at the onset and conclusion of the wet season. Projected climate patterns across semi-arid regions of CONUS are, however, forecasted to increase the seasonality of precipitation, with a reduction in the frequency of storms and an increase in the size of singular events (Wasko et al., 2021; Chang et al.). This shift may impact the timing of precipitation and ultimately the volume of water able to effectively infiltrate and replenish groundwater stores during the wet season, contributing to the increased development of intermittent channels. Expanding ephemerality has serious implications not only for hydrologic, but physical and ecologic processes, disturbing aquatic communities, and sediment and nutrient flux (Datry et al., 2014; Shumilova et al., 2019). It

further holds significant consequences for regional water management strategies. Though current management may consider seasonal variability in stream discharge, this thinking must be expanded to include periods of stream drought. Failure to manage for zero discharge intervals has the potential to exacerbate stream dry downs, increasing their duration, and stressing alternative water sources such as groundwater. Insufficient preparation for novel non-perennial flow will likely have a substantial economic impact, particularly on regional agriculture which relies on stream flow to support irrigation during the dry summer months (Ketchum et al., 2023). Improved understanding of the dominant variables controlling developing stream intermittency is necessary, not only to strengthen both our characterization and prediction, but to mitigate non-perennial stream expansion in vulnerable dryland basins around the globe.

2.6 References

Beck, H.E., Zimmermann, N.E., McVicar, T.R., Vergopolan, N., Berg, A., and Wood, E.F., 2018, Present and future Köppen-Geiger climate classification maps at 1-km resolution: Scientific Data, v. 5, p. 180214, doi:10.1038/sdata.2018.214.

Bouimouass, H., Tweed, S., Marc, V., Fakir, Y., Sahraoui, H., and Leblanc, M., 2024, The importance of mountain-block recharge in semiarid basins: An insight from the High-Atlas, Morocco: Journal of Hydrology, v. 631, p. 130818, doi:10.1016/j.jhydrol.2024.130818.

Boulton, A.J., Rolls, R.J., Jaeger, K.L., and Datry, T., 2017, Chapter 2.3 - Hydrological Connectivity in Intermittent Rivers and Ephemeral Streams, in Datry, T., Bonada, N., and Boulton, A. eds., Intermittent Rivers and Ephemeral Streams, Academic Press, p. 79–108, doi:10.1016/B978-0-12-803835-2.00004-8.

Busch, M.H. et al., 2020, What's in a Name? Patterns, Trends, and Suggestions for Defining Non-Perennial Rivers and Streams: Water, v. 12, p. 1980, doi:10.3390/w12071980.

Chang, W., Stein, M.L., Wang, J., Kotamarthi, V.R., and Moyer, E.J. Changes in Spatiotemporal Precipitation Patterns in Changing Climate Conditions in: Journal of Climate Volume 29 Issue 23 (2016):, https://journals.ametsoc.org/view/journals/clim/29/23/jcli-d-15-0844.1.xml?tab_body=fulltext-display (accessed August 2024).

Chen, X., Tang, G., Chen, T., and Niu, X., 2022, An Assessment of the Impacts of Snowmelt Rate and Continuity Shifts on Streamflow Dynamics in Three Alpine Watersheds in the Western U.S.: Water, v. 14, p. 1095, doi:10.3390/w14071095.

Constantz, J., and Thomas, C.L., 1997, Stream bed temperature profiles as indicators of percolation characteristics beneath arroyos in the Middle Rio Grande Basin, USA: Hydrological Processes, v. 11, p. 1621–1634, doi:10.1002/(SICI)1099-1085(19971015)11:12<1621::AID-HYP493>3.0.CO;2-X.

Costigan, K.H., Daniels, M.D., and Dodds, W.K., 2015, Fundamental spatial and temporal disconnections in the hydrology of an intermittent prairie headwater network: Journal of Hydrology, v. 522, p. 305–316, doi:10.1016/j.jhydrol.2014.12.031.

Costigan, K.H., Jaeger, K.L., Goss, C.W., Fritz, K.M., and Goebel, P.C., 2016, Understanding controls on flow permanence in intermittent rivers to aid ecological research: integrating meteorology, geology and land cover: Integrating Science to Understand Flow Intermittence: Ecohydrology, v. 9, p. 1141–1153, doi:10.1002/eco.1712.

Datry, T., Larned, S.T., and Tockner, K., 2014, Intermittent Rivers: A Challenge for Freshwater Ecology: BioScience, v. 64, p. 229–235, doi:10.1093/biosci/bit027.

Davis, J.C., 2002, Statistics and Data Analysis in Geology: New York, Wiley, https://www.scribd.com/doc/98598695/Statistics-and-Data-Analysis-in-Geology-3rd-ed (accessed September 2023).

DeCicco, L., 2024, Water / dataRetrieval · GitLab: GitLab, https://code.usgs.gov/water/dataRetrieval (accessed August 2024).

Dethier, E.N., Sartain, S.L., Renshaw, C.E., and Magilligan, F.J., 2020, Spatially coherent regional changes in seasonal extreme streamflow events in the United States and Canada since 1950: Science Advances, v. 6, p. eaba5939, doi:10.1126/sciadv.aba5939.

Dudley, R.W., Hirsch, R.M., Archfield, S.A., Blum, A.G., and Renard, B., 2020, Low streamflow trends at human-impacted and reference basins in the United States: Journal of Hydrology, v. 580, p. 124254, doi:10.1016/j.jhydrol.2019.124254.

Eng, K., Wolock, D.M., and Dettinger, M.D., 2016, Sensitivity of Intermittent Streams to Climate Variations in the USA: River Research and Applications, v. 32, p. 885–895, doi:10.1002/rra.2939.

Fakir, Y., Bouimouass, H., and Constantz, J., 2021, Seasonality in Intermittent Streamflow Losses Beneath a Semiarid Mediterranean Wadi: Water Resources Research, v. 57, doi:10.1029/2021WR029743.

Ficklin, D.L., Robeson, S.M., and Knouft, J.H., 2016, Impacts of recent climate change on trends in baseflow and stormflow in United States watersheds: Geophysical Research Letters, v. 43, p. 5079–5088, doi:10.1002/2016GL069121.

Gleeson, T., Cuthbert, M., Ferguson, G., and Perrone, D., 2020, Global Groundwater Sustainability, Resources, and Systems in the Anthropocene: Annual Review of Earth and Planetary Sciences, v. 48, p. 431–463, doi:10.1146/annurev-earth-071719-055251.

Goodrich, D. c., Kepner, W. g., Levick, L. r., and Wigington Jr., P. j., 2018, Southwestern Intermittent and Ephemeral Stream Connectivity: JAWRA Journal of the American Water Resources Association, v. 54, p. 400–422, doi:10.1111/1752-1688.12636.

Hammond, J.C. et al., 2022, Going Beyond Low Flows: Streamflow Drought Deficit and Duration Illuminate Distinct Spatiotemporal Drought Patterns and Trends in the U.S. During the Last Century: Water Resources Research, v. 58, p. e2022WR031930, doi:10.1029/2022WR031930.

Hammond, J.C. et al., 2021, Spatial Patterns and Drivers of Nonperennial Flow Regimes in the Contiguous United States: Geophysical Research Letters, v. 48, doi:10.1029/2020GL090794.

Hirsch, R.M., Slack, J.R., and Smith, R.A., 1982, Techniques of trend analysis for monthly water quality data: Water Resources Research, v. 18, p. 107–121, doi:10.1029/WR018i001p00107.

Jaeger, K.L., Olden, J.D., and Pelland, N.A., 2014, Climate change poised to threaten hydrologic connectivity and endemic fishes in dryland streams: Proceedings of the National Academy of Sciences of the United States of America, v. 111, p. 13894–13899, doi:10.1073/pnas.1320890111.

Jaeger, K., Sando, R., McShane, R.R., Dunham, J.B., Hockman-Wert, D., Kaiser, K., Hafen, K., Risley, J.C., and Blasch, K., 2018, Probability of Streamflow Permanence Model (PROSPER): A spatially continuous model of annual streamflow permanence throughout the Pacific Northwest: Journal of Hydrology X, v. 2, p. 100005, doi:10.1016/j.hydroa.2018.100005.

Kampf, S.K. et al., 2021, Managing nonperennial headwater streams in temperate forests of the United States: Forest Ecology and Management, v. 497, p. 119523, doi:10.1016/j.foreco.2021.119523.

Kelly, B.T., and Bruckerhoff, L.A., 2024, Dry, drier, driest: Differentiating flow patterns across a gradient of intermittency: River Research and Applications, v. n/a, doi:10.1002/rra.4289.

Kendall, M.G., 1948, Rank Correlation Methods: C. Griffin, 182 p.

Ketchum, D., Hoylman, Z.H., Huntington, J., Brinkerhoff, D., and Jensco, K.G., 2023, Irrigation intensification impacts sustainability of streamflow in the Western United States:, doi:https://doi.org/10.1038/s43247-023-01152-2.

Kovach, R. et al., 2019, An Integrated Framework for Ecological Drought across Riverscapes of North America: BioScience, v. 69, doi:10.1093/biosci/biz040.

Lever, J., Krzywinski, M., and Altman, N., 2017, Principal component analysis: Nature Methods, v. 14, p. 641–642, doi:10.1038/nmeth.4346.

Levick, L. et al., 2008, The Ecological and Hydrological Significance of Ephemeral and Intermittent Streams in the Arid and Semi-arid American Southwest: U.S. Environmental Protection Agency and USDA/ARS Southwest Watershed Research Center, doi:EPA/600/R-08/134, ARS/233046.

Lins, H.F., and Slack, J.R., 2005, Seasonal and Regional Characteristics of U.S. Streamflow Trends in the United States from 1940 to 1999: Physical Geography, v. 26, p. 489–501, doi:10.2747/0272-3646.26.6.489.

Maindonald, J., and Braun, W.J., 2003, Data Analysis and Graphics Using R – an Example-Based Approach, Third Edition: Cambridge.

Mann, H.B., 1945, Nonparametric Tests Against Trend: Econometrica, v. 13, p. 245–259, doi:10.2307/1907187.

McLeod, A.I., 2022, Kendall: Kendall Rank Correlation and Mann-Kendall Trend Test. R package version 2.2.1. https://CRAN.R-project.org/package=Kendall:

McMahon, T.A., and Nathan, R.J., 2021, Baseflow and transmission loss: A review: WIREs Water, v. 8, p. e1527, doi:10.1002/wat2.1527.

Meals, D.M., Spooner, J., Dressing, S.A., and Harcum, J.B., 2011, Statistical analysis for monotonic trends: Tech Notes 6, https://www.epa. gov/polluted-runoff-nonpoint-source-pollution/nonpoint-source-monitoringtechnical-notes.

Messager, M.L., Lehner, B., Cockburn, C., Lamouroux, N., Pella, H., Snelder, T., Tockner, K., Trautmann, T., Watt, C., and Datry, T., 2021, Global prevalence of non-perennial rivers and streams: Nature, v. 594, p. 391–397, doi:10.1038/s41586-021-03565-5.

Milewski, A., Elkadiri, R., and Durham, M., 2015, Assessment and Comparison of TMPA Satellite Precipitation Products in Varying Climatic and Topographic Regimes in Morocco: Remote Sensing, v. 7, p. 5697–5717, doi:10.3390/rs70505697.

O'Connor, B.L., Hamada, Y., Bowen, E.E., Grippo, M.A., Hartmann, H.M., Patton, T.L., Van Lonkhuyzen, R.A., and Carr, A.E., 2014, Quantifying the sensitivity of ephemeral streams to land disturbance activities in arid ecosystems at the watershed scale: Environmental Monitoring and Assessment, v. 186, p. 7075–7095, doi:10.1007/s10661-014-3912-5.

Peña-Gallardo, M., Vicente-Serrano, S.M., Hannaford, J., Lorenzo-Lacruz, J., Svoboda, M., Domínguez-Castro, F., Maneta, M., Tomas-Burguera, M., and Kenawy, A.E., 2019, Complex influences of meteorological drought time-scales on hydrological droughts in natural basins of the contiguous Unites States: Journal of Hydrology, v. 568, p. 611–625, doi:10.1016/j.jhydrol.2018.11.026.

R Core Team, 2011, R: A Language and Environment for Statistical Computing:

Sauquet, E., Shanafield, M., Hammond, J.C., Sefton, C., Leigh, C., and Datry, T., 2021, Classification and trends in intermittent river flow regimes in Australia, northwestern

Europe and USA: A global perspective: Journal of Hydrology, v. 597, p. 126170, doi:10.1016/j.jhydrol.2021.126170.

Scamardo, J.E., and Wohl, E., 2024, Recognizing the ephemeral stream floodplain: Identification and importance of flood zones in drylands: Earth Surface Processes and Landforms, v. 49, p. 210–235, doi:10.1002/esp.5754.

Scheff, J., and Frierson, D.M.W., 2012, Robust future precipitation declines in CMIP5 largely reflect the poleward expansion of model subtropical dry zones: Geophysical Research Letters, v. 39, doi:10.1029/2012GL052910.

Schilling, O.S., Cook, P.G., Grierson, P.F., Dogramaci, S., and Simmons, C.T., 2021, Controls on Interactions Between Surface Water, Groundwater, and Riverine Vegetation Along Intermittent Rivers and Ephemeral Streams in Arid Regions: Water Resources Research, v. 57, p. e2020WR028429, doi:10.1029/2020WR028429.

Seager, R., Neelin, D., Simpson, I., Liu, H., Henderson, N., Shaw, T., Kushnir, Y., Ting, M., and Cook, B. Dynamical and Thermodynamical Causes of Large-Scale Changes in the Hydrological Cycle over North America in Response to Global Warming in: Journal of Climate Volume 27 Issue 20 (2014):, https://journals.ametsoc.org/view/journals/clim/27/20/jcli-d-14-00153.1.xml (accessed August 2024).

Sehler, R., Li, J., Reager, J., and Ye, H., 2019, Investigating Relationship Between Soil Moisture and Precipitation Globally Using Remote Sensing Observations: Journal of Contemporary Water Research & Education, v. 168, p. 106–118, doi:10.1111/j.1936-704X.2019.03324.x.

Shanafield, M., and Cook, P.G., 2014, Transmission losses, infiltration and groundwater recharge through ephemeral and intermittent streambeds: A review of applied methods: Journal of Hydrology, v. 511, p. 518–529, doi:10.1016/j.jhydrol.2014.01.068.

Shentsis, I., and Rosenthal, E., 2003, Recharge of aquifers by flood events in an arid region: Hydrological Processes, v. 17, p. 695–712, doi:10.1002/hyp.1160.

Shumilova, O. et al., 2019, Simulating rewetting events in intermittent rivers and ephemeral streams: A global analysis of leached nutrients and organic matter: Global Change Biology, v. 25, p. 1591–1611, doi:10.1111/gcb.14537.

Small, E.E., 2005, Climatic controls on diffuse groundwater recharge in semiarid environments of the southwestern United States: Water Resources Research, v. 41, doi:10.1029/2004WR003193.

Stubbington, R., Acreman, M., Acuña, V., Boon, P.J., Boulton, A.J., England, J., Gilvear, D., Sykes, T., and Wood, P.J., 2020, Ecosystem services of temporary streams differ between wet and dry phases in regions with contrasting climates and economies (A. J. Castro, Ed.): People and Nature, v. 2, p. 660–677, doi:10.1002/pan3.10113.

Ting, M., Seager, R., Li, C., Liu, H., and Henderson, N., 2018, Mechanism of Future Spring Drying in the Southwestern United States in CMIP5 Models: Journal of Climate, https://journals.ametsoc.org/view/journals/clim/31/11/jcli-d-17-0574.1.xml (accessed August 2024).

UNEMG, 2011, Global Drylands: A UN System-Wide Response: Environment Management Group of the United Nations, Geneva.

U.S. Environmental Protection Agency, 2024, Climate Change Indicators in the United States, Fifth Edition: EPA 430-R-24-003, www.epa.gov/climate-indicators.

U.S. Geological Survey, 2001, USGS National Water Information System (NWIS). Water Data for the Nation:, http://waterdata.usgs.gov/nwis/ (accessed May 2024).

U.S. Geological Survey and U.S. Department of Agriculture, Natural Resources Conservation Service, 2013, Federal Standards and Procedures for the National Watershed Boundary Dataset (WBD): v. 4, p. 63.

Venables, W.N., and Ripley, B.D., 2002, Modern Applied Statistics with S: New York, NY, UA, Springer.

Wasko, C., Nathan, R., Stein, L., and O'Shea, D., 2021, Evidence of shorter more extreme rainfalls and increased flood variability under climate change: Journal of Hydrology, v. 603, p. 126994, doi:10.1016/j.jhydrol.2021.126994.

Zimmer, M.A. et al., 2020, Zero or not? Causes and consequences of zero-flow stream gage readings: WIREs Water, v. 7, doi:10.1002/wat2.1436.

Zimmer, M.A., Burgin, A.J., Kaiser, K., and Hosen, J., 2022, The unknown biogeochemical impacts of drying rivers and streams: Nature Communications, v. 13, p. 7213, doi:10.1038/s41467-022-34903-4.

Zipper, S.C. et al., 2021, Pervasive changes in stream intermittency across the United States: Environmental Research Letters, v. 16, p. 084033, doi:10.1088/1748-9326/ac14ec.

Zipper, S.C., Farmer, W.H., Brookfield, A., Ajami, H., Reeves, H.W., Wardropper, C., Hammond, J.C., Gleeson, T., and Deines, J.M., 2022, Quantifying Streamflow Depletion from Groundwater Pumping: A Practical Review of Past and Emerging Approaches for Water Management: JAWRA Journal of the American Water Resources Association, v. 58, p. 289–312, doi:10.1111/1752-1688.12998.

Zowam, F.J., Milewski, A.M., and Richards IV, D.F., 2023, A Satellite-Based Approach for Quantifying Terrestrial Water Cycle Intensity: Remote Sensing, v. 15, p. 3632, doi:10.3390/rs15143632.

CHAPTER 3

QUANTIFYING INTERMITTENT FLOW REGIMES IN UNGAUGED BASINS: OPTIMIZATION OF REMOTE SENSING TECHNIQUES FOR EPHEMERAL CHANNELS USING A FLEXIBLE STATISTICAL CLASSIFICATION

Davidson, L. J., Milewski, A. M., Holland, S. M. 2023. *Remote Sensing*, 15, 5672, DOI: 10.3390/rs15245672. Reprinted here with permission of publisher.

3.1 Chapter Abstract

Intermittent and ephemeral channels are a critical component of the global hydrologic network. The dominant feature in dryland environments, ephemeral channel transmission loss facilitates aquifer recharge. Characterizing flow intermittency improves groundwater storage estimates; however, limited gauging of intermittent systems impedes this understanding. This research develops an improved classification for surface flow, optimized for ephemeral systems using linear discriminant function analysis and remotely sensed imagery. It further applies this methodology to assess temporal and spatial flow patterns across the Souss channel, an ungauged, ephemeral system in central Morocco. Linear discriminant function analysis demonstrates high predictive accuracy for Landsat imagery, with significantly improved classification success as compared to the Modified Normalized Difference Water Index. Application to the Souss channel from 1984 to 2022 points to a decreasing trend in flow frequency. Despite this change, flow events remain concentrated within the wet season, critical for regional aquifer recharge. Spatial flow characteristics further support sustained infiltration, with the majority of events focused within the upstream channel section during both dry and wet seasons. Decreased occurrence moving downstream highlights the likely impact of additional factors such as transmission loss, evapotranspiration, and agricultural abstraction contributing to channel intermittency.

3.2 Introduction

Perennial channels remain the dominant conceptual framework for hydrologic research, yet more than half of the global stream network experiences flow cessation on an annual basis (Datry et al., 2014; Messager et al., 2021). Non-perennial channels (e.g., intermittent, and ephemeral channels) encompass a broad range of dynamic systems, with periods of flow

discontinuity ranging from a single day to the majority of the year (Costigan et al., 2017). Observed across both humid and arid climates, this range of disruption, as well as the primary drivers, vary widely (Hammond et al., 2021; Messager et al., 2021; Zipper et al., 2021). Intermittent flow is a naturally occurring feature of many hydrologic regimes; it may be catalyzed by drought, anthropogenic abstraction, or occur only in response to precipitation events. Key drivers of flow variability include climate, topography, height of the water table, and basin land use (Costigan et al., 2017; Hammond et al., 2021; Messager et al., 2021; Zipper et al., 2021). In conjunction with providing critical water resources, non-perennial channels facilitate key biogeochemical processes and sediment flux as they shift between wet and dry phases (Datry et al., 2014; Stubbington et al., 2020; Stark et al., 2021; Zimmer et al., 2022).

Despite their hydrologic and ecologic significance, intermittent systems remain poorly characterized (Datry et al., 2014; Zimmer et al., 2020). Though increasing work has been carried out to understand their prevalence and global distribution, minimal research has been focused on the dynamic nature and temporal variability of flow. This is particularly relevant as many perennial streams are anticipated to grow increasingly intermittent with projected climate warming and altered patterns of precipitation (Zipper et al., 2021).

Limited characterization is a specific concern within dryland environments, where intermittent and ephemeral channels are the dominant hydrologic feature (Milewski et al., 2009, 2015; Hammond et al., 2021; Messager et al., 2021). Ephemeral channels experience episodic flow only in response to storm events; streamflow is closely tied to precipitation seasonality and is spatially and temporally variable (Fakir et al., 2021). Transmission loss, the vertical infiltration of surface water through channel sediments, represents the primary form of aquifer recharge within arid zones (Shentsis and Rosenthal, 2003; Levick et al., 2008; Shanafield and Cook,

2014). Limited research has focused on quantifying ephemeral channel flow regimes, despite direct implications of channel intermittency for groundwater recharge and water availability. This is, in part, a result of the minimal gauging and limited data history frequently observed in non-perennial systems (Levick et al., 2008; Costa et al., 2013; Costigan et al., 2017). Though under-prioritized, ephemeral channels present specific challenges to monitoring (Krabbenhoft et al., 2022). Extended periods of no-flow, punctuated by large, destructive floods may damage gauge equipment. Flow may further be spatially discontinuous across the channel, with stationary gauges poorly suited to capture flow heterogeneity (Zimmer et al., 2020). In arid regions with already limited water resources, even minor shifts in onset, duration, and distribution of precipitation may have profound implications for ephemeral channel flow and resulting recharge (Fakir et al., 2021). Failure to quantify spatial and temporal patterns of surface flow impedes modeling efforts and water-balance estimates, increasing the likelihood of mismanagement (Döll and Schmied, 2012).

Remote sensing has frequently been used to characterize landscapes, including substantial work in water detection (Alsdorf et al., 2007; Zhou et al., 2017). Common methods include the application of image masks, indices, classification schemes, and proxies to differentiate water pixels from the land surface. These methods however are broadly focused on large, clear water bodies, such as oceans, lakes, and major perennial rivers, which display low, relatively consistent reflectance values over space and time (McFeeters, 1996; Xu, 2006; Feyisa et al., 2014; Fisher et al., 2016). Though interest has increased in recent years, water detection methods developed for open water bodies are poorly suited for water pixel identification within ephemeral channels (Seaton and Mazvimavi, 2020; Maswanganye, 2022). Within these systems, water pixels are frequently mixed, highly turbid, and spatially and temporally inconsistent (Sun

et al., 2012; Tulbure et al., 2016; Borg Galea et al., 2019; Maswanganye, 2022). Common fluvial features such as braided or multi-threaded geomorphology may yield channels too narrow to be resolved at the spatial resolution of common sensors (Levick et al., 2008; Sun et al., 2012). Temporally, ephemeral channels vary greatly, with inundation ranging from a period of hours to days (Levick et al., 2008; Costigan et al., 2017). The limited temporal resolution of publicly available satellites may further fail to capture this variability. Physical properties of arid environments may present challenges, with low topographic gradients and limited vegetation impeding channel delineation (Hamada et al., 2016). Highly turbid flow events may additionally produce high spectral reflectance, reducing contrast between adjacent channel alluvial sediments (Jacobberger et al., 1983; Hamada et al., 2016). Recent work has identified the utility of tailored water pixel detection to specific environments through the use of machine learning algorithms and statistical analyses (Jacobberger et al., 1983; Hamada et al., 2016; Isikdogan et al., 2017). Specific applications include the use of random forest algorithms with satellite-derived variables (TOA bands, NDVI, or common water pixel indices) for water pixel prediction and subsequent mapping (Tulbure et al., 2016; Malinowski et al., 2016; Veh et al., 2018; Chen et al., 2020; Fei et al., 2022). For intermittent systems, this has the potential to improve water pixel classification and identification.

At present, remote sensing analysis of temporary water bodies is minimal and has primarily assessed non-channelized flow, such as generalized flooding, glacial outbursts, or isolated pools (Malinowski et al., 2016; Veh et al., 2018; Seaton and Mazvimavi, 2020; Maswanganye, 2022). Within ephemeral systems, research has focused on the mapping and delineation of channel morphology and connectivity, disregarding fluctuations in inundation (Hamada et al., 2016; Chen et al., 2020; Fei et al., 2022). Across this work, LiDAR is frequently

chosen for high-resolution, spatially focused imagery capable of measuring topographic variation (Hamada et al., 2016; Malinowski et al., 2016). LiDAR scanning however is costly and not readily available, with limited temporal range for trend analysis. Publicly available, passive satellites may be better suited for the assessment of long-term shifts in inundation; imagery is generally available across a longer temporal period, necessary for the evaluation of hydrologic trends (Seaton and Mazvimavi, 2020). Existing research within this area generally struggles with data availability, both temporally and spatially, for the assessment of significant trends at the established 30-year hydrologic reference period (World Meteorological Organization (WMO), 2017). This limits the ability of existing methodologies to quantify statistically significant trends, particularly in intermittent systems which may be experiencing shifting inundation in relation to climate warming.

This research is focused on understanding large-scale hydrologic processes within ungauged basins through the use of remote sensing and a flexible statistical classification. It further explores the application of this remote sensing methodology to quantify streamflow variability within an ungauged, ephemeral channel in central Morocco. This work specifically aims to (1) assess the utility of discriminant function analysis for improved classification of ephemeral channel inundation. In turn, this methodology is applied to (2) quantify the temporal and (3) spatial patterns of flow variability across the Souss channel, an evolving ephemeral system.

Within this study, discriminant function analysis was applied to NASA Landsat imagery (missions 5, 7, and 8) from 1984 to 2022 to develop an optimized water classification scheme based on the unique characteristics of water pixels within ephemeral river systems. Improved water pixel classification was applied to identify patterns of surface flow across upstream,

midstream, and downstream reaches of the channel. Remotely sensed precipitation data (TRMM-TMPA, GPM-IMERG) were applied to validate flood presence. Remote sensing has the potential to resolve data gaps for the past and present characterization of channel intermittency, particularly in data-limited systems. This analysis demonstrates potential in its application to quantify patterns of intermittent surface flow across non-perennial channels, improving management in water-scarce regions.

3.3 Methods

Study Area

The Souss–Massa (27,000 km2) is a semi-arid, highly agricultural basin located in central Morocco (Figure 1) (Bouchaou et al., 2011; Hssaisoune et al., 2016). Bounded by the High-Atlas Mountains to the north and Anti-Atlas Mountains to the south, the Souss channel flows from the Aoulouz reservoir in the foothills to terminate at the Atlantic Ocean. Overall, a gently sloping system, the average stream gradient shifts from 12.2 m/km in the channel upstream to flatten across the midstream and downstream sections (5.7 m/km and 3.1 m/km, respectively). This channel is underlain by alluvial material, primarily gravels, sands, and lacustrine limestones, which comprise a thick Pliocene–Quaternary sequence (Choukr-Allah et al., 2016; Hssaisoune et al., 2019). These sediments contain an unconfined regional aquifer with variable thickness; depth to the water table is shown to increase moving westward and with distance from the channel (Dindane et al., 2003; Ait Brahim et al., 2017). The unconfined aquifer is shallowest adjacent to the Souss, ranging from an average of 10–30 m below the surface (Dindane et al., 2003; Ait Brahim et al., 2017). Historically an ephemeral system, surface flow is seasonal, supported by tributaries originating in the High-Atlas Mountains and precipitation during the wet season from

November–March (Bouchaou et al., 2011; Hssaisoune et al., 2016). Post-1990, discharge has been modulated through releases by the Aoulouz dam, located at the channel headwaters (Bouragba et al., 2011). As a result of flow intermittency and limited infrastructure, data are scarce across the basin. Discharge measurements are restricted to only two gauges located in the upstream and midstream channel sections, with intermittent measurements beginning in 1999 (Bouizrou et al., 2023).

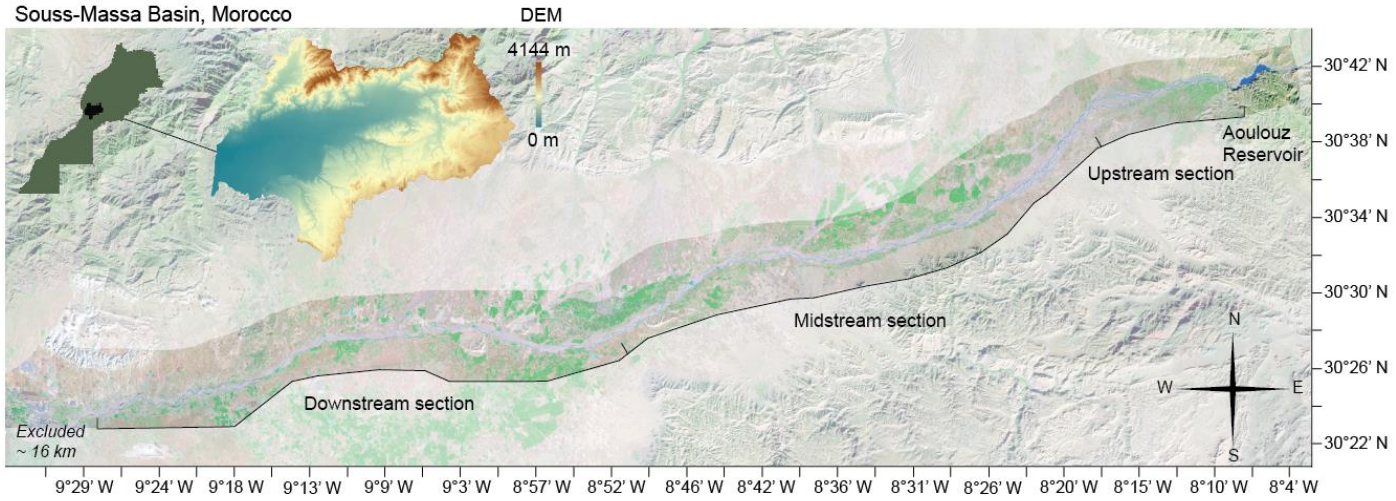

Figure 3-1. The Souss channel, located in central Morocco. The channel is broken into three distinct sections based on basin morphology: upstream, midstream, and downstream. The final 16 km of the downstream section of the channel was excluded from analysis, as the reach from Drarga to the terminus at the Atlantic Ocean experiences rare surface flow and common saltwater intrusion. In the upper left, a DEM of the Souss–Massa basin displays variable elevation, ranging from 4144 m in the channel uplands to 0 m across the downstream section of the plain.

Across this basin, precipitation is heterogenous, with annual averages ranging from 500 mm in the uplands to 250 mm across the plain (Hssaisoune et al., 2019). Decreased precipitation intensity and increased mean annual temperature have been observed in recent decades, with inter-annual variability resulting in a higher frequency of drought (Bouragba et al., 2011; Bouchaou et al., 2011). Despite limited water resources, the Souss–Massa basin relies heavily on irrigation via surface and groundwater pumping to support critical citrus and vegetable exports, accounting for greater than 50% and 85%, respectively, of the national total (Ait Brahim et al., 2017; Almulla et al., 2022). The basin additionally is widely utilized for cereal and almond production (Almulla et al., 2022). Since the 1970s, over-pumping for agriculture, in tandem with reduced precipitation, has driven steady declines in the height of the unconfined Souss aquifer (Ait Brahim et al., 2017). Though surface flow in the channel plays a vital role in supporting regional agriculture, a limited understanding of flow intermittency creates a challenge for sustainable water management.

Data

Using Google Earth Engine, satellite imagery of the Souss channel was acquired from NASA Landsat missions 5, 7, and 8, spanning a combined 38-year period from 1984 to 2022. Top of Atmosphere (TOA) reflectance imagery (Tier 1) was selected, and dark-object subtraction was applied for atmospheric correction (Chavez, 1988). Landsat imagery is available approximately every 16 days; however images were filtered for low cloud cover (less than 5% of the image), reducing the number of available images (Table 3-1). The Souss channel was divided into three sections of varying length corresponding to upstream, midstream, and downstream reaches, delineated on the basis of channel morphology and geographic markers. In particular,

the upstream and midstream sections were separated at a distinct bend in the channel, which is further the approximate location of reduced flow frequency. The midstream and downstream channel sections were delineated at the mid-sized town of Taroudant, which is further correlated to qualitative observations of reduced surface flow (Figure 1). Channel reaches were used to spatially filter imagery to regions of interest (Figure 2). Only images which entirely cover channel sections were selected to avoid edge pixels, which commonly have incomplete band information. An exception, however, was made for the downstream section, with the inclusion of four additional images which only partially cover the section (ranging from 0.69 to 5.11% fewer pixels) to support a more complete time span for Landsat 5 path 203/row 39 (WRS-2). Though the number of images per section is in part an artifact of variable cloud cover, Landsat 5 path 203/row 39 has approximately one-third fewer images collected than path 202/row 39. From visual inspection, the truncated images included were entirely dry and devoid of surface flow. Across all selected imagery, band values were extracted for each pixel in the image (Figure 3). For comparison across bands, each pixel value was converted to a percent range, standardizing the scale of all values from 0 to 1, as demonstrated in Equation (1).

$$\text{Pixel Percent Range} = \frac{(\text{Pixel Value} - \text{Band Minimum})}{(\text{Band Maximum} - \text{Band Minimum})} \qquad (1)$$

Table 3-1. Landsat 5, 7, and 8 satellite information. Across the three satellites, the Panchromatic and Thermal bands (1 and 2) were excluded from linear discriminant function analysis due to their varied spatial resolutions.

Satellite	Filtered Temporal Range	Bands	Range	Resolution
Landsat 5 TM TOA Collection 1, Tier 1	May 1984–September 2011	Band 1: Blue	30 m	0.45–0.52 µm
		Band 2: Green	30 m	0.52–0.60 µm
		Band 3: Red	30 m	0.63–0.69 µm
		Band 4: NIR	30 m	0.76–0.90 µm
		Band 5: SWIR 1	30 m	1.55–1.75 µm
		Band 6: Thermal Infrared	60 m	10.40–12.50 µm
		Band 7: SWIR 2	30 m	2.08–2.35 µm
Landsat 7 TOA Collection 1, Tier 1	October 2011–April 2013	Band 1: Blue	30 m	0.45–0.52 µm
		Band 2: Green	30 m	0.52–0.60 µm
		Band 3: Red	30 m	0.63–0.69 µm
		Band 4: NIR	30 m	0.77–0.90 µm
		Band 5: SWIR 1	30 m	1.55–1.75 µm
		Band 6: Thermal Infrared	60 m	10.40–12.50 µm
		Band 7: SWIR 2	30 m	2.08–2.35 µm
		Band 8: Panchromatic	15 m	0.52–0.90 µm
Landsat 8 TOA Collection 2, Tier 1	April 2013–May 2023	Band 1: Coastal aerosol	30 m	0.43–0.45 µm
		Band 2: Blue	30 m	0.45–0.51 µm
		Band 3: Green	30 m	0.53–0.59 µm
		Band 4: Red	30 m	0.64–0.67 µm
		Band 5: NIR	30 m	0.85–0.88 µm
		Band 6: SWIR 1	30 m	1.57–1.65 µm
		Band 7: SWIR 2	30 m	2.11–2.29 µm
		Band 8: Panchromatic	15 m	0.52–0.90 µm
		Band 9: Cirrus	30 m	1.36–1.38 µm
		Band 10: Thermal Infrared 1	100 m	10.60–11.19 µm
		Band 11: Thermal Infrared 2	100 m	11.50–12.51 µm

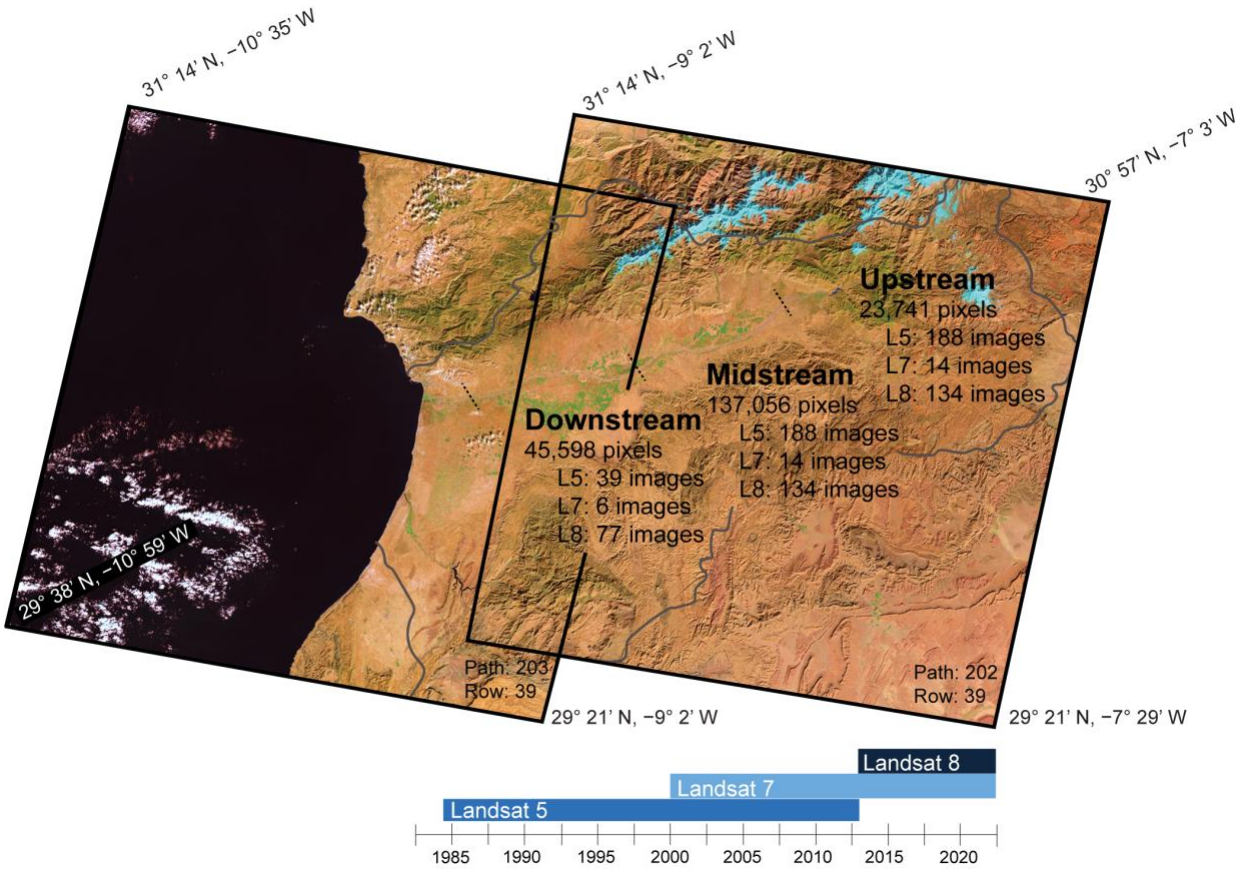

Figure 3-2. Footprint of Landsat imagery within the Souss–Massa basin (outlined in gray). Across the channel, the differing section length translates to a variable number of pixels per section. The upstream and midstream reach both fall within the path 202/row 39 Landsat image, while the downstream stretch falls entirely within the path 203/row 39 image and partially in the path 202/row 39 image (WRS-2).

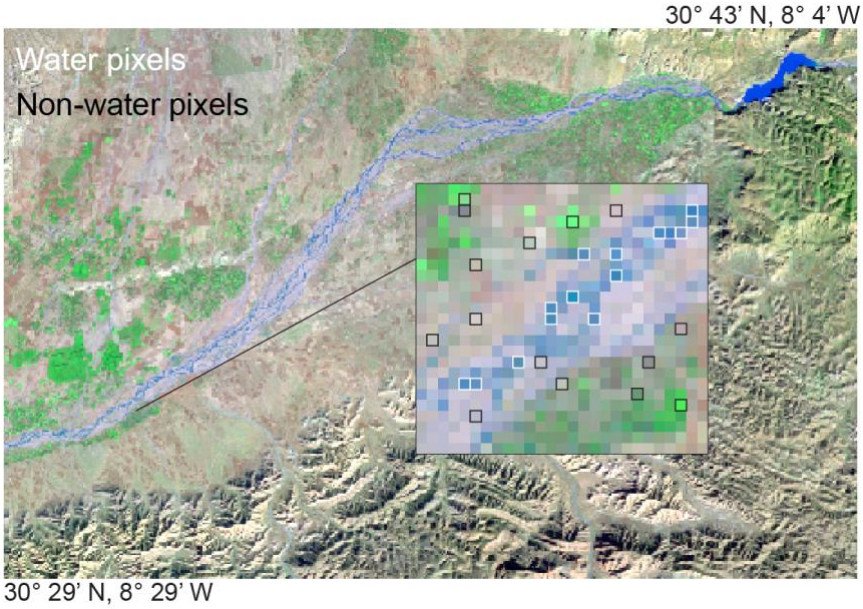

Figure 3-3. Example of water and non-water pixel selection within the training dataset. Pixels outlined in white indicate water, while pixels outlined in black indicate non-water.

Statistical Analysis

Discriminant function analysis is a statistical method used to identify known, categorical groups within unknown, continuous data. For remotely sensed images, this statistical procedure allows for a computationally simple, supervised pixel classification based on a combination of variables. Within ephemeral channels where water pixels do not closely align with those of clear and open water bodies, water pixel identification can be tailored to site-specific reflectance values across multiple bands. Discriminant function analysis provides the advantage of rapid, computationally inexpensive, and flexible classification for binary groups without overfitting, an advantage over similar machine learning classifiers such as decision trees or random forest models. Linear Discriminant Analysis (LDA) generates a linear function which maximizes the distinction between groups, in this study, water and non-water pixels (Davis, 2002). This

function uses the visible and near-infrared bands of each satellite as explanatory variables, producing loadings for each. Larger loadings, positive or negative, identify the bands which have the greatest impact on group determination (Davis, 2002; Maindonald and Braun, 2003). For each pixel within the training dataset, group membership is determined as a classification probability. The predictive accuracy of an LDA is evaluated through a comparison of a pixel's group classification via linear function and its known group membership (Maindonald and Braun, 2003). This is further evaluated using jackknife validation, which generates a predictive accuracy free of resubstitution error (Maindonald and Braun, 2003). When appropriate accuracy has been determined, an LDA is free to be applied to pixels outside of the training dataset, those with unknown group membership.

For Landsat 5 and 8, an image corresponding to a flood event within the midstream section of the ephemeral channel was visually identified in natural color and used to construct a training dataset. Water and non-water pixels were manually selected (1600 pixels per group, 3200 total) for the training dataset (Table A1). The selection prioritized pixels with clear group membership and avoided edge or mixed pixels. Using R Statistical Software (v4.1.1) and the MASS R package (v7.3–60), a separate LDA was then trained for each satellite based on the known pixel values of the training dataset (Venables and Ripley, 2002; R Core Team, 2011). When appropriate predictive accuracy was determined via jackknife validation, the LDA function was applied across all previously identified images for that satellite, predicting group membership for each pixel. This was then translated to a percent of water pixels per image, used to determine whether an image displays inundation or dry conditions.

As the Souss channel is predominantly dry, the majority of images are expected to display water pixel percentages near zero. Flood events represent atypical behavior in this

system, resulting in significantly fewer images with elevated water pixel percentages. Surface flow has qualitatively been observed less frequently with increasing distance from source. Flood events which originate in the upstream section of the channel may extend only partially into midstream and downstream channel reaches, though this spatial variability is poorly understood. Small percentages of water pixels may be identified within images lacking surface flow as a result of either anthropogenic water storage adjacent to the channel or analysis error. Such percentages, however, are expected to be minimal due to the high predictive accuracy of both LDAs.

The cutoff between wet and dry channel conditions was determined via Receiver Operator Characteristic (ROC) curves, calculated for each satellite. Cutoffs aim to maximize the number of true positives, correctly identified flood events, while minimizing false positives. For each satellite, 10% of the evaluated imagery was randomly sampled and visually analyzed for inundation. Random samples maintained the same proportion of channel sections present in the evaluated imagery. ROC curves for each satellite were compared for both percentages and counts of water pixels per image to identify the cutoff value associated with the greatest sensitivity and specificity. Both percentage and counts were included to explore a greater number of classification thresholds in the random subsample. For Landsat 5, images with greater than 0.55% water pixels were determined to represent flood conditions within the channel (TPR = 0.85, FPR = 0.18). For Landsat 8, images with more than 1200 pixels were identified as flood conditions (TPR = 0.71, FPR = 0.24) (Figure 4).

The Landsat 7 satellite sustained a failure in its scan line corrector in mid-2003, resulting in a scan line error and artifact within the subsequent imagery. As a result, the number of pixels per image was reduced by approximately 20% (Andrefouet et al., 2003). This artifact further

significantly increased the number of edge pixels per image, pixels in which one or more bands lack a value. Due to these errors, use of Landsat 7 imagery was minimized to only the temporal period not covered by Landsat 5 and Landsat 8, December 2011 through April 2013. As a result, the small number of available images eliminates the need for automated image classification and instead enables visual analysis of flood presence. Additionally, the inconsistent exclusion of band values within the edge pixels is poorly suited for LDA construction and application, as this method assumes an equal number of variables within all cases.

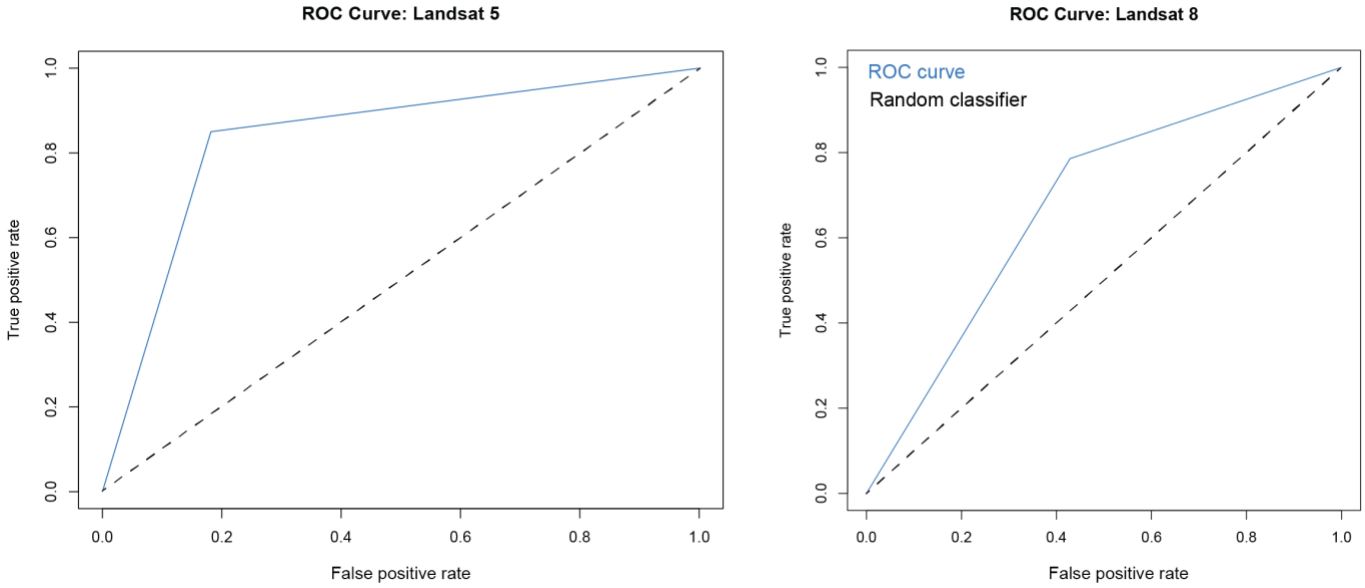

Figure 3-4. ROC curves for Landsat 5 and Landsat 8 flood cutoffs. ROC curves for both counts and water pixel percentages were compared for each satellite. For all satellites, the majority of images have water pixel values which cluster near zero percent. This is consistent with our understanding of a default dry channel, with intermittent periods of surface flow.

Validation

Within the Souss–Massa basin, precipitation gauging is limited and temporally variable. Gauges are further poorly spatially distributed and concentrated in the midstream and downstream sections of the channel, despite higher precipitation in channel uplands (Bouizrou et al., 2023). Due to its ephemeral nature, antecedent precipitation is considered necessary for surface flow within the Souss basin. Satellite-based precipitation estimates thus may serve as a tool to validate flood presence. NASA and JAXA TRMM-TMPA (Daily Accumulated Precipitation, TRMM-3B42 V7) and GPM-IMERG (Daily Accumulated Precipitation—Final Run V06) products were used for validation of channel inundation from January 1998 through August 2021. Estimates from the TRMM-TMPA satellite were used from 1998 to 1999, while 2000 to 2021 utilizes the GPM-IMERG algorithm which fuses TRMM and GPM estimates across the overlap period from 2000 to 2015. Precipitation estimates were aggregated into a cumulative total precipitation across the seven-day period prior to a satellite image. Estimates of less than 10 mm per seven-day period were excluded, as previous work has identified elevated error in estimation of light precipitation events, including false precipitation (Tian et al., 2009).

The utility of the TRMM product for precipitation estimates across Morocco has demonstrated accuracy at elevations less than 1000 m (Milewski et al., 2015; Tramblay et al., 2016). This is in line with global observations of reduced estimate accuracy over variable topography. Within the Souss–Massa basin, TRMM-TMPA was found to provide accurate estimates of daily precipitation, outperforming similar precipitation estimates (CHIRPS, and PERSIANN) when compared to in situ measurements (Bouizrou et al., 2023). Precipitation estimates were further improved with the launch of the GPM satellite in 2014, equipped with a dual-frequency precipitation radar capable of better distinguishing the light precipitation events

characteristic of arid environments (Saouabe et al., 2020). Evaluation of GPM estimate accuracy in a mountainous Moroccan basin found strong agreement with observed precipitation, improved in lower elevation sections of the basin (Saouabe et al., 2020). Though GPM-IMERG Final Run is regarded as a research-level product, it is important to note the potential for introduced biases from retrospective processing (Tang et al., 2020). Research focused on the resampled period (2000–2015), however, found suitable accuracy at the daily scale, with increased accuracy moving from 2001 to 2018 through the addition of passive microwave samples (Tang et al., 2020). Studies in arid environments further indicate GPM-IMERG Final Run suitability for precipitation estimates (Shawky et al., 2019).

Following flood validation, Mann–Kendall trend analysis was applied to identify statistically significant monotonic trends in flood events across the time period. Trend analysis was explored at monthly, seasonal, and annual flood occurrence aggregations across individual and grouped channel sections.

3.4 Results

LDA Training

The Landsat 5 LDA was trained on the midstream section of a flood image from 30 September 1997 (Figure 5). This LDA has high predictive accuracy when applied to the training dataset, with 100% accuracy in group classification with and without jackknife validation (Table 2). The resulting LDA demonstrates similar classification success when applied to unknown pixels in images with and without channel flooding (Table 2). Plotted, this LDA supports distinct group classification without overlap, with loadings that indicate that the Red (0.63–0.69 μm) and

SWIR 2 (2.08–2.35 μm) bands have the greatest influence on the linear function (Table 3-3) (Figure 3-6)

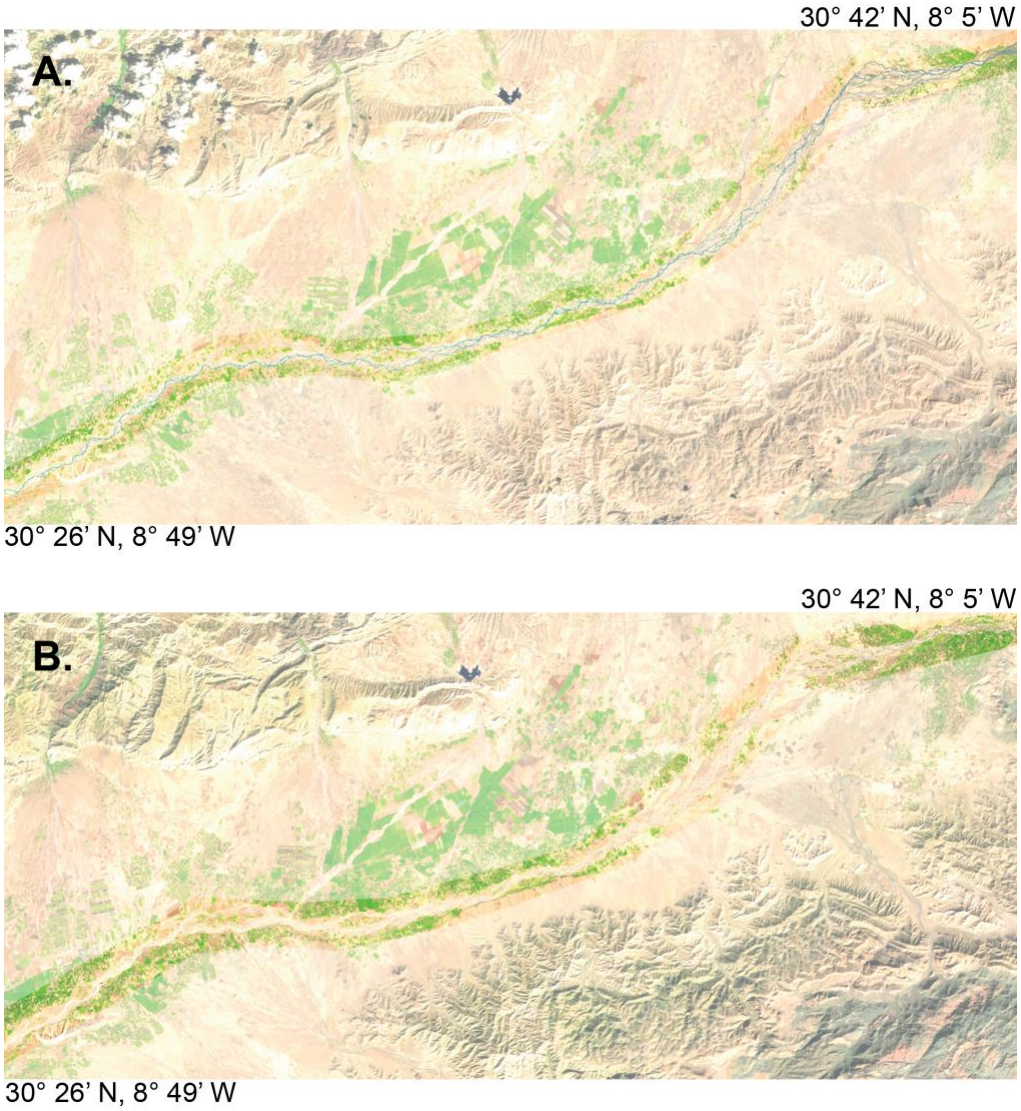

Figure 3-5. (A) Landsat 5 image of a midstream channel flood, 30 September 1997. (B) Landsat 5 image of midstream channel without surface flow, 17 November 1997.

Table 3-2. Predictive accuracies calculated for the training dataset used to construct the LDA. Both achieve 100% accuracy in classifying test pixels correctly into the two groups. Classification was then tested on unknown pixels within a flood and non-flood image in the midstream channel region. The classifier correctly infers a much greater number of water pixels (5.80% vs. 0.20%) in the flood image.

Landsat 5 LDA		**Training Pixels**	**Predictive Accuracy**	**Jackknife Predictive Accuracy**
Training Dataset	Water pixels	1600	100%	100%
Flood Image 30 September 1997	Non-water pixels	1600	100%	100%
Test Classification		**Pixels per Image**	**Predicted Water pixels**	**Predicted Non-water pixels**
Flood Image Midstream 30 September 1997		137,056 pixels	7956 pixels (5.80%)	129,100 pixels (94.20%)
Non-flood Image Midstream 17 November 1997		137,056 pixels	271 pixels (0.20%)	136,785 pixels (99.80%)

Table 3-3. Landsat 5 LDA loadings. Bolded values signify bands which have the greatest contribution.

Bands	**Loadings**
Blue	−2.64
Green	3.38
Red	**10.28**
NIR	−4.44
SWIR 1	−5.32
SWIR 2	**−9.61**

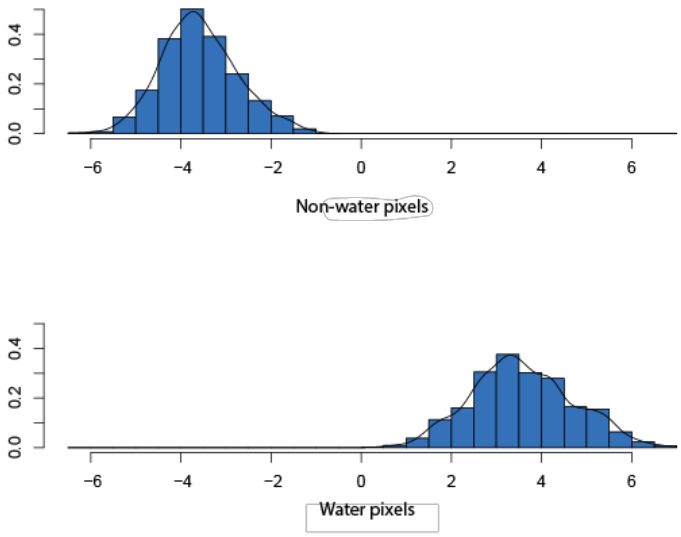

Figure 3-6**.** Graphical distribution of Landsat 5 discriminant function analysis for water vs. non-water pixels. Lack of overlap, as well as tight within-group pixel distribution indicates strong group separation and a successful LDA.

The Landsat 8 LDA was constructed using a midstream flood image from 7 December 2016 (Figure 3-7). High predictive accuracy was achieved with the training dataset, yielding a 98.13% and 98.75% accuracy for the water and non-water pixels, respectively (Table 3-4). This LDA demonstrates successful group classification with minimal overlap, with loadings which identify the Blue (0.45–0.51 µm) and Coastal aerosol bands (0.43–0.45 µm) as most significant to the discriminant function (Table 3-5) (Figure 3-8). Application to unknown pixels within flood and non-flood images (12 July 2016 and 16 July 2016, respectively) align with these observations; water pixels are predicted to comprise 11.68% of the flood image and 0.71% of the non-flood image (Figure 3-7) (Table 3-4).

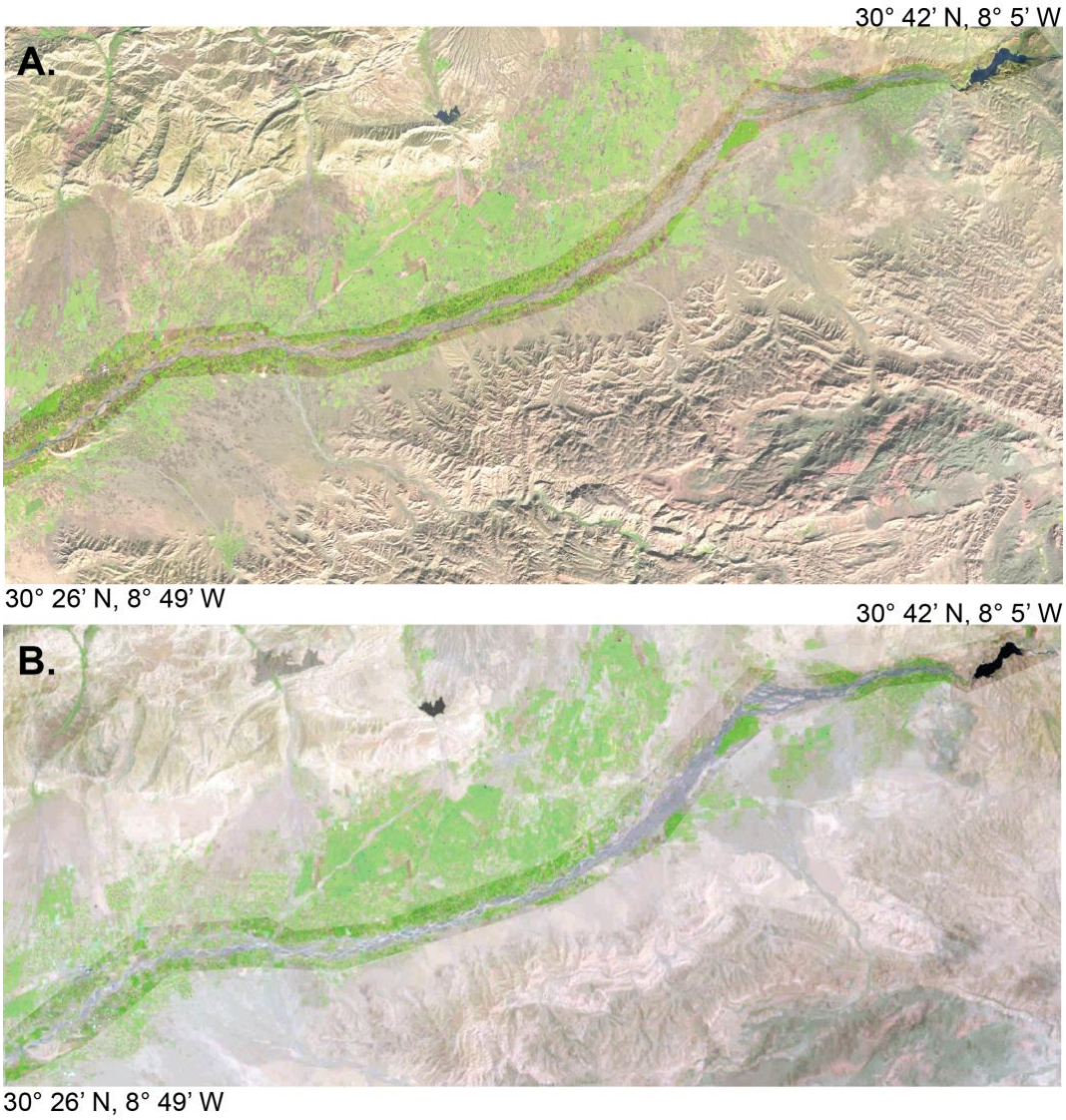

Figure 3-7. (A) Landsat 8 image of a channel flood across the midstream section, 7 December 2016. (B) Landsat 8 image without surface flow, midstream section, 16 July 2016. Images were used for testing LDA classification on unknown pixels.

Table 3-4. Predictive accuracies calculated for the training dataset of the Landsat 8 DFA. Both achieve near 100% accuracy in classifying the pixels correctly into the two groups. Classification testing of water pixel predictions for flood vs. non-flood images successfully identified higher water pixel percentages with known water presence (11.68% vs. 0.71%).

Landsat 8 LDA		**Training Pixels**	**Predictive Accuracy**	**Jackknife Predictive Accuracy**
Training Dataset	Water pixels	1600	98.13%	98.13%
Flood Image: 12 July 2016	Non-water pixels	1600	98.75%	98.69%
Test Classification		Pixels per Image	Predicted Water pixels	Predicted Non-water pixels
Flood Image Midstream, 12 July 2016		137,056 pixels	16,014 pixels (11.68%)	88.32%
Non-flood Image Midstream, 16 July 2016		137,056 pixels	970 pixels (0.71%)	99.29%

Table 3-5. Landsat 8 LDA loadings. Bolded values signify bands with the greatest contribution.

Bands	**Loadings**
Coastal aerosol	**38.19**
Blue	**−44.28**
Green	8.01
Red	−2.25
NIR	7.25
SWIR 1	−10.63
SWIR 2	11.37
Cirrus	−1.76

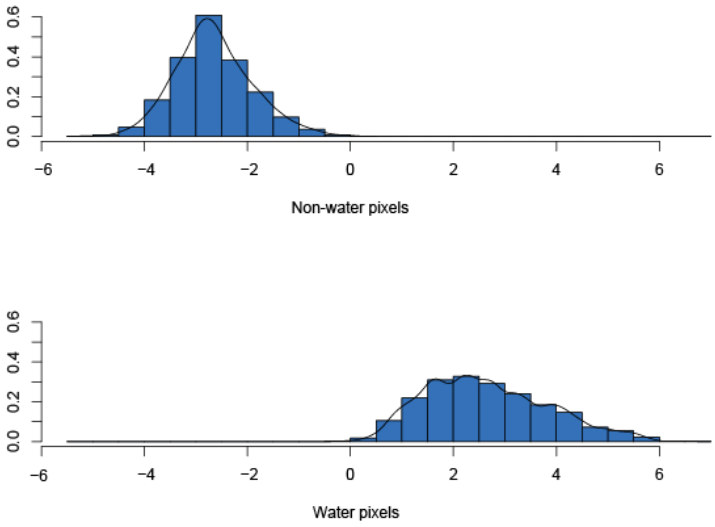

Figure 3-8. Graphical depiction of group classification for Landsat 8 LDA, indicating successful delineation with minimal overlap.

Due to the scan line artifact and minimal imagery spanning from December 2011 through April 2013, Landsat 7 imagery was visually analyzed. With only 14 images in the upstream and midstream sections, respectively, and six images in the downstream section, only one upstream image displayed channel surface flow (26 March 2013). This Landsat 7 flood image was assigned a value of 5.01% water pixels, the average water pixel percent for Landsat 5 and Landsat 8 upstream flood imagery.

Modified NDWI Comparison

Predictions from the LDA pixel classifications were compared to a widely accepted and commonly used classification index, the Modified Normalized Difference Water Index (modified NDWI) (Xu, 2006). Developed to minimize built-up land noise in water pixel extraction, the

modified NDWI has proven successful in open water delineation through the use of the SWIR and green bands (Xu, 2006). It has been further shown to effectively identify turbid water bodies, a feature particularly suited to ephemeral channels (Xu, 2006). The modified NDWI was applied to the Landsat 5 and 8 LDA training datasets, as well as flood and non-flood test imagery. Using the commonly applied threshold of zero, positive values are characterized as water pixels, while zero and negative values are considered land (Xu, 2006). Across both the Landsat 5 and 8 LDAs, the modified NDWI proved to be less sensitive in its identification of water pixels, misclassifying 9.38% (Landsat 5) and 98.06% (Landsat 8) of the training dataset's water pixels as non-water (Table 3-6). In contrast, the index had high accuracy in identification of non-water pixels, with 100% (Landsat 5) and 99.94% (Landsat 8) non-water pixels correctly classified. For both satellites, the modified NDWI leaned heavily toward over classification of land pixels while failing to identify observed water. This further supports our concern that commonly utilized water classification indices may be poor classifiers of the water features within ephemeral channels, failing to accurately quantify water presence in these systems.

Table 3-6. Comparison of Landsat 5 and 8 LDA classifications to modified NDWI.

		Modified NDWI		LDA	
		Water Pixels	**Non-Water Pixels**	**Water Pixels**	**Non-Water Pixels**
Landsat 5	Training dataset, Water pixels 30 September 1997	1450	150	1600	0
	Training dataset, Non-water pixels 30 September 1997	0	1600	0	1600
	Flood Image, 30 September 1997	2647 (1.93%)	134,409 (98.07%)	7956 (5.80%)	129,100 (94.20%)
	Non-flood Image, 17 November 1997	3 (0.002%)	137,053 (99.99%)	271 (0.20%)	136,785 (99.80%)
Landsat 8	Training Dataset, Water pixels 12 July 2016	31	1569	1570	30
	Training Dataset, Non-water pixels 12 July 2016	1	1599	20	1580
	Flood Image, 12 July 2016	90 (0.07%)	136,966 (99.93%)	16,014 (11.68%)	121,042 (88.32%)
	Non-flood Image, 16 July 2016	0 (0%)	137,056 (100%)	970 (0.71%)	136,086 (99.29%)

Validation

For images correlated to the period of TRMM-TMPA and GPM-IMERG estimates, flood presence as identified by ROC curve cutoff values (>0.55% water pixels for Landsat 5, >1200 water pixels for Landsat 8) was validated through combined precipitation estimates of 10 mm or greater for the preceding seven-day period (Appendix Chapter 3, Figure 1). Results indicate a higher number of non-precipitation-validated floods further upstream in the channel, with the number of precipitation-validated events increasing moving further downstream (Table 3-7) (Figure 3-9). As the Souss channel is an ephemeral system supported by surface runoff and experiencing transmission losses, increased distance from the headwaters would be expected to correlate with an increase in precipitation-linked flow. Surface flow is further frequently observed in the upstream section of the channel, likely supported by precipitation and runoff in

the adjacent mountain block, and less tied to precipitation adjacent to the channel. Orographic precipitation may not directly translate to precipitation (and thus satellite estimates) on the plain. This may additionally highlight increased error in satellite precipitation estimates with increasing elevation (Shawky et al., 2019). Several minor tributary channels originating in the adjacent mountain block may further be supported by this precipitation, with confluences in the midstream and downstream sections contributing to non-precipitation-validated flow. In addition, dam installation at the channel headwaters post-1990 has resulted in infrequent dam releases uncorrelated to precipitation. Dam releases may produce limited surface flow in the channel upstream and midstream sections, and account for instances of non-precipitation-validated flow.

Across the three channel sections, a cumulative 336 upstream, 336 midstream, and 122 downstream images were evaluated, spanning from 1984 through 2023. Of these images, 43.88% percent were identified as containing channel surface flow, while 56.17% represent dry conditions. Separated by section, the highest frequency of surface flow is observed within the upstream channel (50.28%), which is consistent with visual observation. The midstream and downstream sections demonstrate notably fewer flood events (33.62%, 16.09%), with the least occurring downstream (Table 3-8).

Table 3-7. Validation of flood presence through prior precipitation, separated by channel section.

	Precipitation-Validated Flood	Non-Precipitation-Validated Flood
Upstream	43 (50.59%)	42 (49.41%)
Midstream	36 (54.55%)	30 (45.45%)
Downstream	37 (80.43%)	9 (19.57%)

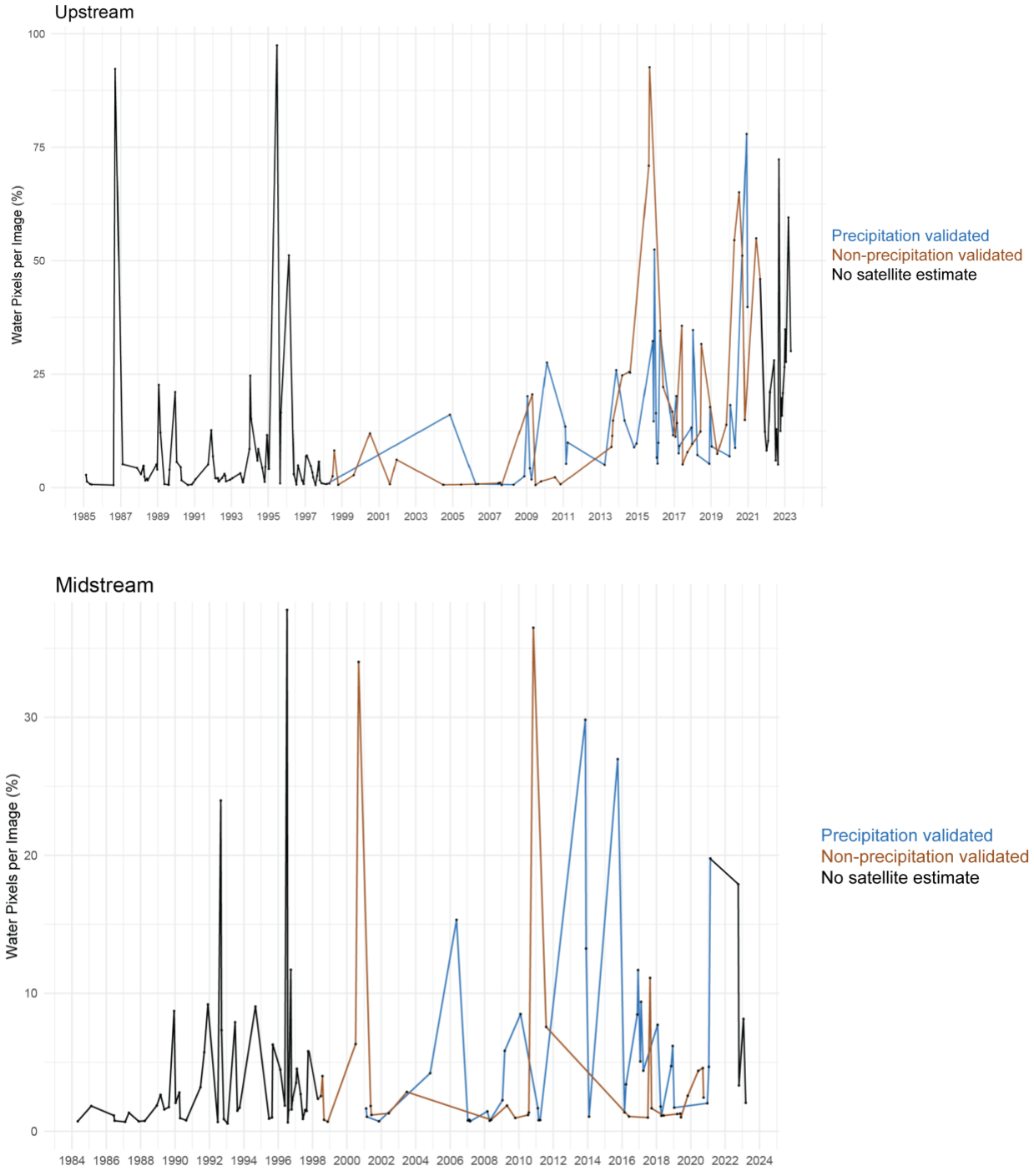

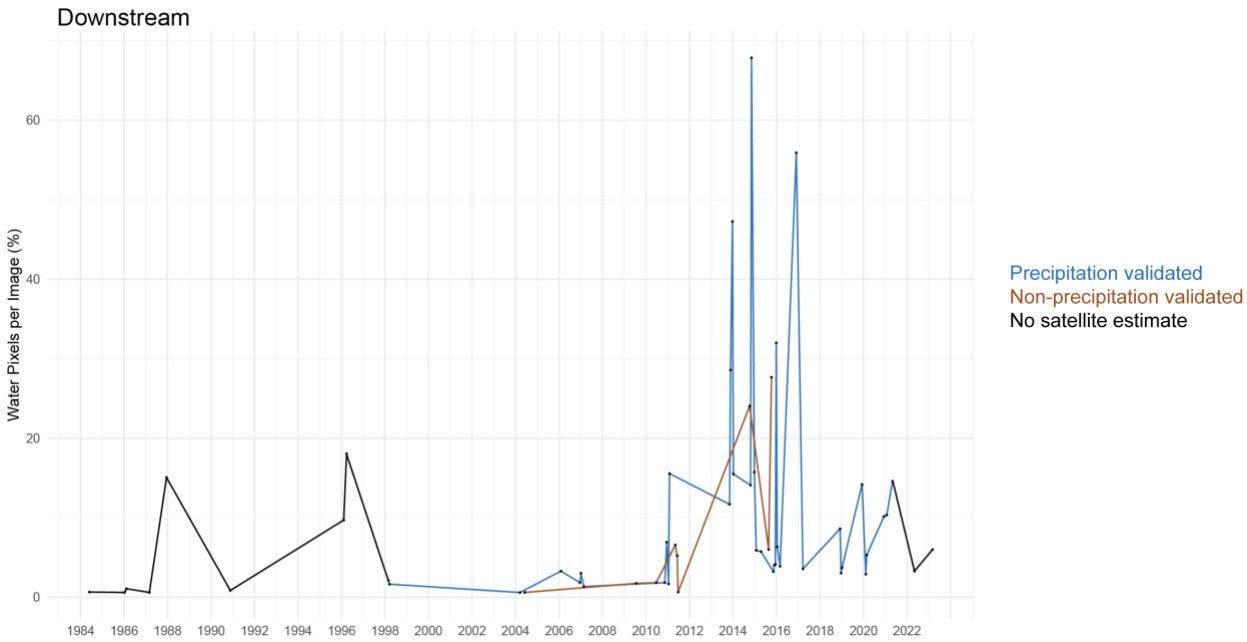

Figure 3-9. Flood events across the observation period, separated by channel section and satellite precipitation validation. Periods in black indicate events which fall outside the range of available TRMM-TMPA and GPM-IMERG estimates. The majority of non-precipitation-validated events (blue) are observed in the upstream section of the channel, decreasing further downstream. This is consistent with runoff patterns which support flow within an ephemeral system.

Flood Assessment

Across the three channel sections, a cumulative 336 upstream, 336 midstream, and 122 downstream images were evaluated, spanning from 1984 through 2023. Of these images, 43.88% percent were identified as containing channel surface flow, while 56.17% represent dry conditions. Separated by section, the highest frequency of surface flow is observed within the upstream channel (50.28%), which is consistent with visual observation. The midstream and

downstream sections demonstrate notably fewer flood events (33.62%, 16.09%), with the least occurring downstream (Table 3-8).

Table 3-8. Flood event frequency across channel sections and satellite images.

	Landsat 5	Landsat 7	Landsat 8	Total
Upstream	103	1 (0.57%)	71	175 (50.28%)
Midstream	81	0 (0%)	36	117 (33.62%)
Downstream	25	0 (0%)	31	56 (16.09%)
Total	209	1	138	

Temporal Variability

Across the observation period, the temporal frequency of flood events remained relatively consistent, with surface flow representing a sporadic, but regular event within the Souss channel (Figure 3-10). From 1998 to 2008, however, a period of reduced flow frequency was observed across all channel sections. Evaluation of seasonal patterns of channel inundation further highlight the overall reduction in both wet and dry season events during this period (Figure 3-11). This is consistent with significant droughts, which occurred from 1998 to 2001, 2005, and in 2007 (Verner et al., 2018). Pre-1998, dry season flood events are observed as a significant proportion of all channel inundation. Post-2008, however, the contribution of dry season events decreases, while wet season floods increase in overall occurrence.

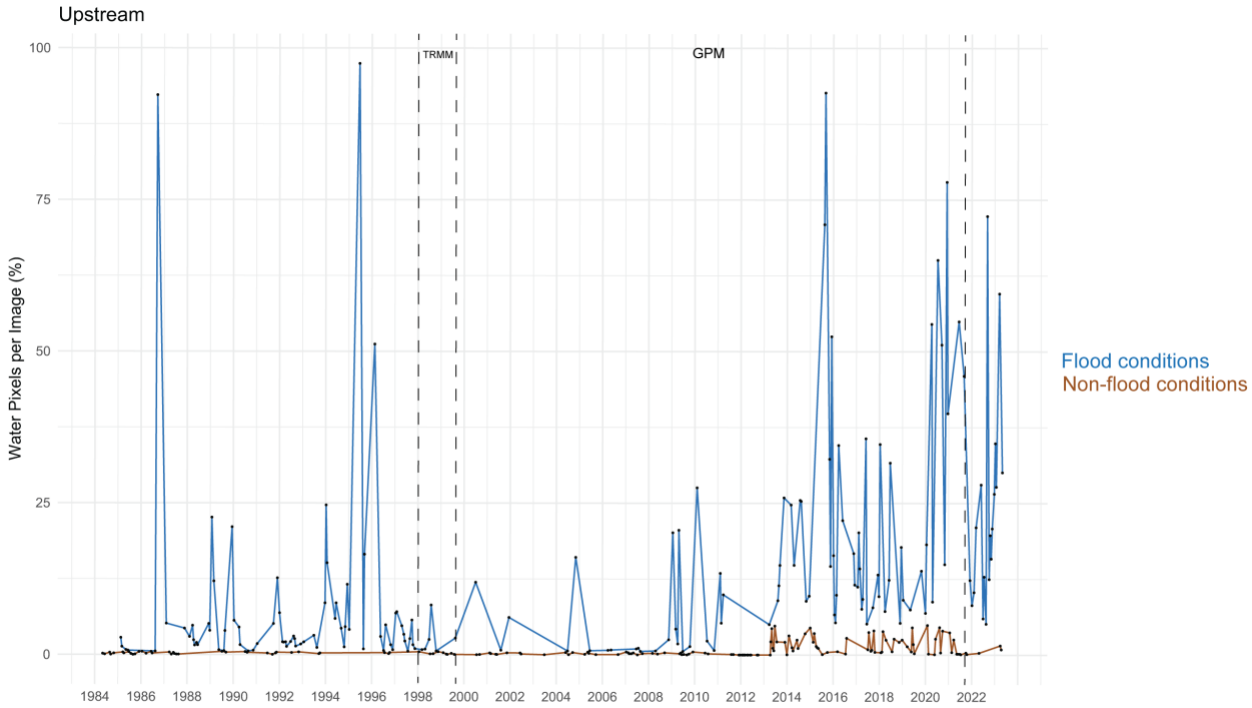
Upstream
TRMM
GPM
Water Pixels per Image (%)
100
75
50
25
0
1984
1986
1988
1990
1992
1994
1996
1998
2000
2002
2004
2006
2008
2010
2012
2014
2016
2018
2020
2022
Flood conditions
Non-flood conditions

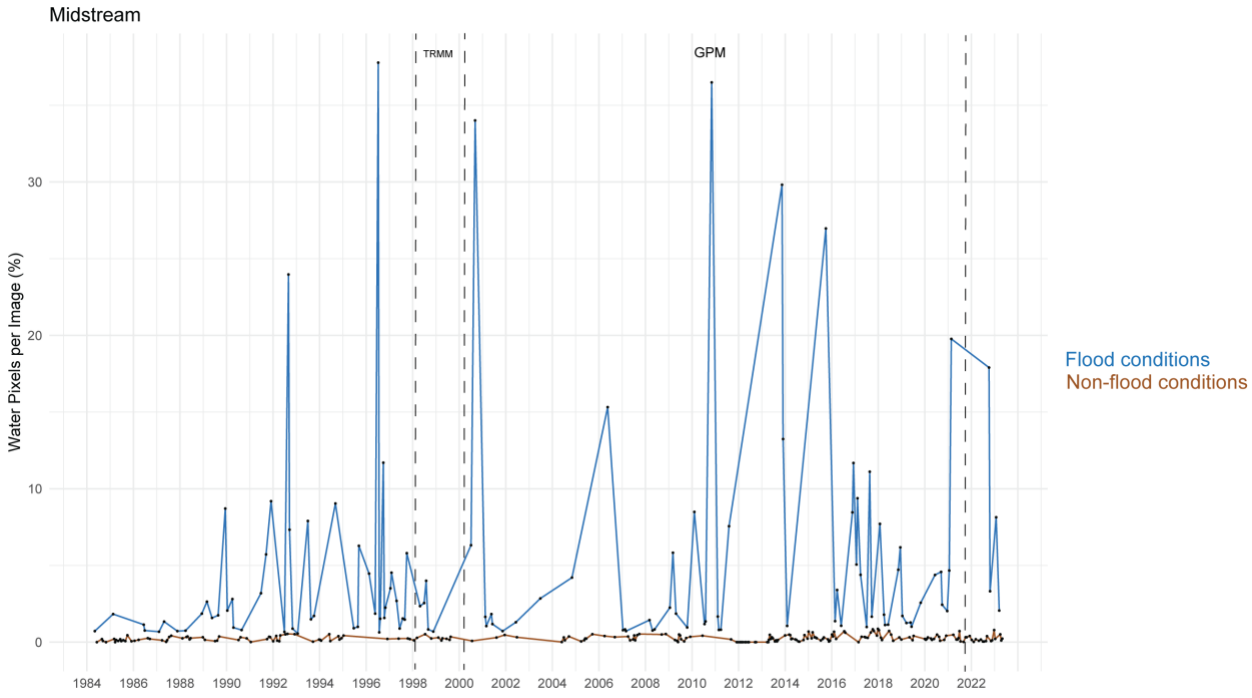
Midstream
TRMM
GPM
Water Pixels per Image (%)
30
20
10
0
1984
1986
1988
1990
1992
1994
1996
1998
2000
2002
2004
2006
2008
2010
2012
2014
2016
2018
2020
2022
Flood conditions
Non-flood conditions

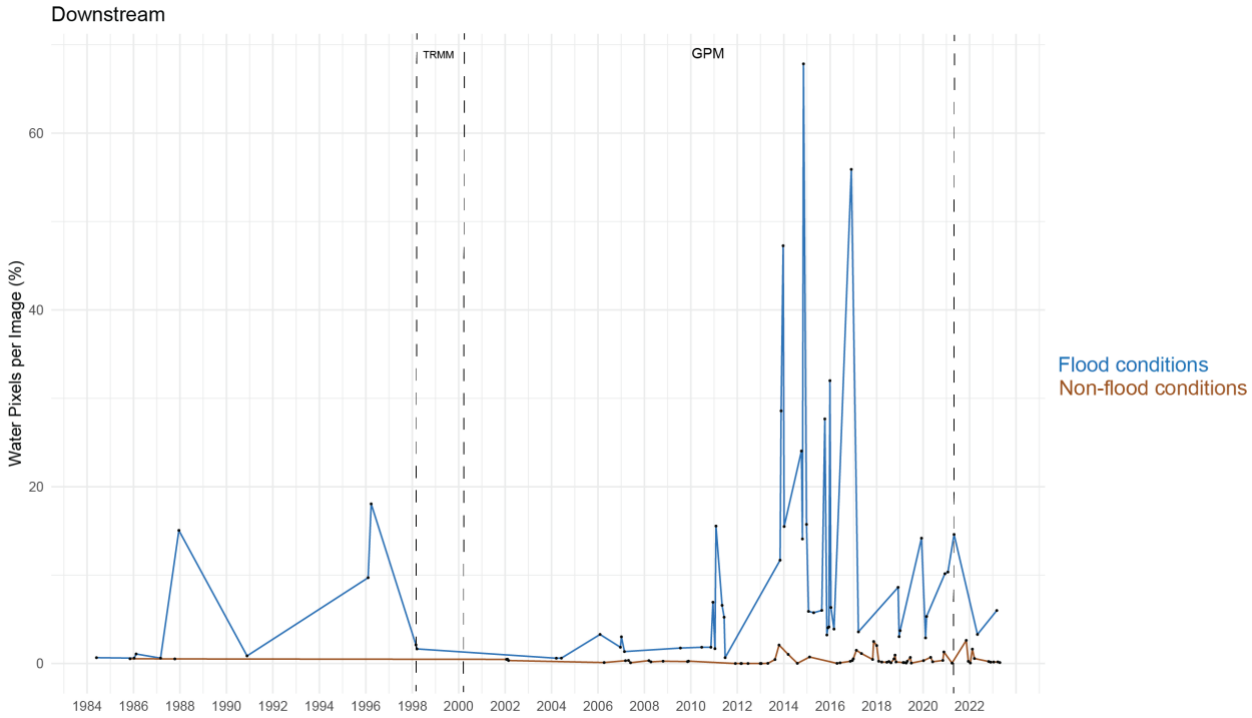

Figure 3-10. Flood frequency across the observation period, separated by channel section. Events are delineated as flood (blue) or non-flood conditions (brown). Monotonic trends in water pixels per image for flood events across the period are not observed.

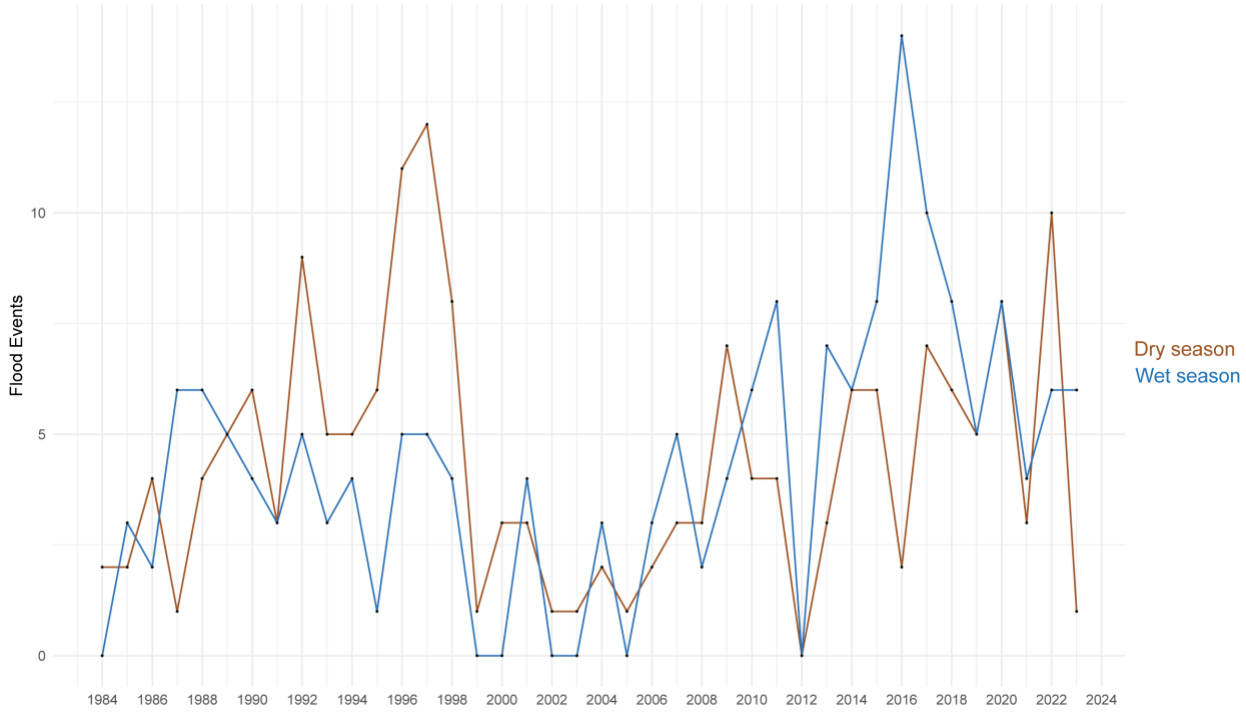

Figure 3-11. Seasonal flood frequency across the observation period. From 1984 to 2023, the dominant season of flood contribution shifts from the dry season (April–October) to the wet season (November–March). This shift begins to occur in 2001, correlated with the same period of reduced channel flooding from 2001 to 2008.

Mann–Kendall trend analysis was applied to assess monotonic trends in the number of flood events from 1984 through 2023 (Table 3-9) (Figure 3-12). With flood occurrence aggregated annually, Mann–Kendall analysis identified statistically significant (i.e., non-zero) positive trends in flood events across the observation period for a combination of all three sections, and the downstream section individually. For non-flood events, statistically significant positive trends were observed for all channel sections, both grouped and individually. It further identified a statistically significant positive trend in the number of flood events across all

sections when aggregated monthly, and for the wet season specifically. No statistically significant trend, either positive or negative, was observed for flood events during the dry seasons. For non-flood events, a statistically significant positive trend in the number of flood events was found when aggregated monthly, and for both wet and dry seasons.

Table 3-9. Mann–Kendall trend analysis.

Aggregation	All Channel Sections	Upstream	Midstream	Downstream
Annual Flood events	**tau = 0.234** ***p* = 0.0403**	tau = 0.143 *p* = 0.2134	tau = 0.0703 *p* = 0.5539	**tau = 0.347** ***p* = 0.0043**
Annual Non-flood events	**tau = 0.335** ***p* = 0.0029**	**tau = 0.279** ***p* = 0.0163**	**tau = 0.231** ***p* = 0.0436**	**tau = 0.59** ***p* = 1.0729e-06**
Wet Season Flood Events	**tau = 0.302** ***p* = 0.0089**			
Wet Season Non- flood events	**tau = 0.457** ***p* = 0.0002**			
Dry Season Flood events	tau = 0.0753 *p* = 0.5181			
Dry Season Non-flood events	**tau = 0.254** ***p* = 0.0293**			
Monthly Flood events	**tau = 0.222** ***p* =< 2.22 × 10^{-16}**			
Monthly Non-flood events	**tau = 0.227** ***p* =< 2.22 × 10^{-16}**			

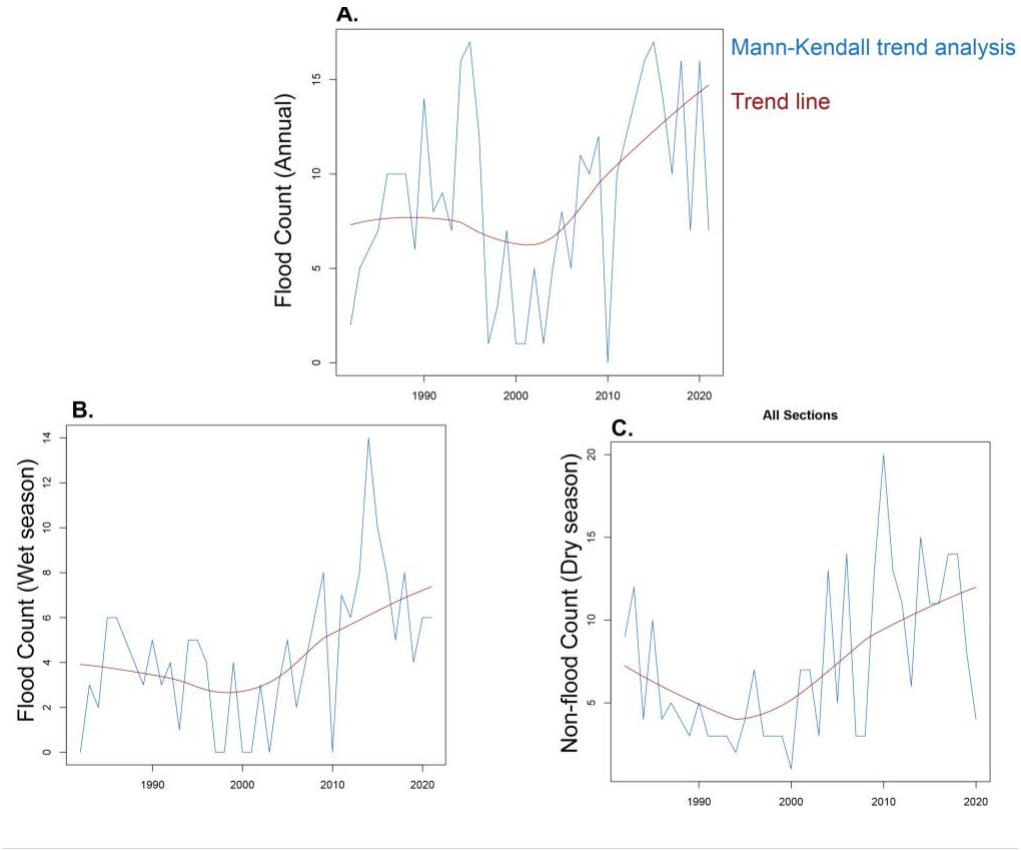

Figure 3-12. Mann–Kendall trend analysis. Aggregations vary, however each represents analysis of all three channel sections. (A) Annual aggregation for all flood events. (B) Wet season aggregation for all flood events. (C) Dry season aggregation for non-flood events.

Spatial Variability

Due to the twice-monthly return of the Landsat satellites, quantifying the spatial connectivity of surface flow for a specific inundation event is challenging via satellite imagery. The assessment of larger trends in the spatial variability of flood events across the Souss upstream, midstream, and downstream sections, however, demonstrates a decreased frequency of inundation moving downstream (Table 3-10) (Appendix Chapter 3, Figure 2). This is consistent with visual observation, in which flow rarely extends to downstream reaches and instead

fluctuates between upstream and midstream sections. It is further logical within an arid, ephemeral system, in which surface water is lost to evapotranspiration and transmission losses. Across the observation period, occurrence of flood events within the downstream section of the channel is observed to increase following 2004, in tandem with the previously observed increased frequency of wet season inundation events (Figure 3-12). Across the wet season, flood frequency is observed as relatively balanced across the midstream and downstream channel sections, with approximately half of all events occurring within the upstream section (Table 3-10). In contrast, however, the proportion of flood events occurring within the downstream section drops significantly during the dry season, shifting from 24.28% to only 8.00% of all flood events. The upstream section continues to represent approximately half of all events during this season.

Table 3-10. Spatial distribution of flood events by season.

Season	Upstream	Midstream	Downstream
Wet	81 (46.8%)	50 (28.90%)	42 (24.28%)
Dry	94 (53.71%)	67 (38.29%)	14 (8.00%)

3.5 Discussion

LDA Classification

Commonly used water classification indices are broadly tailored to identify clear, consistent, open water bodies, the antithesis of the shallow, turbid, and temporal pixels observed within ephemeral channels. As a result, the application of these indices for the assessment of surface water presence within intermittent systems may fail to capture the reality of flow within the channel. The high predictive accuracy of linear discriminant function analysis (LDA) when applied to both the Landsat 5 and Landsat 8 imagery presents a novel solution to this challenge. As a highly flexible and exploratory statistical method, LDA classification allows for tailoring to site-specific features, both spectral and physical. Within the Souss basin, the Red and SWIR 2 bands (Landsat 5), and Blue and Coastal aerosol bands (Landsat 8) were identified as key parameters in the distinction between water and non-water pixels for each group of satellite imagery. For Landsat 5, identification of the Red band may highlight the relevance of bare soil, a dominant component of a landscape with minimal vegetation. The SWIR 2 band has previously been identified as effectively distinguishing water from the landscape, particularly adjacent agricultural fields. For Landsat 8, the Blue band is commonly associated with the reflectance of surface water, while the Coastal aerosol band may capture heavily turbid water pixels, a key characteristic of ephemeral systems like the Souss. Though these bands have been identified as the dominant contributors to their respective LDAs, it is important to recognize that the remaining five bands additionally play an important role in the linear function.

The overall poor performance of the modified NDWI confirms the previous intuition that existing classifiers may be poorly suited to ephemeral and intermittent systems. The modified NDWI index utilizes the Green and SWIR 1 bands, both of which did not appear as primary

factors in differentiating water and non-water pixels in this channel. Of the loadings for each LDA, the Green band ranked fifth (both for Landsat 5 and 8) and the SWIR 1 band ranking third and fourth (Landsat 5 and Landsat 8, respectively). This may indicate the minimized significance of vegetation and soil moisture when differentiating surface water presence in this system. For the Green band, this is somewhat intuitive within an arid basin like the Souss–Massa, where riparian vegetation is minimal. SWIR 1 reflectance, however, is understood to increase with drier soil, a common feature in this basin. Interestingly, the mid-ranking of the SWIR 1 band for both LDAs indicates that this band likely does play some role, though is not the dominant factor, in distinguishing water and non-water pixels.

Optimizing water classification schemes is critical for improved estimates of large-scale hydrologic processes within data-scarce environments. This is specifically relevant in ephemeral systems, where improved understanding of surface flow directly informs estimates of transmission loss, groundwater storage, and shifting flow patterns as a result of climate and anthropogenic influence. With minimal gauging, remotely sensed imagery and precipitation estimates are the primary means of understanding the variability of these hydrologic processes across time. Satellite imagery, however, does present specific challenges to time-series analysis. The infrequent, bi-monthly return of Landsat imagery, paired with filtering for cloud cover and image quality, significantly reduces the number of images available for analysis. The offset image collection dates for the upstream–midstream channel sections and the downstream section further make it difficult to track the progression of an individual flood event within the system. Instead, the analysis of patterns of surface water within the Souss is forced to focus more broadly on temporal and spatial shifts in flow across the time period. The spatial resolution of Landsat pixels may further fail to capture variations in braided flow commonly observed in the Souss and

other ephemeral systems. Spatial resolution may lack the detail necessary to distinguish the shifting fluvial geomorphology of a system, resulting in mixed pixels. Additional physical features of the landscape and riparian vegetation may result in shadowing; however, impacts are likely minimized within similarly arid systems which are frequently topographically uniform and vegetation sparse.

The use of satellite precipitation estimates for validation presents additional challenges, particularly with spatial resolution. TRMM-TMPA (0.25° × 0.25°) and GPM-IMERG (0.1° × 0.1°) grid cells are significantly coarser than Landsat pixels and further aggregated to an average precipitation upstream of the channel section of interest. Estimates may fail to capture the spatial heterogeneity of precipitation across the basin. TRMM-TMPA and GPM-IMERG have further demonstrated varied estimation accuracy with elevation and aridity, factors which may introduce error into precipitation estimates for the Souss (Milewski et al., 2015). Additionally, from 2000 to 2021, precipitation estimates are derived from fusion of TRMM-TMPA and GPM-IMERG, retrospective processing which may introduce an additional layer of error for estimates over this period (Tian et al., 2009). Despite these considerations, remotely sensed precipitation estimates are an effective comparative tool for the assessment of precipitation-driven ephemeral channel flow. Results from this work identify the increasing percentage of precipitation-validated flood events moving downstream within the channel (upstream = 5.59%, midstream = 54.55%, downstream = 80.43%). This is in line with the previous understanding of regional flow processes, in which channel flow is predominantly derived from precipitation and surface runoff. As the ephemeral system moves downstream, an increasing proportion of surface water is hypothesized to be transferred to the subsurface via transmission losses. To support flow in the downstream section, an increasing input of precipitation is needed. The upstream section of the

basin may additionally derive runoff form the adjacent mountain block, resulting in the reduced need for prior precipitation adjacent to the channel.

Temporal and Spatial Variability

The optimized LDA classification was applied to the Souss channel to analyze temporal and spatial patterns of flow intermittency. Mann–Kendall analysis initially identified a positive trend in the number of flood events when aggregated annually, monthly, and by wet season. This trend, however, is identifying the increase in available imagery for the Landsat 8 period. For this study, Landsat 5 imagery spans 27 years, with an identified 209 floods out of 415 total images (50.36%). In contrast, Landsat 8 imagery spans only a 10-year period, with 138 floods out of 290 total images (47.59%). Though there is certainly a positive trend in increased image density over the time period, we can observe that, in fact, the percentage of flood events actually decreases by 2.77%.

Focused on non-flood events, Mann–Kendall analysis identified a similar statistically significant positive trend for the upstream, midstream, and downstream sections individually and grouped, when aggregated annually. This was additionally supported via aggregation monthly, and by wet and dry season. Of Landsat 5 imagery, 50.84% is observed to represent non-flood events, compared to 81.03% of Landsat 8 imagery. This increase in the temporal frequency of non-flood events further supports our understanding of decreased flooding across the time period.

In contrast to the channel as a whole, Mann–Kendall analysis of flood events by section identified a statistically significant positive trend within only the downstream section, aggregated annually. Within the downstream section of Landsat 5, 25 of 39 images were identified as flood

events (64.10%), while Landsat 8 imagery identified 31 of 32 events as representative of surface flow (96.88%). This observation of increased temporal frequency of flooding is at odds with the results for the upstream and midstream sections, which display a trend toward decreased flooding. Increased frequency of surface flow within the downstream section of the channel may in fact be supported by tributary contribution, as opposed to source-derived flow. It may additionally indicate the increased occurrence and distance of saltwater intrusion, a phenomenon that has been frequently observed near the channel mouth (Choukr-Allah et al., 2016).

Overall, decreased frequency of flood events within the channel from 1984 through 2023 is consistent with broad decadal warming trends for Morocco, in which precipitation is projected to decrease and temperatures are expected rise (Verner et al., 2018). Decreased inputs paired with elevated evapotranspiration may result in the increased frequency of drought in dryland environments. Analyzed seasonally, flood frequency appears to shift around 1998, with the preceding period dominated by dry season flood events and the following period experiencing increased wet season flood frequency. Within the Souss–Massa basin, the sharpest seasonal increase in flood events occurs during the dry season from 1990 to 1998. This may be partially driven by the creation of the Aoulouz dam at the channel headwaters in 1990. The dam is intended to support irrigation needs and artificial recharge through channel infiltration, leading to dam releases when the channel lacks consistent flow (Dindane et al., 2003). Previous work on ephemeral channel transmission loss has identified prior sediment moisture as crucial for infiltration and sustained aquifer recharge (Fakir et al., 2021). Flood events concentrated within the wet season thus may have a higher likelihood of recharging the regional aquifer, as transmission losses have the potential for deeper percolation. Within the Souss, the trend toward increased flood events within the wet season represents a positive shift for regional water

storage. Despite an overall decreasing trend in the frequency of channel flooding, the impact on the regional water balance may be mitigated if reductions are concentrated within the dry season.

Spatial characteristics of flood variability additionally play an important role in sustained groundwater recharge. Across the wet season, flood events are relatively balanced, with 46.8% occurring with the upstream, 28.90% the midstream, and 24.28% the downstream channel sections. The reduction between the upstream and midstream sections points to external factors likely impacting the extent of channel flow. Specifically, transmission loss may be partially responsible for the decreased flow frequency within the midstream and downstream sections. Over pumping and abstraction to support agriculture additionally occurs broadly across the plain adjacent to the channel midsection, and likely contributes to reduced surface flow (Bouchaou et al., 2011; Ait Brahim et al., 2017). Increased transmission loss during the wet season period has positive implications for aquifer recharge, with infiltration between the upstream–midstream sections reducing the overall time surface water remains on the landscape and potentially contributing to reductions in PET (Fakir et al., 2021). During the dry season, the majority of flood events are concentrated within the upstream section of the channel (53.71%). This may further be to the benefit of regional aquifer recharge, as the higher number of flood events within this section increase the likelihood of antecedent sediment moisture and sustained infiltration (Fakir et al., 2021).

3.6 Conclusions

Within data-limited, ephemeral systems, remotely sensed imagery paired with linear discriminant function analysis has the potential to improve our understanding of large-scale hydrologic processes. Despite overall reductions in the frequency of flow within the Souss

channel, the preservation of events within the wet seasons increases the likelihood that sustained aquifer recharge can persist. The spatial distribution of surface water further contributes to the potential for recharge, with the majority of events concentrated within the upstream reaches of the channel. The addition of in situ measurements of precipitation and related discharge across channel sections has the potential to further refine and validate these observations, at the scale of both pixel classification and flood variability. The incorporation of subsurface monitors of infiltration and sustained recharge would further help connect this work to regional estimates of transmission loss and optimal conditions for aquifer recharge. Field measurements may ultimately help expand the application of this method to intermittent systems across varied environments, quantifying broad shifts in regional flow patterns.

3.7 References

Ait Brahim, Y., Seif-Ennasr, M., Malki, M., N'da, B., Choukrallah, R., El Morjani, Z.E.A., Sifeddine, A., Abahous, H., and Bouchaou, L., 2017, Assessment of Climate and Land Use Changes: Impacts on Groundwater Resources in the Souss-Massa River Basin, in Choukr-Allah, R., Ragab, R., Bouchaou, L., and Barceló, D. eds., The Souss-Massa River Basin, Morocco, Cham, Springer International Publishing, The Handbook of Environmental Chemistry, p. 121–142, doi:10.1007/698_2016_71.

Almulla, Y., Ramirez, C., Joyce, B., Huber-Lee, A., and Fuso-Nerini, F., 2022, From participatory process to robust decision-making: An Agriculture-water-energy nexus analysis for the Souss-Massa basin in Morocco: Energy for Sustainable Development, v. 70, p. 314–338, doi:10.1016/j.esd.2022.08.009.

Alsdorf, D.E., Rodríguez, E., and Lettenmaier, D.P., 2007, Measuring surface water from space: Reviews of Geophysics, v. 45, doi:10.1029/2006RG000197.

Andrefouet, S., Bindschadler, R., Brown de Colstoun, E., and Choate, M., 2003, Preliminary assessment of the value of Landsat-7 ETM+ data following scan line corrector malfunction: US Geological Survey, EROS Data Center.

Borg Galea, A., Sadler, J.P., Hannah, D.M., Datry, T., and Dugdale, S.J., 2019, Mediterranean intermittent rivers and ephemeral streams: Challenges in monitoring complexity: Ecohydrology, v. 12, p. e2149, doi:10.1002/eco.2149.

Bouchaou, L., Tagma, T., Boutaleb, S., Hssaisoune, M., and El Morjani, Z.E.A., 2011, Climate change and its impacts on groundwater resources in Morocco: The case of the Souss-Massa basin, in Climate Change Effects on Groundwater Resources: A Global Synthesis of Findings and Recommendations, p. 129–144.

Bouizrou, I., Bouadila, A., Aqnouy, M., and Gourfi, A., 2023, Assessment of remotely sensed precipitation products for climatic and hydrological studies in arid to semi-arid data-scarce region, central-western Morocco: Remote Sensing Applications: Society and Environment, v. 30, p. 100976, doi:10.1016/j.rsase.2023.100976.

Bouragba, L., Mudry, J., Bouchaou, L., Hsissou, Y., Krimissa, M., Tagma, T., and Michelot, J.L., 2011, Isotopes and groundwater management strategies under semi-arid area: Case of the Souss upstream basin (Morocco): Applied Radiation and Isotopes, v. 69, p. 1084–1093, doi:10.1016/j.apradiso.2011.01.041.

Chavez, P.S., 1988, An improved dark-object subtraction technique for atmospheric scattering correction of multispectral data: Remote Sensing of Environment, v. 24, p. 459–479, doi:10.1016/0034-4257(88)90019-3.

Chen, H., Liang, Q., Liang, Z., Liu, Y., and Ren, T., 2020, Extraction of connected river networks from multi-temporal remote sensing imagery using a path tracking technique: Remote Sensing of Environment, v. 246, p. 111868, doi:10.1016/j.rse.2020.111868.

Choukr-Allah, R., Ragab, R., Bouchaou, L., and Barcelo, D., 2016, The Souss-Massa River Basin, Morocco:

Costa, A.C., Foerster, S., de Araújo, J.C., and Bronstert, A., 2013, Analysis of channel transmission losses in a dryland river reach in north-eastern Brazil using streamflow series, groundwater level series and multi-temporal satellite data: Hydrological Processes, v. 27, p. 1046–1060, doi:10.1002/hyp.9243.

Costigan, K.H., Kennard, M.J., Leigh, C., Sauquet, E., Datry, T., and Boulton, A.J., 2017, Chapter 2.2 - Flow Regimes in Intermittent Rivers and Ephemeral Streams, in Datry, T.,

Bonada, N., and Boulton, A. eds., Intermittent Rivers and Ephemeral Streams, Academic Press, p. 51–78, doi:10.1016/B978-0-12-803835-2.00003-6.

Datry, T., Larned, S.T., and Tockner, K., 2014, Intermittent Rivers: A Challenge for Freshwater Ecology: BioScience, v. 64, p. 229–235, doi:10.1093/biosci/bit027.

Davis, J.C., 2002, Statistics and Data Analysis in Geology: New York, Wiley, https://www.scribd.com/doc/98598695/Statistics-and-Data-Analysis-in-Geology-3rd-ed (accessed September 2023).

Dindane, K., Bouchaou, L., Hsissou, Y., and Krimissa, M., 2003, Hydrochemical and isotopic characteristics of groundwater in the Souss Upstream Basin, southwestern Morocco: Journal of African Earth Sciences, v. 36, p. 315–327, doi:10.1016/S0899-5362(03)00050-2.

Döll, P., and Schmied, H.M., 2012, How is the impact of climate change on river flow regimes related to the impact on mean annual runoff? A global-scale analysis: Environmental Research Letters, v. 7, p. 014037, doi:10.1088/1748-9326/7/1/014037.

Fakir, Y., Bouimouass, H., and Constantz, J., 2021, Seasonality in Intermittent Streamflow Losses Beneath a Semiarid Mediterranean Wadi: Water Resources Research, v. 57, doi:10.1029/2021WR029743.

Fei, J., Liu, J., Ke, L., Wang, W., Wu, P., and Zhou, Y., 2022, A deep learning-based method for mapping alpine intermittent rivers and ephemeral streams of the Tibetan Plateau from Sentinel-1 time series and DEMs: Remote Sensing of Environment, v. 282, p. 113271, doi:10.1016/j.rse.2022.113271.

Feyisa, G.L., Meilby, H., Fensholt, R., and Proud, S.R., 2014, Automated Water Extraction Index: A new technique for surface water mapping using Landsat imagery: Remote Sensing of Environment, v. 140, p. 23–35, doi:10.1016/j.rse.2013.08.029.

Fisher, A., Flood, N., and Danaher, T., 2016, Comparing Landsat water index methods for automated water classification in eastern Australia: Remote Sensing of Environment, v. 175, p. 167–182, doi:10.1016/j.rse.2015.12.055.

Hamada, Y., O'Connor, B.L., Orr, A.B., and Wuthrich, K.K., 2016, Mapping ephemeral stream networks in desert environments using very-high-spatial-resolution multispectral remote sensing: Journal of Arid Environments, v. 130, p. 40–48, doi:10.1016/j.jaridenv.2016.03.005.

Hammond, J.C. et al., 2021, Spatial Patterns and Drivers of Nonperennial Flow Regimes in the Contiguous United States: Geophysical Research Letters, v. 48, doi:10.1029/2020GL090794.

Hssaisoune, M., Bouchaou, L., Matsumoto, T., Araguas, L., Kraml, M., and Aggarwal, P., 2019, New evidences on groundwater dynamics from the Souss-Massa system (Morocco): Insights gained from dissolved noble gases: Applied Geochemistry, v. 109, p. 104395, doi:10.1016/j.apgeochem.2019.104395.

Hssaisoune, M., Boutaleb, S., Benssaou, M., and Bouaakkaz, B., 2016, (PDF) Physical Geography, Geology, and Water Resource Availability of the Souss-Massa River Basin: Springer Berlin Heidelberg, 1–30 p., https://www.researchgate.net/publication/308497276_Physical_Geography_Geology_and_Water_Resource_Availability_of_the_Souss-Massa_River_Basin (accessed March 2023).

Isikdogan, F., Bovik, A.C., and Passalacqua, P., 2017, Surface Water Mapping by Deep Learning: IEEE Journal of Selected Topics in Applied Earth Observations and Remote Sensing, v. 10, p. 4909–4918, doi:10.1109/JSTARS.2017.2735443.

Jacobberger, P.A., Arvidson, R.E., and Rashka, D.L., 1983, Application of Landsat multispectral scanner data and sediment spectral reflectance measurements to mapping of the Meatiq Dome, Egypt: Geology, v. 11, p. 587–591, doi:10.1130/0091-7613(1983)11<587:AOLMSD>2.0.CO;2.

Krabbenhoft, C.A. et al., 2022, Assessing placement bias of the global river gauge network: Nature Sustainability, v. 5, p. 586–592, doi:10.1038/s41893-022-00873-0.

Levick, L. et al., 2008, The Ecological and Hydrological Significance of Ephemeral and Intermittent Streams in the Arid and Semi-arid American Southwest: U.S. Environmental Protection Agency and USDA/ARS Southwest Watershed Research Center, doi:EPA/600/R-08/134, ARS/233046.

Maindonald, J., and Braun, W.J., 2003, Data Analysis and Graphics Using R – an Example-Based Approach, Third Edition: Cambridge.

Malinowski, R., Höfle, B., Koenig, K., Groom, G., Schwanghart, W., and Heckrath, G., 2016, Local-scale flood mapping on vegetated floodplains from radiometrically calibrated airborne LiDAR data: ISPRS Journal of Photogrammetry and Remote Sensing, v. 119, p. 267–279, doi:10.1016/j.isprsjprs.2016.06.009.

Maswanganye, S.E., 2022, Remotely sensed applications in monitoring the spatio-temporal dynamics of pools and flows along non-perennial rivers: a review | South African Geographical Journal.

McFeeters, S.K., 1996, The use of the Normalized Difference Water Index (NDWI) in the delineation of open water features: International Journal of Remote Sensing, v. 17, p. 1425–1432, doi:10.1080/01431169608948714.

Messager, M.L., Lehner, B., Cockburn, C., Lamouroux, N., Pella, H., Snelder, T., Tockner, K., Trautmann, T., Watt, C., and Datry, T., 2021, Global prevalence of non-perennial rivers and streams: Nature, v. 594, p. 391–397, doi:10.1038/s41586-021-03565-5.

Milewski, A., Elkadiri, R., and Durham, M., 2015, Assessment and Comparison of TMPA Satellite Precipitation Products in Varying Climatic and Topographic Regimes in Morocco: Remote Sensing, v. 7, p. 5697–5717, doi:10.3390/rs70505697.

Milewski, A., Sultan, M., Yan, E., Becker, R., Abdeldayem, A., Soliman, F., and Gelil, K.A., 2009, A remote sensing solution for estimating runoff and recharge in arid environments: Journal of Hydrology, v. 373, p. 1–14, doi:10.1016/j.jhydrol.2009.04.002.

R Core Team, 2011, R: A Language and Environment for Statistical Computing:

Saouabe, T., El Khalki, E.M., Saidi, M.E.M., Najmi, A., Hadri, A., Rachidi, S., Jadoud, M., and Tramblay, Y., 2020, Evaluation of the GPM-IMERG Precipitation Product for Flood Modeling in a Semi-Arid Mountainous Basin in Morocco: Water, v. 12, p. 2516, doi:10.3390/w12092516.

Seaton, D., and Mazvimavi, D., 2020, Use of multi-temporal satellite data for monitoring pool surface areas occurring in non-perennial rivers in semi-arid environments of the Western Cape, South Africa: ISPRS Journal of Photogrammetry and Remote Sensing, v. 167, p. 375–384, doi:10.1016/j.isprsjprs.2020.07.018.

Shanafield, M., and Cook, P.G., 2014, Transmission losses, infiltration and groundwater recharge through ephemeral and intermittent streambeds: A review of applied methods: Journal of Hydrology, v. 511, p. 518–529, doi:10.1016/j.jhydrol.2014.01.068.

Shawky, M., Moussa, A., Hassan, Q.K., and El-Sheimy, N., 2019, Performance Assessment of Sub-Daily and Daily Precipitation Estimates Derived from GPM and GSMaP Products over an Arid Environment: Remote Sensing, v. 11, p. 2840, doi:10.3390/rs11232840.

Shentsis, I., and Rosenthal, E., 2003, Recharge of aquifers by flood events in an arid region: Hydrological Processes, v. 17, p. 695–712, doi:10.1002/hyp.1160.

Stark, K., Cadol, D., Varyu, D., and Laronne, J.B., 2021, Direct, continuous measurements of ultra-high sediment fluxes in a sandy gravel-bed ephemeral river: Geomorphology, v. 382, p. 107682, doi:10.1016/j.geomorph.2021.107682.

Stubbington, R., Acreman, M., Acuña, V., Boon, P.J., Boulton, A.J., England, J., Gilvear, D., Sykes, T., and Wood, P.J., 2020, Ecosystem services of temporary streams differ between wet and dry phases in regions with contrasting climates and economies (A. J. Castro, Ed.): People and Nature, v. 2, p. 660–677, doi:10.1002/pan3.10113.

Sun, F., Sun, W., Chen, J., and Gong, P., 2012, Comparison and improvement of methods for identifying waterbodies in remotely sensed imagery: International Journal of Remote Sensing - INT J REMOTE SENS, v. 33, p. 6854–6875, doi:10.1080/01431161.2012.692829.

Tang, G., Clark, M.P., Papalexiou, S.M., Ma, Z., and Hong, Y., 2020, Have satellite precipitation products improved over last two decades? A comprehensive comparison of GPM IMERG with nine satellite and reanalysis datasets: Remote Sensing of Environment, v. 240, p. 111697, doi:10.1016/j.rse.2020.111697.

Tian, Y., Peters-Lidard, C.D., Eylander, J.B., Joyce, R.J., Huffman, G.J., Adler, R.F., Hsu, K., Turk, F.J., Garcia, M., and Zeng, J., 2009, Component analysis of errors in satellite-based

precipitation estimates: Journal of Geophysical Research: Atmospheres, v. 114, doi:10.1029/2009JD011949.

Tramblay, Y., Thiemig, V., Dezetter, A., and Hanich, L., 2016, Evaluation of satellite-based rainfall products for hydrological modelling in Morocco: Hydrological Sciences Journal, v. 61, p. 2509–2519, doi:10.1080/02626667.2016.1154149.

Tulbure, M.G., Broich, M., Stehman, S.V., and Kommareddy, A., 2016, Surface water extent dynamics from three decades of seasonally continuous Landsat time series at subcontinental scale in a semi-arid region: Remote Sensing of Environment, v. 178, p. 142–157, doi:10.1016/j.rse.2016.02.034.

Veh, G., Korup, O., Roessner, S., and Walz, A., 2018, Detecting Himalayan glacial lake outburst floods from Landsat time series: Remote Sensing of Environment, v. 207, p. 84–97, doi:10.1016/j.rse.2017.12.025.

Venables, W.N., and Ripley, B.D., 2002, Modern Applied Statistics with S: New York, NY, UA, Springer.

Verner, D., Treguer, D., Redwood, J., Christensen, J., McDonnell, R., Elbert, C., Konishi, Y., and Belghazi, S., 2018, Climate Variability, Drought, and Drought Management in Morocco's Agricultural Sector: World Bank, Washington, DC, doi:10.1596/30603.

World Meteorological Organization (WMO), 2017, Guidelines on the Calculation of Climate Normals: WMO-TD 341.

Xu, H., 2006, Modification of normalised difference water index (NDWI) to enhance open water features in remotely sensed imagery: International Journal of Remote Sensing, v. 27, p. 3025–3033, doi:10.1080/01431160600589179.

Zhou, Y., Dong, J., Xiao, X., Xiao, T., Yang, Z., Zhao, G., Zou, Z., and Qin, Y., 2017, Open Surface Water Mapping Algorithms: A Comparison of Water-Related Spectral Indices and Sensors: Water, v. 9, p. 256, doi:10.3390/w9040256.

Zimmer, M.A. et al., 2020, Zero or not? Causes and consequences of zero-flow stream gage readings: WIREs Water, v. 7, doi:10.1002/wat2.1436.

Zimmer, M.A., Burgin, A.J., Kaiser, K., and Hosen, J., 2022, The unknown biogeochemical impacts of drying rivers and streams: Nature Communications, v. 13, p. 7213, doi:10.1038/s41467-022-34903-4.

Zipper, S.C. et al., 2021, Pervasive changes in stream intermittency across the United States: Environmental Research Letters, v. 16, p. 084033, doi:10.1088/1748-9326/ac14ec.

CHAPTER 4

SPATIAL VARIABILITY IN POTENTIAL RECHARGE: QUANTIFYING TRANSMISSION LOSS AND CONTROLS ON INFILTRATION ACROSS DISPARATE RECHARGE ZONES IN SEMI-ARID ENVIRONMENTS

Davidson, L.J. To be submitted to a peer reviewed journal, Water Resources Research.

4.1 Chapter Abstract

Transmission losses frequently constitute the majority of aquifer recharge in semi-arid environments and are a key hydrologic feature of ephemeral channels. Despite this understanding, infiltration variability and its primary controls remain poorly characterized. In this study, the spatial and temporal variability of transmission loss through ephemeral channels is explored across disparate recharge environments in central Morocco. Continuous temperature monitoring within the near-surface sediments of two ephemeral channels was used to record infiltration events across both wet and dry seasons in upstream and midstream channel reaches. Temperature time series were then used to estimate rates of infiltration at specific depth and compared to sediment-based estimates of saturated hydraulic conductivity. Thermographs indicate distinct spatial patterns of infiltration, both longitudinally across stream channels and vertically within channel sediment. Specifically, observations support the role of near-surface sediment, both its sorting and antecedent moisture, in controlling sustained infiltration during surface flow events. Improved understanding of transmission loss and its controls is critical for estimates of potential groundwater recharge, particularly in data-scarce, arid systems.

4.2 Introduction

Focused recharge through stream channels represents the primary form of aquifer recharge in arid environments, particularly within ephemeral systems which are estimated to constitute more than half of all river length globally (Datry et al., 2014; Shanafield and Cook, 2014; Di Ciacca et al., 2023). Transmission loss, or streamflow infiltration through channel sediments, has frequently been used as a proxy for groundwater recharge. This is despite the uncertainty that infiltrating water will be transported to depths sufficient to reach the water table

and not re-evaporated (Shanafield and Cook, 2014). Quantifying channel infiltration is critical for sustainable water management in water-limited environments, but largely depends on understanding drivers of its spatial and temporal variability.

The physical and climatic characteristics which shape ephemeral channel development further predispose a system to transmission loss. Though they can occur in both high-elevation and plains environments, ephemeral channels frequently evolve in response to limited or seasonal precipitation patterns. Non-perennial systems generally lack baseflow inputs from groundwater and are disconnected from deeper, unconfined aquifers. Channels are regularly characterized by highly permeable sediment, such as coarse-grained sand or alluvium, ideal for rapid infiltration of surface water. Previous work has identified the role of antecedent sediment moisture in facilitating deep infiltration, as well as the impact of subsurface geology and heterogeneity (Shanafield and Cook, 2014; Fakir et al., 2021). With these variable controls, patterns of transmission loss are considered non-standard across arid regions and in individual basins, varying both spatially and temporally across recharge environments.

The connection between transmission loss and sustained recharge remains poorly quantified, despite the development of a robust theoretical framework through controlled studies within experimental watersheds. In part, research has been concentrated within heavily instrumented ephemeral channels in the western USA, with more limited analysis of systems abroad which lack gaging equipment (Shanafield and Cook, 2014; Portoghese et al., 2022). Significant gaps remain in our understanding of regional controls of ephemeral channel infiltration and thus our ability to quantify groundwater recharge via ephemeral systems. This deficiency may only become more urgent with the current expansion of non-perennial systems under warming climate conditions. Climate change is projected to extend drylands globally,

which currently encompass approximately 40% of the global land surface, increasing intermittent flow and overall contribution of transmission loss to aquifer recharge (Eng et al., 2016; Costigan et al., 2016; Gaur and Squires, 2018; Jaeger et al., 2018).

This research focuses on quantifying regional differences in transmission loss and potential recharge through streambed-sediment thermographs, as well as explores associated controls, in semi-arid basins. Specifically, this work examines patterns of transmission loss within ephemeral channels across both mountain front and plain recharge zones in central Morocco. The goals of this research are (1) quantify temporal frequency and rate of infiltration events in differing recharge environments, (2) understand spatial patterns of transmission loss, both intra-channel and across systems, and (3) identify primary controls driving regional differences in potential recharge.

4.3 Methods

Study Area: Mountain Front Recharge, Tensift Basin

The Ourika sub-basin (507 km^2) is a semi-arid mountain front basin located in the larger Tensift basin of central Morocco (Figure 1) (Bouimouass et al., 2024). Originating at the high elevation mountain front of the High Atlas (4,167 m.a.s.l.), Oued Ourika flows north across the Haouz plain (1,070 m) before joining with the larger Oued Tensift (Daoudi and Saidi, 2008; Rhoujjati et al., 2021; Bouimouass et al., 2024). Surface flow in Oued Ourika is intermittent and largely driven by seasonal inputs of precipitation and snowmelt, which results in peak flows during April (wet season, October– April) (Bouimouass et al., 2024). Precipitation is heterogeneous across the basin, with an average of 700 mm/year in the High Atlas Mountains upstream and 300 mm/year in the mid- and downstream plain (Daoudi and Saidi, 2008;

Delcaillau et al., 2010; Fakir et al., 2021; Bell et al., 2022). Concentrated seasonal moisture inputs, paired with a steep gradient of 11% and a narrow, incising valley, predispose the channel to extreme flooding (Daoudi and Saidi, 2008; Delcaillau et al., 2010; Fakir et al., 2021).

The Haouz plain Is underlain by heterogeneous Quaternary alluvial deposits while high-elevation regions of the basin, near Oukaïmeden, are comprised of Precambrian crystalline rocks (Ayt Ougougdal et al., 2020; Bouimouass et al., 2024). An unconfined alluvial aquifer is the primary source of groundwater in the plain, extending up to 150 m beneath the stream. A deeper confined aquifer is comprised of both Eocene marls and Turonian-Cenomanian limestones (Bouimouass et al., 2024). Regionally, mountain-front recharge through stream infiltration represents the primary form of recharge to the unconfined aquifer (Markovich et al., 2019; Bouimouass et al., 2024). In part, this is due to concentration of precipitation and snowmelt concentrated at higher elevations, which extend the seasonal duration of hydrologic inputs to the more arid downstream reaches. This impact has led to the High Atlas Mountains to be colloquially referred to as “water towers” (Pascon, 1978; Jarlan et al., 2015).

Intermittent flow within Oued Ourika is used in conjunction with the unconfined Haouz aquifer to support regional agriculture. Stream diversion is essential to irrigation within the basin, with olive and winter cereal production representing the primary land use and economic activity within the mountain-front region (Modeste et al., 2016; Bouimouass et al., 2024). In recent decades, increased pressure on regional groundwater has caused average water-table declines of two meters annually (Bouimouass et al., 2020). This has likely been exacerbated by recurring droughts and reduced total precipitation, falling by 28% in the last half-century (Ouassanouan et al., 2022). Total discharge has similarly declined by 40% within the mountain front sub-basins of the Tensift (Ouassanouan et al., 2022).

Plains Recharge: Souss-Massa Basin

The Souss-Massa basin (27,000 km^2) is located in west-central Morocco, nestled between the High Atlas Mountains to the north and Anti-Atlas Mountains to the south (Figure 1) (Bouchaou et al., 2008; Hssaisoune et al., 2019). Situated on the basin plain (4,200 km^2), Oued Souss is an ephemeral stream which stretches 180 km from the upstream Aoulouz reservoir to the Atlantic Ocean (Hssaisoune et al., 2019). The plain is gradually sloping, ranging in elevation from 700 m at Aoulouz to sea level at the terminus (Hssaisoune et al., 2019). Classified as semi-arid, the plain receives an average of 250 mm of precipitation annually, with the majority concentrated during the wet-season from October through April (Hssaisoune et al., 2019). Evapotranspiration exceeds 2000 mm annually, and temperature fluctuates on both daily and seasonal cycles (Bouchaou et al., 2008). It is this distinct seasonality which facilitates the majority of groundwater recharge across the Souss plain, with wet season precipitation supporting surface flow and direct infiltration through channels sediments. Outside of the plain, additional recharge occurs from precipitation at higher elevations (Bouchaou et al., 2008; Hssaisoune et al., 2017).

The plain and Souss river channel are underlain by multilayered, unconsolidated Pliocene-Quaternary sediments, deposited by alluvial fans (Ait Hssaine and Bridgland, 2009). These sediments (primarily gravels and sands) and lacustrine limestones extend up to 300 m in depth and are underlain by Senonian marls, which confine a deeper aquifer of Turonian limestone (Hssaisoune et al., 2019, 2021). The unconfined aquifer is shallowest beneath upstream sections of Oued Souss, within 10 m to 30 m of the surface, and deepens downstream (westward) and away from the channel (Dindane et al., 2003; Ait Brahim et al., 2017). Surface-water abstraction and groundwater pumping, primarily from the unconfined aquifer, are

necessary to support regional irrigation. The Souss basin is an economically critical agricultural region, producing the majority of national citrus and vegetable exports, along with cereals and almonds (Bouchaou et al., 2008; Choukr-Allah et al., 2016; Almulla et al., 2022). Over-pumping of regional aquifers has been well documented in the past five decades, manifesting as water level declines ranging from 0.5 to 2.5 m/year (Hssaisoune et al., 2016). Rapid declines in aquifer storage have given rise to basin subsidence and salinization, particularly in the downstream reach (Bouchaou et al., 2008; Richards and Milewski, 2022). Similar to patterns of projected climate warming in arid regions globally, in recent decades the Souss has experienced a shift toward increased mean annual temperatures and decreased precipitation intensity, with elevated frequency of drought (Bouragba et al., 2011; Bouchaou et al., 2011). Controlled releases from the Aoulouz Dam have been irregularly employed to artificially recharge the unconfined aquifer and support irrigation during drought periods (Bouragba et al., 2011). Though historically ephemeral, the frequency of surface flow within Oued Souss has shifted with changing precipitation, resulting in a reduction in flood events, which may impact regional groundwater recharge patterns (Davidson et al., 2023).

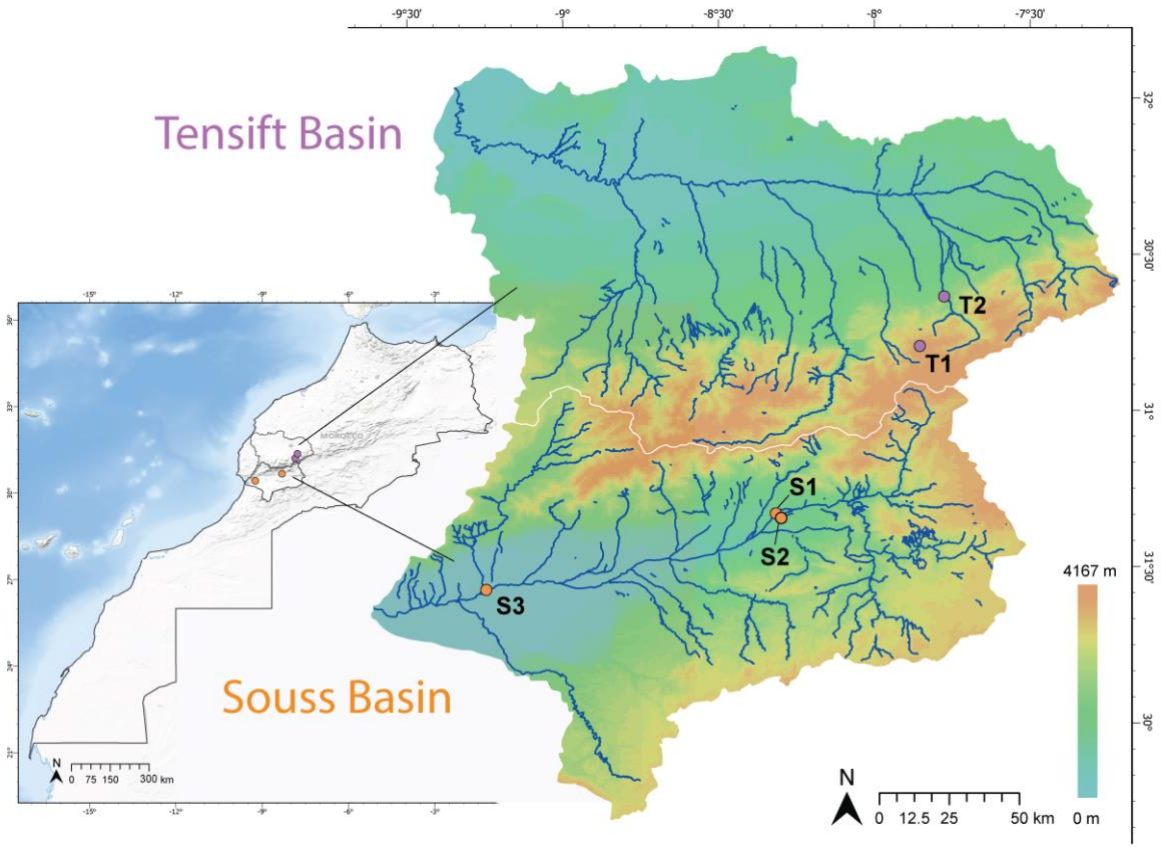

Figure 4-1. Research basins, located in central Morocco. Transects 1, 2, and 3 are located in the upstream section of the Tensift basin, at Oukaïmeden, High Atlas Mountains (T1). Transect 4 is located within the midstream section of the Tensift basin on the Haouz plain (T2). The upstream section of the Souss basin has two distinct transect sites installed laterally across the channel, near Aoulouz. Transects 6 and 7 are established in the channel center (S1) and transect 5 is located near the channel left bank (S2). Transect 8 was deployed in the midstream section of the Souss channel, near Issen (S3). Basin elevation highlights the location of upstream sites in higher elevation zones.

Detection of Potential Recharge through Sediment Temperature

Streambed sediment temperature profiles have historically been employed to detect surface flow and channel infiltration (Constantz and Thomas, 1997; Constantz et al., 2001; Constantz, 2008). Heat is a particularly useful tracer in ephemeral channels, where streambed sediment is generally saturated only in response to surface flow conditions. Dry sediments exhibit greater diurnal temperature fluctuations than saturated material, as a result of adsorption of solar radiation and heat propagation via conduction (Constantz, 2008; Shanafield and Cook, 2014). In a flowing stream with saturated sediment, radiation is both reflected and absorbed prior to advection (Constantz, 2008). In both saturated and unsaturated material, diurnal temperature fluctuations are further attenuated with depth due to heat absorption by stream sediments (Constantz, 2008). This behavior allows for the calculation of infiltration rates from subsurface temperature data collected at variable depths, as distinct changes in temperature pattern co-occur with infiltration events. For ephemeral systems with limited gaging, subsurface temperature probes offer an effective alternative to surface-water monitoring. They further allow for exploration of the connection between periodic surface flow and aquifer recharge via transmission losses (Constantz et al., 2001; Blasch et al., 2004; Fakir et al., 2021).

Our study deployed temperature loggers in vertical transects beneath bed sediments of two ephemeral channels to quantify intermittent streamflow and related infiltration. Eight vertical transects were installed during no-flow channel conditions, and transect depth was dependent on near-surface sediment sorting and height of the water table. Each transect consisted of a minimum of three HOBO temperature pendants (Onset Computer, Bourne, MA, USA) attached to a wire and spaced at a set distance, ranging from 10 to 35 cm depending on transect depth. Pendant measurement range is from -4° to 158° F (± 0.95°F). The temperature pendant

nearest the surface (Pendant A) was buried between 5 and 25 cm, while the deepest pendant (Pendant C or D) reached depths between 40 and 105 cm. Temperature measurements were recorded at 15-minute intervals, with variable length of the collection period (3 months – 1 year) as a result of battery failures. Previous studies in subsurface temperature monitoring have identified a minimum depth of 15 cm as ideal to mitigate temperature anomalies related to atmospheric events and diurnal temperature fluctuations (Constantz et al., 2001; Blasch et al., 2004).

In the Ourika basin, Transects 1, 2, and 3 were deployed at the upstream site, near Oukaïmeden (October 2015–October 2016, June 2022–June 2023, and June 2023–May 2024, respectively) (Table 4-1). Transect 4 was deployed at the channel midstream, near Ourika, from June to August 2022. In the Souss basin, four transects were deployed across upstream and midstream sites, spanning a two-year period. At the upstream location, Transects 6 and 7 were deployed in the channel midstream (S1), recording from June to October 2022 and June 2023 to May 2024, respectively. Transect 5 was deployed parallel to S1 along the channel bank (S2) and recorded data from June to November 2022. This transect utilized an Onset HOBO U12 temperature logger as an alternative to temperature pendants, which recorded temperature hourly. At the midstream location, Transect 8 was installed from June 2023 to May 2024 (Table 4-1). Within the Souss basin, sediment samples were additionally collected at all transect locations, with material fining upward similar to stacked sediment patterns commonly observed in ephemeral systems (Jadoon et al., 2016).

Table 4-1. Study Basin Transect Locations

Mountain Front System		Plain System		
Upstream (Oukaïmeden, Tensift)	Midstream (Ourika, Tensift)	Upstream (Aoulouz, Souss)		Midstream (Issen, Souss)
T1	T2	S1	S2	S3
Transect 1 Transect 2 Transect 3	Transect 4	Transect 6 Transect 7	Transect 5	Transect 8

Event Detection through Statistical Anomalies

Temperature data for each transect were statistically evaluated using seasonal z-scores for detection of anomalies associated with potential infiltration events. Infiltration of water into unsaturated sediment is characterized by a distinct drop in temperature and loss of diurnal pattern. Atmospheric events, such as cold fronts preceding a storm, may present similar temperature patterns to legitimate infiltration (Jadoon et al., 2016). Statistical anomaly detection is thus necessary to accurately differentiate true hydrologic events, and a variety of techniques have been employed. Common methodologies work to mitigate seasonal variability, through data smoothing and the application of weighted or moving windows (Blasch et al., 2004; Partington et al., 2021). As sensors are insulated from diurnal temperature fluctuations with increasing depth, potential infiltration events were required to exhibit a sharp temperature drop across all sensors in the transect (Blasch et al., 2004).

To address the distinct seasonality of climate in our research basins, temperature data from each pendant were separated into wet- and dry-season subsets prior to the calculation of z-scores (Zhou and Tang, 2016). Scores within the 5^{th} percentile were flagged as negative anomalies indicative of a potential infiltration event. Anomalies were further visually confirmed within the temperature data for loss of diurnal pattern during the event. Six events (two within

the Tensift basin, four within the Souss) were statistically flagged as infiltration events, though visually mimicked the appearance of cold fronts. Specifically, this was due to the maintenance of their diurnal pattern despite an overall drop in temperature. A potential event in February 2023 at the upstream site of the Tensift basin was not statistically identified as being within of the lowest 5th percentile, but it visually demonstrated a pattern indicative of infiltration and significant prior precipitation. The anomaly for this event fell within the lowest 5.5% of the temperature data, and expansion of the cutoff to this value did not identify any additional events. Omission of these seven events did not substantially alter estimated rates of infiltration for each site (both increasing by less than 1.00 cm/h) and were included in these results (though identified).

Validation via Satellite-based Precipitation Estimates

Due to limited availability of in-situ stream gaging, precipitation prior to and during potential infiltration events was used to validate presence of surface flow. Stream and precipitation gage data within Morocco are not publicly available and, furthermore, fail to capture local climate conditions at upstream and midstream sections of both basins. GPM-IMERG multi-satellite precipitation estimates with gage calibration (half-hourly, averaged daily–Final Run V07) satellite precipitation estimates were utilized to validate potential infiltration events. Application of final run GPM precipitation estimates within Morocco have been found to have suitable accuracy across arid, mountainous basins, with strongest agreement in lower elevation portions of the basin (Shawky et al., 2019; Saouabe et al., 2020).

Multimodal Estimation of Infiltration Rate

Infiltration rates were calculated for potential recharge events via two methods: 1) the time lag observed between temperature anomalies across pendants in a transect versus the

vertical distance traveled, and 2) based on saturated hydraulic conductivity estimated from sediment analysis. Infiltration rates determined via time lag were calculated for each pendant in a single event, representing infiltration rates spanning from the near surface to depths with a dampened diurnal signal. An average overall rate was further calculated for each individual event, as well as for each pendant within the transect. In the case of pendant battery failure during the observation period, infiltration rates are calculated based on remaining pendants and denoted with an asterisk. Hydraulic conductivity estimates were calculated from sediment samples within the Souss basin and determined from literature analysis within the Tensift. Sediment samples were collected at depths ranging from 75 to 85 cm for better representation of subsurface material. A low-permeability layer at the surface of channel bed sediment is a common feature in arid systems, in part due to the upward fining and sorting of alluvial sediments (Fakir et al., 2021). Analysis was conducted via wet sieve and Meter PARIO Soil Particle Analyzer to produce particle distribution curves and taxonomic identification via soil texture (Appendix Chapter 4, Figure 2). Particle distribution curves were applied to the Kozeny-Carman formula for estimation of saturated hydraulic conductivity in channel sediments (Table 4-2). Kozeny-Carman is a widely accepted empirical method successfully applied to unconsolidated porous media of varying sizes, particularly coarse material (Kozeny, 1927; Freeze and Cherry, 1979; Taheri et al., 2017). Though saturated hydraulic conductivity is a property of the porous material, as infiltration approaches steady-state, this value becomes equivalent to saturated hydraulic conductivity. For transect locations within the Tensift basin, saturated hydraulic conductivity values were derived from previous studies of vertical infiltration and sediment composition in close proximity to upstream and midstream sites (Table 4-3). Fakir et al. (2021) sampled bed sediment at 100 cm depth, utilizing sieve and textural analysis to

estimate saturated hydraulic conductivity. At the upstream site, previous studies have reported soil erodibility (K factor) based on a calculation of detailed soil properties, including sand percentage (Ayt Ougougdal et al., 2020). Sand percentage paired with field analysis of sediment texture during transect installation led to its characterization as a sandy clay loam. This classification strongly agreed with previous characterization of soils at this location, and a standard hydraulic conductivity value associated with saturated and loosened conditions for this soil class was assigned (Rawls et al., 1998; Alaoui Haroni et al., 2009). Saturated hydraulic conductivity values were further compared to sensor-based estimates of infiltration rate at depth.

Table 4-2. Souss Basin Sediment Analysis

Site	Taxonomy	Depth (cm)	Coarse Sand (>1000 µm – 500 µm)	Medium Sand (500 µm – 250 µm)	Fine Sand (250 µm– 53 µm)	Fines (<53 µm)	Kozeny-Carman Sat. Hydraulic Conductivity (m/s)
S1 Upstream (center)	Loamy Sand	85	47.17%	23.47%	12.10%	17.26%	2.66×10^{-7}
S2 Upstream (bank)	Loamy Sand	80	39.00%	34.00%	7.77%	19.23%	3.47×10^{-8}
S3 Midstream	Sandy Clay Loam	75	22.17%	23.03%	13.57%55	41.23%	4.34×10^{-7}

Table 4-3. Tensift Basin Sediment Analysis

Site	Taxonomy	Depth (cm)	Gravel (>2000 µm)	Coarse sand (250 µm – 2,000 µm)	Fine sand (50 µm – 250 µm)	Silt (2 µm – 50 µm)	Clay (<2 µm)	Sediment Analysis Sat. Hydraulic Conductivity (m/s)
T1 Upstream	Loam	–	–	49%	–	40%	11%	2.18×10^{-6}
T2 Midstream	Medium Sand	100	58.30%	27.4 %	5.1 %	0.5 %	8.7%	4.00×10^{-5}

Exploration of Infiltration Controls through Principal Component Analysis

Principal components analysis (PCA) was applied to evaluate a subset of variables correlated to infiltration across the upstream and midstream sites of both the Tensift and Souss basins (Table 4-4). Variables of primary interest were related to channel geomorphology (channel width, length, and slope), bed sediment composition (sand, clay, and silt percentage based on sample analysis), and properties of the unconfined aquifer (estimated hydraulic conductivity and maximum depth) (Cataldo et al., 2013). PCA is a statistical analysis used to identify complex relationships between variables and reduce dataset dimensionality (Lever et al., 2017). Three principal components were generated, explaining 99.82% of the data variance. A correlation biplot was used to visualize the relationship between variables and transect locations.

Table 4-4. PCA Variables

Site	Basin	Location	Sand %	Clay %	Silt %	Sat. Hydraulic Conductivity (m/s)	Channel length (m)	Channel width (m)	Elevation (m)	Slope	Maximum Depth of Unconfined Aquifer (m)
S1	Souss	Upstream	0.83	0.08	0.08	2.66×10^{-7}	17,299	113	556	0.83	300 (1)
S2	Souss	Upstream	0.81	0.12	0.08	3.47×10^{-8}	17.299	113	555	0.83	300 (1)
S3	Souss	Midstream	0.59	0.28	0.13	4.34×10^{-7}	985,665	44	86	0.53	140 (2)
T1	Tensift	Upstream	0.49	0.11	0.4	2.18×10^{-6}	86.25	3	2,588	3.48	0 (3)
T2	Tensift	Midstream	0.91	0.087	0.005	4.00×10^{-5} (1)	24,036	73	883	2.59	150 (4)

Note: Sediment and saturated hydraulic conductivity values for the Souss basin derived from sample analysis. Values for channel length, width, and slope derived from Google Earth, 2020.[1] Fakir et al., 2021;[2] Bouchaou et al., 2008; [3] Hssaisoune et al., 2021; [4] N'da et al., 2018; [5] Bouimouass et al., 2024.

4.4 Results

Anomaly Detection for Potential Infiltration

Across the eight research transects, 33 events were identified as seasonal anomalies, and hypothesized to represent infiltration within the channels (Table 5). Potential infiltration events were observed at every site except Transect 4, located in the midstream section of the Tensift basin. The sensors in this transect recorded the shortest period of data collection, approximately

two months, prior to battery failure. This period was during the summer months when fewer surface flow events are expected to occur.

The Tensift and Souss basins demonstrated comparable numbers of potential infiltration events across the study period (Tensift = 16, Souss = 17), with a greater portion of events observed in the upstream channel reaches (Tensift = 16, Souss = 10). With lack of in situ stream gaging, these events were corroborated with GPM satellite precipitation estimates (Table 4-5). Anomalies within the Souss basin demonstrated notably lower precipitation estimates, both for the seven days prior and across the duration of the events (averages of 6.8 mm and 7.65 mm, respectively, as compared to 12.6 mm and 21.4 mm for Tensift). This is in line with lower precipitation levels across this basin, in particular when compared to the high elevation upstream section of the Tensift (Bouimouass et al., 2020). Precipitation events generally occurred in tandem with potential infiltration anomalies, with an average precipitation of 9.1 mm in the week prior, and 14.1 mm during the duration of the event. Across both basins, 63.6% were validated by precipitation estimates greater than 5 mm prior to or during the event.

Seasonally, 48.5% of potential infiltration events occurred during the wet season (November–March) across both the Souss and Tensift basins. The final month of the dry season, October, exhibited the highest percentage of events across both basins (18.2%), followed by March, April, and December (15.2%, respectively). Considered individually, both October and April, which bookend the onset and conclusion of the dry season, encompass the highest number of potential infiltration events in the Tensift basin. Within the Souss there was less concentration, with an equally high number of events in March, October, and December. Potential infiltration events within the midstream section of the Souss channel predominantly occurred during the wet season (85.7%), while upstream reaches of both systems had a larger share of dry-season events.

Table 4-5. Potential Infiltration Events based on Temperature Anomalies and Precipitation Estimates

Basin	Section	Transect	Event	Date of Initiation	Total precipitation 7-days prior (mm)	Total precipitation for duration of event (mm)
Tensift	T1: Upstream	Transect 1	1	2/15/16	1.62	39.46
			2	3/21/16	17.41	76.99
			3	4/20/16	2.09	2.46
			4	5/10/16	55.39	1.22
		Transect 2	5	9/25/22	12.12	8.10
			6	10/12/22	16.53	1.31
			7	10/16/22	14.16	9.15
			8	12/1/22	1.34	40.54
			9	4/4/23	0.00	3.58
			10	1/17/23	0.75	64.52
			11	2/23/23*	14.50	46.14
			12	5/17/23	4.30	14.47
		Transect 3	13	10/14/23	11.30	1.38
			14	12/13/23	41.39	11.43
			15	3/23/24	1.60	1.14
			16	4/26/24	7.50	20.57
	T2: Midstream	Transect 4		NA	NA	NA
Souss	S2: Upstream	Transect 5	17	6/21/22	3.36	1.12
			18	10/12/22	0.72	7.51
	S1: Upstream	Transect 6	19	6/13/22	2.36	6.28
			20	9/24/22	5.14	16.18
		Transect 7	21	10/19/23	3.76	0.81
			22	12/16/23	0.00	0.02
			23	2/9/24	21.39	21.19
			24	3/25/24	4.29	3.30
			25	3/29/24	8.46	7.02
			26	4/18/24	0.00	0.00
	S3: Midstream	Transect 8	27	10/21/2023	2.06	0.33
			28	12/1/2023	36.06	35.38
			29	12/18/23	0.00	0.00
			30	1/7/24	0.23	0.00
			31	2/9/24	21.39	21.19
			32	3/25/24	4.29	9.66
			33	4/27/24	0.00	0.00

*Note: Events highlighted in grey indicate events statistically flagged as anomalies, but which visually mimic atmospheric events due to maintenance of diurnal temperature pattern. * Event 11 was included based on visual pattern and statistical proximity to the standard cut off (z-score was in the lowest 5.5% of the data).*

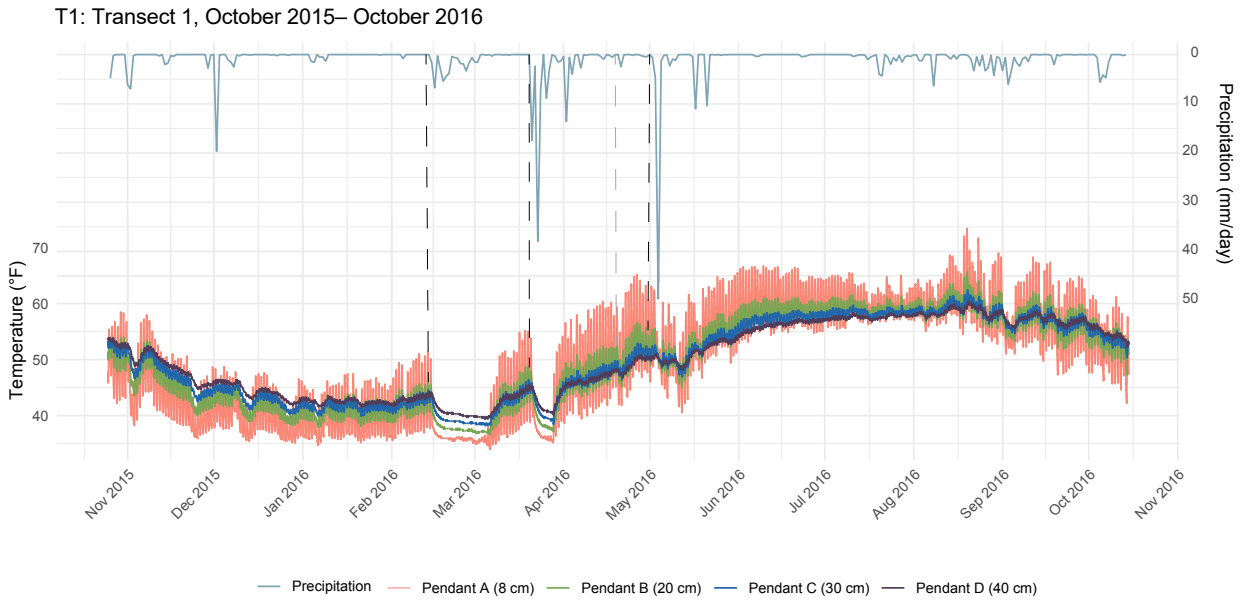

Figure 4-2. Transect 1 Thermograph, Upstream, Tensift Basin

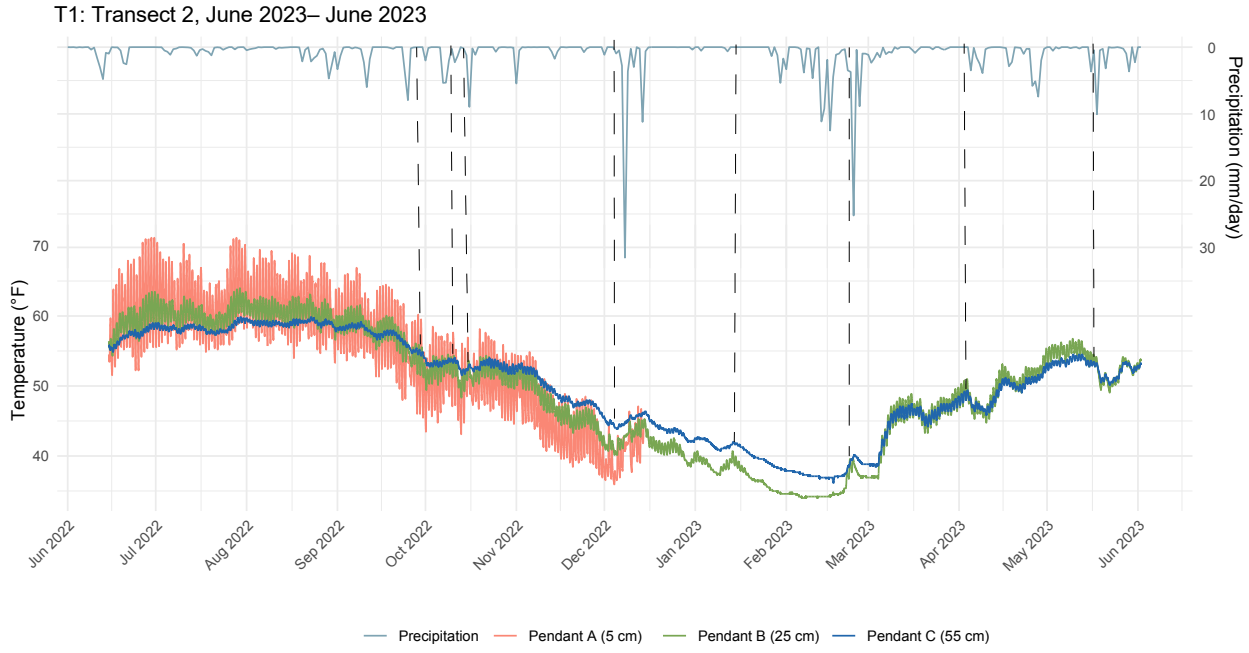

Figure 4-3. Transect 2 Thermograph, Upstream, Tensift Basin

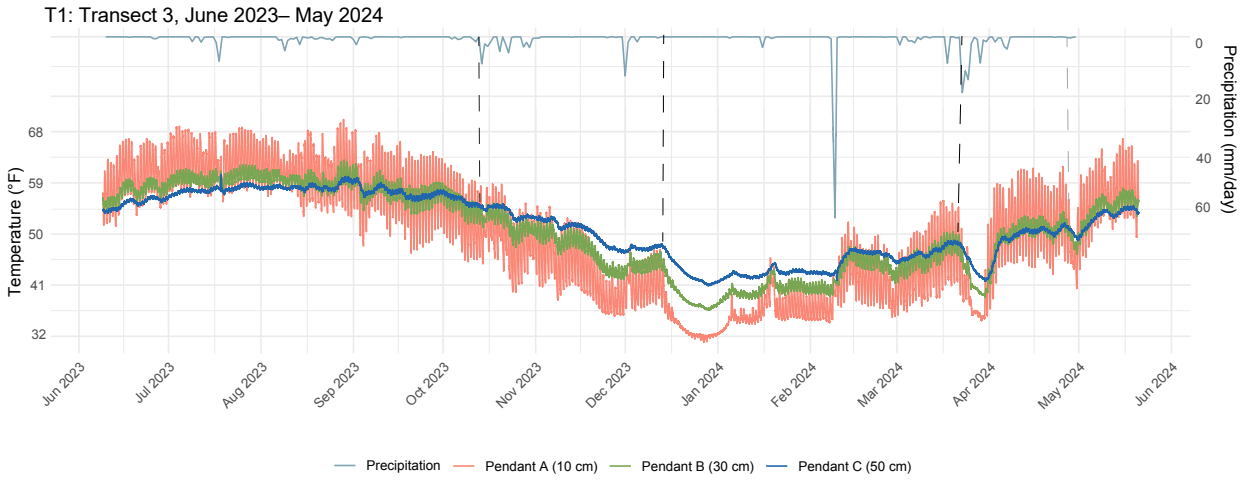

Figure 4-4. Transect 3 Thermograph, Upstream, Tensift Basin

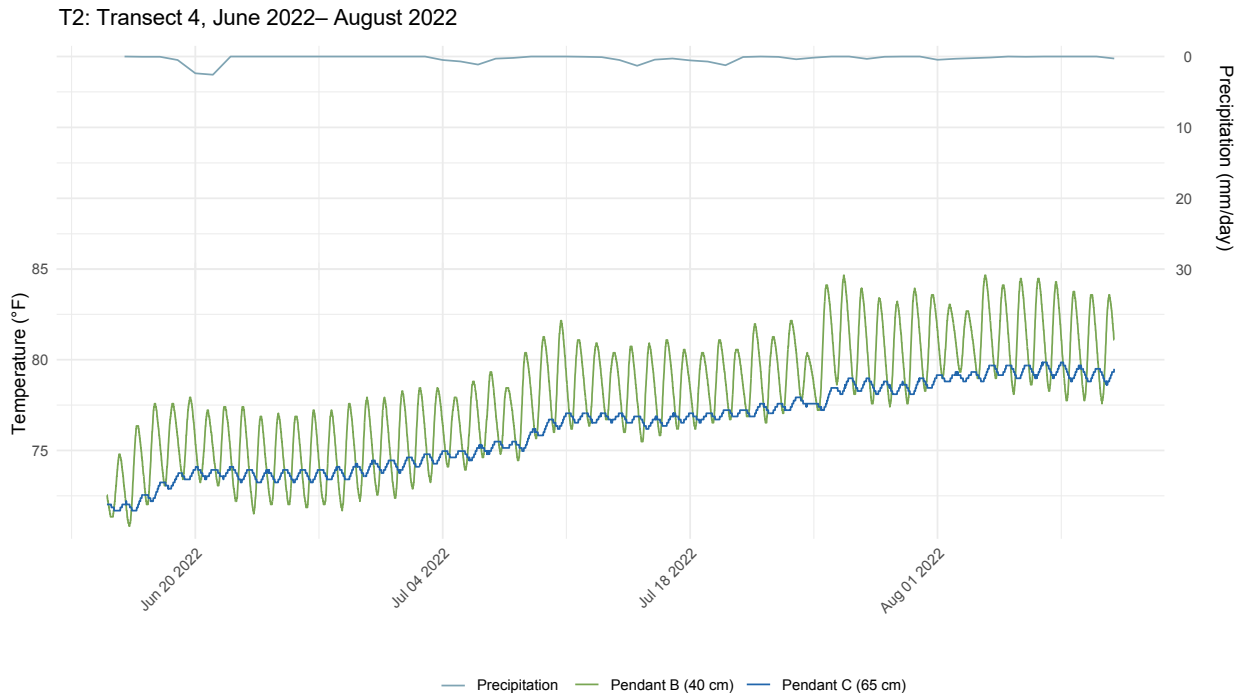

Figure 4-5. Transect 4 Thermograph, Midstream, Tensift Basin

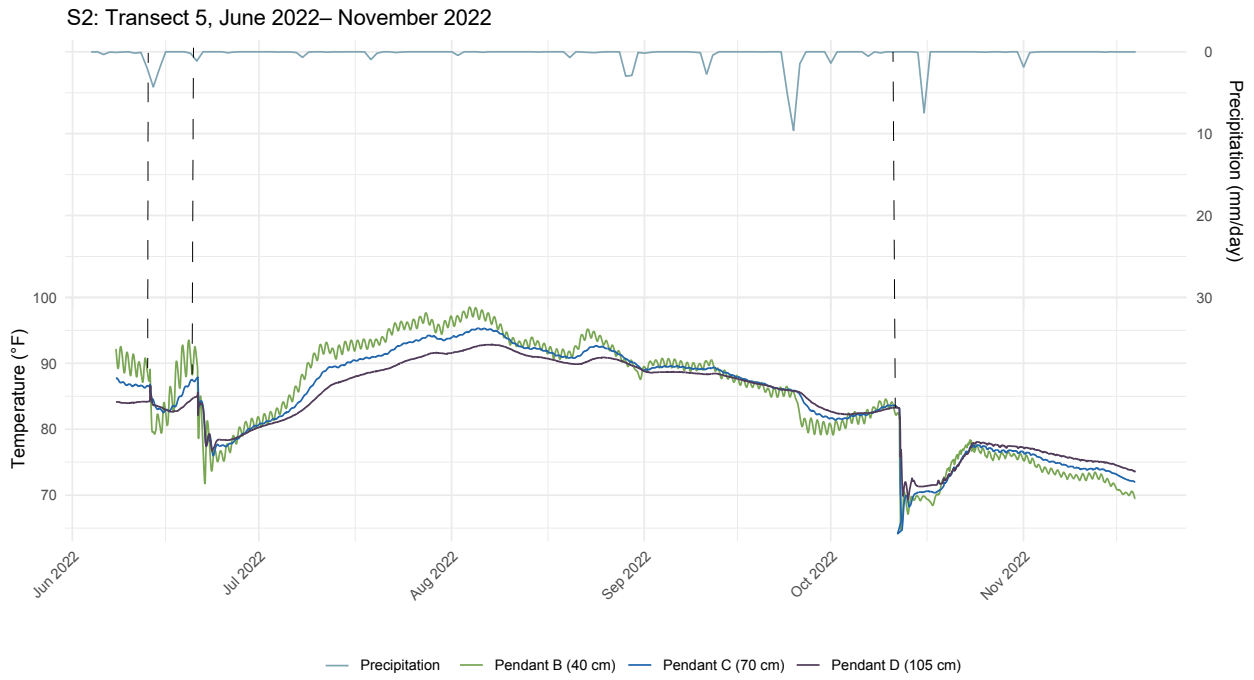

Figure 4-6. Transect 5 Thermograph, Upstream, Souss Basin

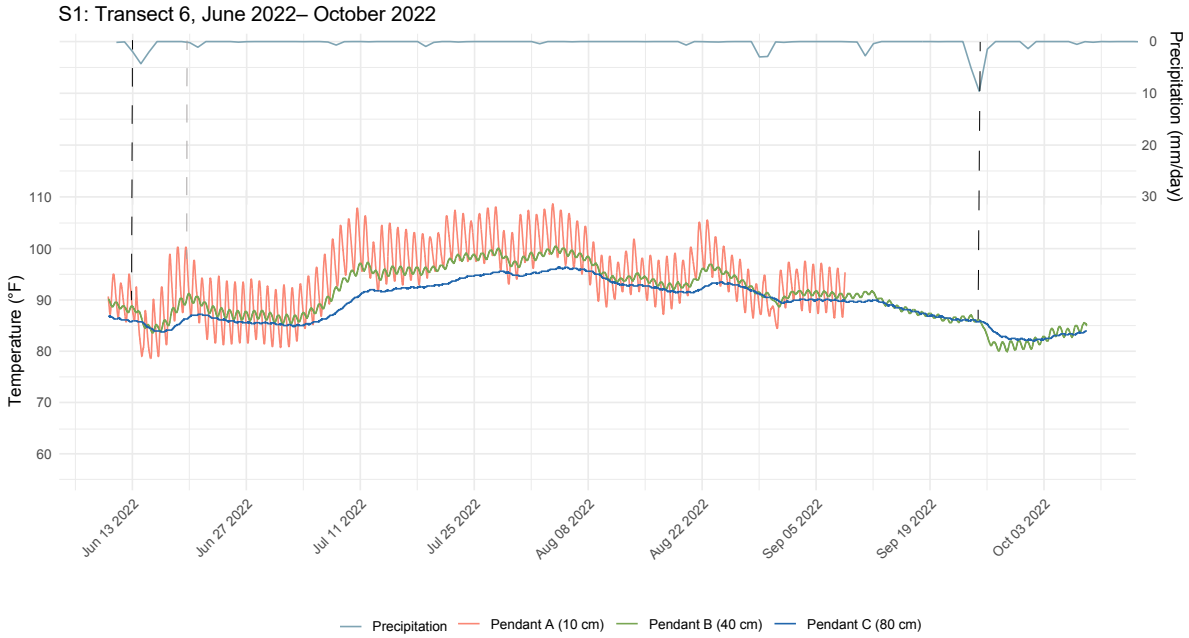

Figure 4-7. Transect 6 Thermograph, Upstream, Souss Basin

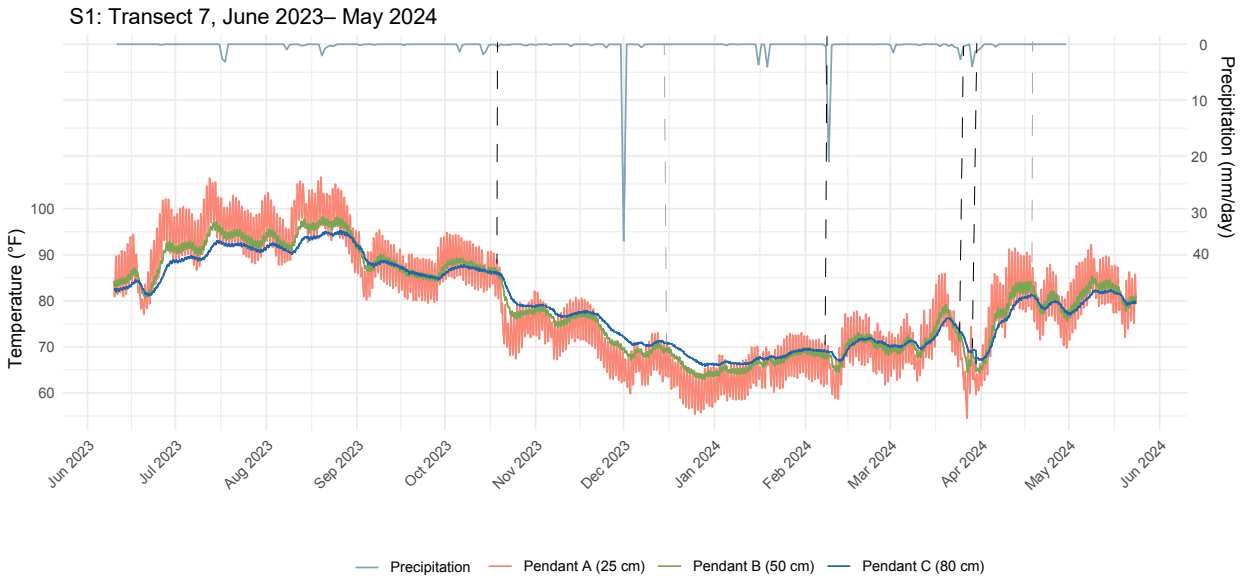

Figure 4-8. Transect 7 Thermograph, Upstream, Souss Basin

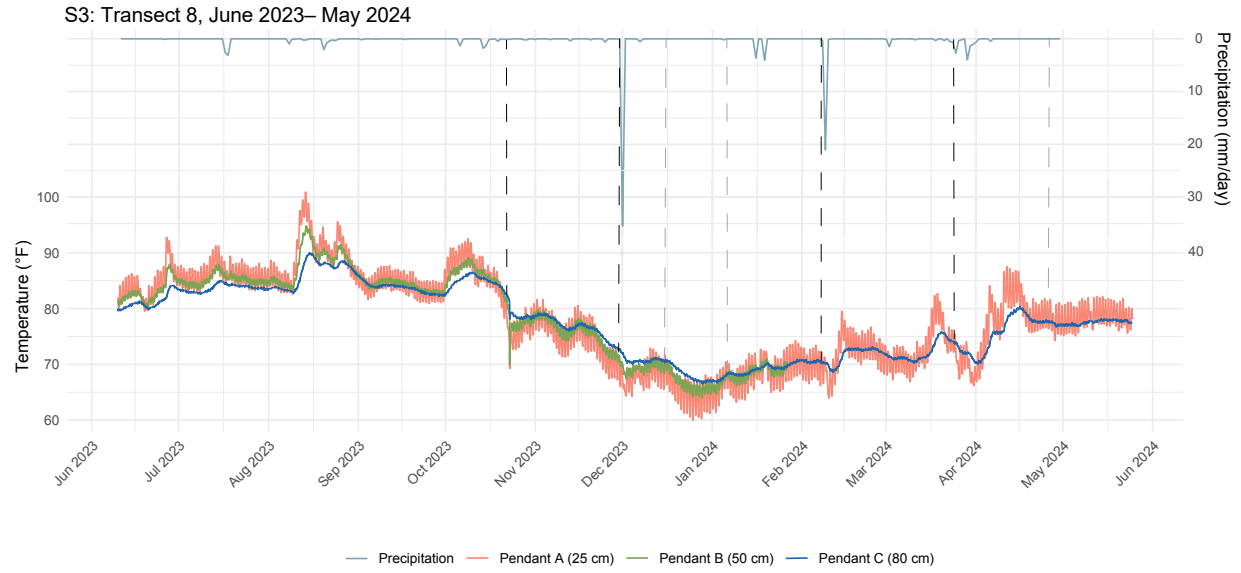

Figure 4-9. Transect 8 Thermograph, Midstream, Souss Basin

Saturated Hydraulic Conductivity and Estimated Rates of Infiltration

The Souss basin sites displayed an overall faster average rate of infiltration than the Tensift basin sites (Table 4-6). Though both locations recorded a comparable number of potential infiltration events, the Tensift basin had no record of events in its midstream section. Within the Souss basin (Table 4-7), infiltration rates slowed significantly moving from the upstream to the midstream section of the channel (13.00 cm/h vs. 6.12 cm/h), however without a comparison within the Tensift it is difficult to know if this is a consistent trend. If true, a lack of midstream events may result in an overall lower rate of average infiltration for the Tensift basin than reported.

Across transects in both basins, infiltration rate was observed to increase with vertical depth in the channel subsurface. This was particularly distinct within the Souss basin, where temperature pendants at the shallowest depth recorded infiltration rates on average 3.43 cm/h lower than those deeper. This is consistent with previous assertions that ephemeral channels commonly display finer, relatively impervious layers near the channel surface with increased coarsening with depth (Fakir et al., 2021).

Seasonally, potential events during the dry season demonstrate greater rates of infiltration than those within the wet season. However, dry-season rates display a greater range and overall variability (standard deviation of 9.88 cm/h for dry season vs. 2.60 cm/h for wet season). With the exclusion of outliers (rates >8.67 cm/h), the average rate of wet-season infiltration is marginally faster than that of the dry season events (5.19 cm/h, vs. 4.45 cm/h for dry-season events). Transect 5 specifically reported elevated rates of infiltration (30.00 cm/h and greater). This may be partially due to the larger sampling window of this sensor, which recorded

temperature measurements hourly as opposed to 15-min increments. In this transect, infiltration rates may in fact be greater, but are obscured by the coarse sampling window.

Overall, infiltration rates calculated from individual events were markedly more rapid than rates based on estimated saturated hydraulic conductivities (Table 6, Table 7). This may in part be due to the influence of the entire sediment profile on in-situ infiltration calculations, where permeability is variable with depth. Additionally, for unsaturated systems, saturated hydraulic conductivity is influenced by preexisting sediment moisture, a metric not accounted for in this value, but inherent to in-situ calculations.

Table 4-6. Estimated Rate of Infiltration: Tensift Basin

Transect	Event	Date of Initiation	Estimated Rate of Infiltration: Temperature anomaly (cm/h)				Average (cm/h)
			Pendant A	Pendant B	Pendant C	Pendant D	
Depth (cm)			8	20	30	40	
Transect 1	1	2/15/16		8.00	3.75	1.07	4.27
	2	3/21/16		8.96	5.00	4.00	5.99
	3	4/20/16		1.31	1.50	2.07	1.63
	4	5/10/16		3.43	5.99	1.76	3.73
Average				*5.43*	*4.06*	*2.23*	*3.91*
Estimated Infiltration: Saturated Hydraulic Conductivity							0.762
Depth			5	25	55		
Transect 2	5	9/25/22		4.44	3.16		3.80
	6	10/12/22		5.71	5.45		5.58
	7	10/16/22		6.67	5.00		5.83
	8	12/1/22		6.67	3.53		5.10
	9	4/4/23		X	20.00		20.00
	10	1/17/23		X	9.23		9.23
	11	2/23/23		X	2.40		2.40
	12	5/17/23		X	8.00		8.00
Average				*5.87*	*7.10*		*7.49*
Estimated Infiltration: Saturated Hydraulic Conductivity							0.762
Depth			10	30	50		
Transect 3	13	10/14/23		1.74	12.27		7.00
	14	12/13/23		4.61	1.71		3.16
	15	3/23/24		4.28	13.48		8.88
	16	4/26/24		2.50	2.92		2.71
Average				*3.28*	*7.60*		*5.44*
Estimated Infiltration: Saturated Hydraulic Conductivity							0.762

Note: 'X' indicates that a sensor ceased recording, generally due to battery failure. For Transect 2, pendant A ceased to function mid-December 2022, with subsequent data based on measurements from pendant B and C. All reported events displayed infiltration to the depth of the deepest pendant. Rows colored in grey indicate potential events occurring during the dry season; white rows to potential events during the dry season.

Table 4-7. Estimated Rate of Infiltration: Souss Basin

Transect	Event	Date of Initiation	Estimated Rate of Infiltration: Temperature anomaly (cm/h)				Average (cm/h)
			Pendant A	Pendant B	Pendant C	Pendant D	
Depth			10	40	70	105	
Transect 5	17	6/21/22		X	30.00	35.00	32.50
	18	10/12/22		X	30.00	35.00	32.50
Average					*30.00*	*35.00*	*32.50*
Estimated Infiltration: Saturated Hydraulic Conductivity							0.0125
Depth			10	40	80		
Transect 6	19	6/13/22		5.29	3.53		4.41
	20	9/24/22		X	2.08		2.08
Average				*5.29*	*2.80*		*3.25*
Estimated Infiltration: Saturated Hydraulic Conductivity							0.0958
Depth			25	50	80		
Transect 7	21	10/19/23		2.50	2.79		2.65
	22	12/16/23		3.03	2.35		2.69
	23	2/9/24		3.70	4.62		4.16
	24	3/25/24		5.00	2.73		3.87
	25	3/29/24		3.70	1.88		2.79
	26	4/18/24		3.57	3.00		3.29
Average				*3.58*	*2.89*		*3.24*
Estimated Infiltration: Saturated Hydraulic Conductivity							0.0958
Depth			25	50	80		
Transect 8	27	10/21/2023		8.33	3.64		5.99
	28	12/1/2023		5.88	17.14		11.51
	29	12/18/23		5.56	1.45		3.505
	30	1/7/24		6.67	4.00		5.335
	31	2/9/24		X	5.64		5.64
	32	3/25/24		X	4.58		4.58
	33	4/27/24		X	5.64		5.64
Average				*6.61*	*6.01*		*6.03*
Estimated Infiltration: Saturated Hydraulic Conductivity							0.1560

Note: 'X' indicates that a sensor ceased recording, generally due to battery failure. In Transect 5, pendant A displayed an instrument error and was excluded, with all reported measurements related to pendants B, C, and D. All reported events displayed infiltration to the depth of the deepest pendant. Rows colored in grey indicate potential events occurring during the dry season; white rows to potential events during the dry season.

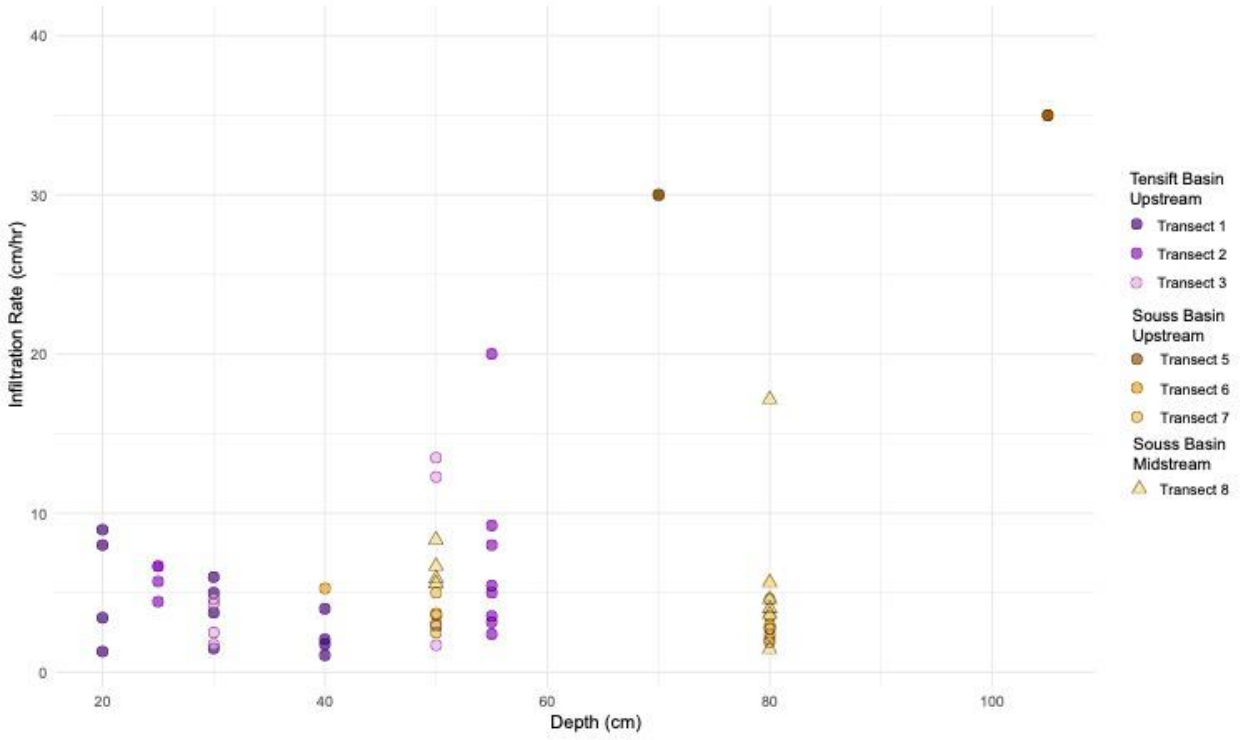

Figure 4-10. Estimated rate of infiltration by depth. Despite their marginally deeper installation, transects within the Souss basin demonstrate comparable infiltration rates. The height of the water table precluded deeper installation within the Tensift basin.

Variable Controls on Recharge

Analysis of physical variables across both basin and stream locations reinforce observed spatial variability in infiltration (Table 4-8; Figure 4-11; Appendix Chapter 4, Figure 1). Specifically, channel length was negatively correlated to saturated hydraulic conductivity, in line with observed decreases in infiltration rate moving from upstream to midstream sites. Sediment sand percentage is further negatively correlated to channel length, potentially indicating that a reduction in coarse material and increase in clay percentage may be a primary control on

declining infiltration. Broadly, elevation and maximum depth of the unconfined aquifer exert the greatest influence on distinguishing transect locations. Upstream sites within the Souss basin plotted together, but distinct from the upstream site in the Tensift basin. Midstream locations for both basins were shown to be distinct from one another, as well as upstream transect locations.

Table 4-8. PCA Output Table

	PC1	PC2	PC3
Maximum depth of unconfined aquifer (m)	**-0.403**	-0.150	-0.178
Channel width (m)	**-0.386**	-0.238	-0.115
Basin location	**-0.352**	0.224	-0.278
Sand %	-0.294	**-0.371**	0.187
Channel length (m)	-0.088	**0.506**	0.197
Clay %	-0.058	**0.524**	0.136
Location in channel	-0.053	0.183	**0.603**
Sat. hydraulic conductivity (m/s)	0.038	-0.286	**0.547**
Silt %	**0.373**	0.149	-0.288
Slope	**0.394**	-0.214	0.122
Elevation (m)	**0.410**	-0.143	-0.154

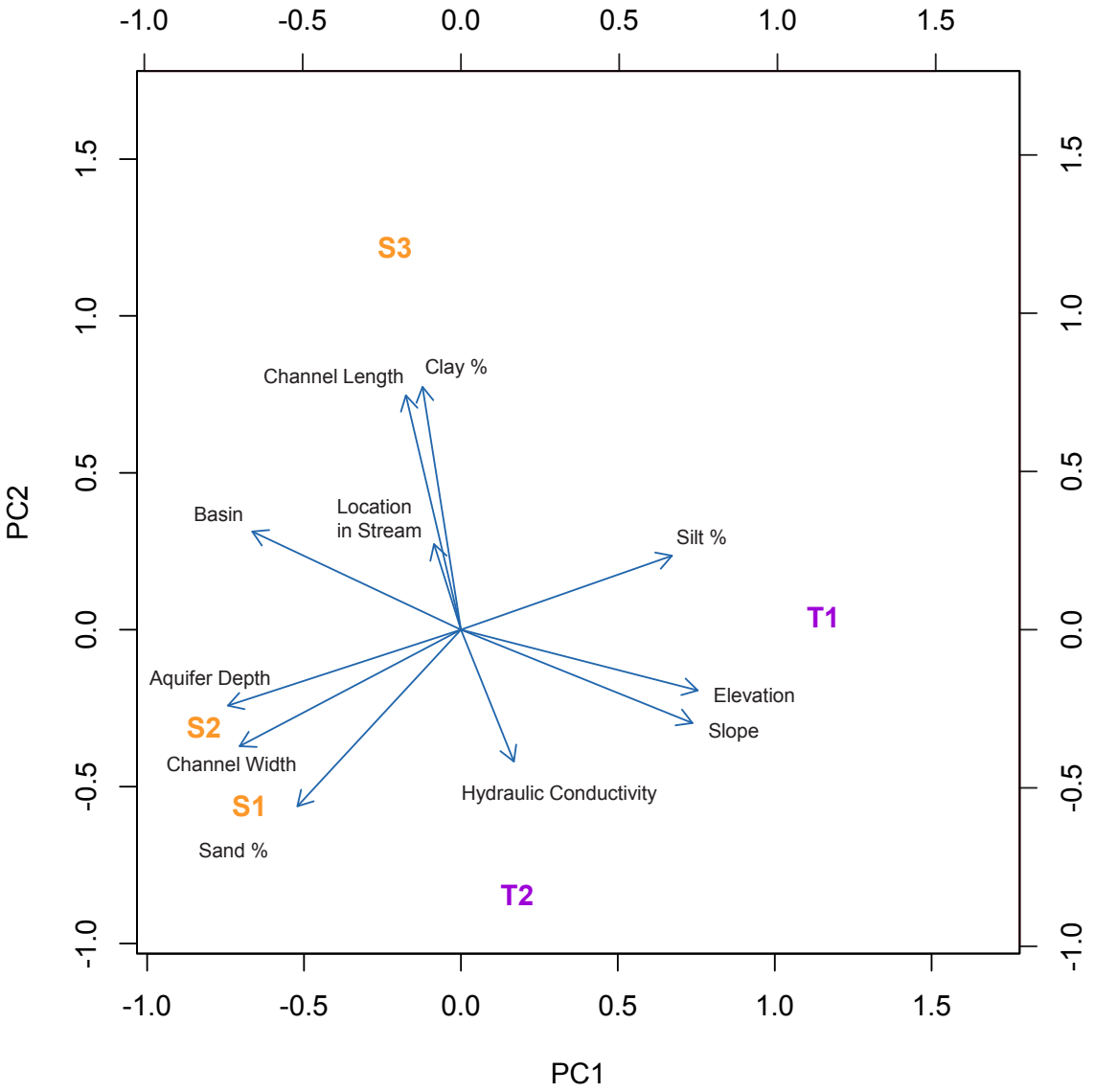

Figure 4-11. PCA Correlation Biplot of physical variables related to infiltration across transect locations. Transects within the Tensift basin (purple) and Souss basin (orange) show distinct based on basin and location in channel. S1, S2, and T1 represent upstream locations, while S3 and T2 represent the channel midstream.

4.5 Discussion

Spatial and temporal variability in transmission loss has significant implications for local groundwater recharge. Previous work on ephemeral channel infiltration has identified the importance of antecedent sediment moisture and preferential flow paths through partially saturated sediments in facilitating deeper infiltration, leading to aquifer recharge as opposed to re-evaporation (Fakir et al., 2021). This is in part supported by the understanding that saturated hydraulic conductivity may be orders of magnitude greater than unsaturated hydraulic conductivity (Elzeftawy and Cartwright, 1981). Not all infiltration events will not have equal impact on regional recharge, however their temporal variability may be crucial to prime the system for future infiltration. A spread of infiltration events across a multi-month period, and not simply concentrated within the wet season, has the potential to increase antecedent sediment moisture during drier periods of the year and allow for meaningful infiltration outside of the wet season (e.g., Transect 1, Transect 3).

High-elevation and upstream channel locations generally receive more precipitation than those within the midstream or on the plain. This supports the observation of increased infiltration events in high-elevation and upstream locations, which have the necessary moisture to facilitate them. It may additionally suggest that when infiltration events do occur, they lead to deeper vertical movement and aquifer recharge, producing anomalies which can statistically be identified. Indeed, visual analysis of all transect thermographs indicate many small perturbations, particularly in pendants nearest the surface. Whether this variability is a result of atmospheric events being detected in unsaturated sediments, or minor infiltration events that are re-evaporated, requires further study. Future work is necessary to quantify infiltration events which

do not continue to move deeper and work to disentangle potential barriers preventing further infiltration.

Though hydraulic conductivity estimates serve as a useful comparison, they may not represent a true analog for infiltration rates within the subsurface. This is due to the in-situ reality of sediment heterogeneity and sorting, both vertically and laterally. Sediment samples were collected from depth and may fail to represent saturated hydraulic conductivity in the near surface. The inherent impact of instrument installation, which despite best efforts may result in some degree of preferential pathways, may further serve to increase local rates of infiltration. Despite these concerns, saturated hydraulic conductivity values from sediment analysis were comparable to those reported within the literature (Fakir et al., 2021; Hssaisoune et al., 2021).

Future work to understand transmission loss variability across ephemeral systems must work to better constrain pre-existing moisture in the subsurface and quantify its seasonal variability. The addition of streamflow gaging equipment would be further useful to quantify the lag between channel flow and initiation of infiltration. This is particularly interesting because of the presence of a near-surface, low-permeability layer which may cause initial infiltration to be slower than in situ observations at depth. Additional work is needed to better appreciate the role of this layer, and whether it hinders initial infiltration during surface flow or acts as a barrier to re-evaporation. Finally, prior work has referenced, but not explored, the potential contribution of lateral infiltration (Fakir et al., 2021). This may be significant in its contribution to antecedent sediment moisture and increased rates of infiltration. Though not the focus of this study, the horizontal installation of sites S1 and S2 within the upstream section of the Souss basin indicates the potential contribution of lateral infiltration. Specifically, Transect 6, located in the center of the channel at site S1, identified potential infiltration on June 13 2022 and September 24 2022.

Events were flagged in Transect 5, located on the left bank of the channel at site S2, approximately 50 meters away, on June 21 2022, (8 days later) and October 12 2022, (18 days later). Transect 5 had rates of infiltration (average 32.5 cm/h) significantly greater than those observed throughout other transects in the study, including Transect 6 (average 3.25 cm/h). This may suggest that surface flow within the channel was initially more focused, before expanding laterally with greater discharge to reach Transect 5 near the bank over a period of days. This lag may additionally suggest that surface flow itself did not expand, but that subsurface infiltration moved laterally, which may account for the near simultaneous occurrence of moisture at all depths in Transect 5. These infiltration events occurred during the dry season, when antecedent sediment moisture was presumed to be minimal. In the following year, Transect 7 (installed in the same location in the channel center) recorded comparable rates of infiltration as in Transect 6.

4.6 Conclusions

Within ephemeral channels, improved understanding of transmission loss informs estimates of regional groundwater recharge and supports sustainable management. This is particularly important in water-scarce, arid systems which lack sufficient stream gaging and groundwater monitoring infrastructure. Across central Morocco, subsurface temperature probes were installed in vertical transects beneath two ephemeral channels to improve our understanding of spatial and temporal variability in transmission loss. Thermographs recorded over multiple years identified 33 potential infiltration events across both wet and dry seasons. Patterns of infiltration highlight the potential role of pre-existing sediment moisture in facilitating rapid infiltration for sustained groundwater recharge. They further suggest the role of near-surface

sediments in both constraining and augmenting vertical infiltration. Within each basin, infiltration rates were observed to decrease with distance downstream, while infiltration was shown to accelerate with increased depth. Sites on the alluvial plain of the Souss basin demonstrated faster rates of infiltration than sites in the high-elevation mountain front of the Tensift basin. In data-limited systems, expanded understanding of local controls on transmission loss processes has the potential to improve current and future estimates of groundwater recharge, particularly within arid basins vulnerable to changing climate.

4.7 References

Ait Brahim, Y., Seif-Ennasr, M., Malki, M., N'da, B., Choukrallah, R., El Morjani, Z.E.A., Sifeddine, A., Abahous, H., and Bouchaou, L., 2017, Assessment of Climate and Land Use Changes: Impacts on Groundwater Resources in the Souss-Massa River Basin, *in* Choukr-Allah, R., Ragab, R., Bouchaou, L., and Barceló, D. eds., The Souss-Massa River Basin, Morocco, Cham, Springer International Publishing, The Handbook of Environmental Chemistry, p. 121–142, doi:10.1007/698_2016_71.

Ait Hssaine, A., and Bridgland, D., 2009, Pliocene–Quaternary fluvial and aeolian records in the Souss Basin, southwest Morocco: A geomorphological model: Global and Planetary Change, v. 68, p. 288–296, doi:10.1016/j.gloplacha.2009.03.002.

Alaoui Haroni, S., Alifriqui, M., and Simonneaux, V., 2009, Recent dynamics of the wet pastures at Oukaimeden plateau (High Atlas mountains, Morroco): Biodiversity and Conservation, v. 18, p. 167–189, doi:10.1007/s10531-008-9465-6.

Almulla, Y., Ramirez, C., Joyce, B., Huber-Lee, A., and Fuso-Nerini, F., 2022, From participatory process to robust decision-making: An Agriculture-water-energy nexus analysis for the Souss-Massa basin in Morocco: Energy for Sustainable Development, v. 70, p. 314–338, doi:10.1016/j.esd.2022.08.009.

Ayt Ougougdal, H., Khebiza, M.Y., Messouli, M., Bounoua, L., and Karmaoui, A., 2020, Delineation of vulnerable areas to water erosion in a mountain region using SDR-InVEST model: A case study of the Ourika watershed, Morocco: Scientific African, v. 10, p. e00646, doi:10.1016/j.sciaf.2020.e00646.

Bell, B., Hughes, P., Fletcher, W., Cornelissen, H., Rhoujjati, A., Hanich, L., and Braithwaite, R., 2022, Climate of the Marrakech High Atlas, Morocco: Temperature lapse rates and precipitation gradient from piedmont to summits: Arctic, Antarctic, and Alpine Research, v. 54, p. 78–95, doi:10.1080/15230430.2022.2046897.

Blasch, K., Ferré, T.P.A., Hoffmann, J., Pool, D., Bailey, M., and Cordova, J., 2004, Processes controlling recharge beneath ephemeral streams in southern Arizona, *in* Hogan, J.F., Phillips, F.M., and Scanlon, B.R. eds., Water Science and Application, Washington, D. C., American Geophysical Union, v. 9, p. 69–76, doi:10.1029/009WSA05.

Bouchaou, L., Michelot, J.L., Vengosh, A., Hsissou, Y., Qurtobi, M., Gaye, C.B., Bullen, T.D., and Zuppi, G.M., 2008, Application of multiple isotopic and geochemical tracers for investigation of recharge, salinization, and residence time of water in the Souss–Massa aquifer, southwest of Morocco: Journal of Hydrology, v. 352, p. 267–287, doi:10.1016/j.jhydrol.2008.01.022.

Bouchaou, L., Tagma, T., Boutaleb, S., Hssaisoune, M., and El Morjani, Z.E.A., 2011, Climate change and its impacts on groundwater resources in Morocco: The case of the Souss-Massa basin, *in* Climate Change Effects on Groundwater Resources: A Global Synthesis of Findings and Recommendations, p. 129–144.

Bouimouass, H., Fakir, Y., Tweed, S., and Leblanc, M., 2020, Groundwater recharge sources in semiarid irrigated mountain-fronts: Hydrological Processes, v. 34, p. 1598–1615, doi:10.1002/hyp.13685.

Bouimouass, H., Tweed, S., Marc, V., Fakir, Y., Sahraoui, H., and Leblanc, M., 2024, The importance of mountain-block recharge in semiarid basins: An insight from the High-Atlas, Morocco: Journal of Hydrology, v. 631, p. 130818, doi:10.1016/j.jhydrol.2024.130818.

Bouragba, L., Mudry, J., Bouchaou, L., Hsissou, Y., Krimissa, M., Tagma, T., and Michelot, J.L., 2011, Isotopes and groundwater management strategies under semi-arid area: Case of the Souss upstream basin (Morocco): Applied Radiation and Isotopes, v. 69, p. 1084–1093, doi:10.1016/j.apradiso.2011.01.041.

Cataldo, J.C., Behr, C., Monalto, F.A., and Pierce, R.J., 2013, Prediction of Transmission Losses in Ephemeral Streams, Western U.S.A: The Open Hydrology Journal, v. 4, p. 19–34, doi:10.2174/1874378101004010019.

Choukr-Allah, R., Ragab, R., Bouchaou, L., and Barcelo, D., 2016, The Souss-Massa River Basin, Morocco: Cham, Springer International Publishing, The Handbook of Environmental Chemistry, doi:10.1007/978-3-319-51131-3

Constantz, J., 2008, Heat as a tracer to determine streambed water exchanges: Water Resources Research, v. 44, doi:10.1029/2008WR006996.

Constantz, J., Stonestorm, D., Stewart, A.E., Niswonger, R., and Smith, T.R., 2001, Analysis of streambed temperatures in ephemeral channels to determine streamflow frequency and duration: Water Resources Research, v. 37, p. 317–328, doi:10.1029/2000WR900271.

Constantz, J., and Thomas, C.L., 1997, Stream bed temperature profiles as indicators of percolation characteristics beneath arroyos in the Middle Rio Grande Basin, USA:

Hydrological Processes, v. 11, p. 1621–1634, doi:10.1002/(SICI)1099-1085(19971015)11:12<1621::AID-HYP493>3.0.CO;2-X.

Costigan, K.H., Jaeger, K.L., Goss, C.W., Fritz, K.M., and Goebel, P.C., 2016, Understanding controls on flow permanence in intermittent rivers to aid ecological research: integrating meteorology, geology and land cover: Integrating Science to Understand Flow Intermittence: Ecohydrology, v. 9, p. 1141–1153, doi:10.1002/eco.1712.

Daoudi, L., and Saidi, M.E., 2008, Floods in a Semi-arid zone: Example of the Ourika (High Atlas of Marrakech, Morocco) International Scientific Journal for Alternative Energy and Ecology. ISJAEE, v. 5, p. 117–123.

Datry, T., Larned, S.T., and Tockner, K., 2014, Intermittent Rivers: A Challenge for Freshwater Ecology: BioScience, v. 64, p. 229–235, doi:10.1093/biosci/bit027.

Davidson, L., Milewski, A., and Holland, S., 2023, Quantifying Intermittent Flow Regimes in Ungauged Basins: Optimization of Remote Sensing Techniques for Ephemeral Channels Using a Flexible Statistical Classification: Remote Sensing, v. 15, p. 5672, doi:10.3390/rs15245672.

Delcaillau, B., Laville, E., Amhrar, M., Namous, M., Dugué, O., and Pedoja, K., 2010, Quaternary evolution of the Marrakech High Atlas and morphotectonic evidences of the Tizi N'Test Fault activity, Morocco: Geomorphology, v. 118, p. 262–279, doi:10.1016/j.geomorph.2010.01.006.

Di Ciacca, A., Wilson, S., Kang, J., and Wöhling, T., 2023, Deriving transmission losses in ephemeral rivers using satellite imagery and machine learning: Hydrology and Earth System Sciences, v. 27, p. 703–722, doi:10.5194/hess-27-703-2023.

Dindane, K., Bouchaou, L., Hsissou, Y., and Krimissa, M., 2003, Hydrochemical and isotopic characteristics of groundwater in the Souss Upstream Basin, southwestern Morocco: Journal of African Earth Sciences, v. 36, p. 315–327, doi:10.1016/S0899-5362(03)00050-2.

Elzeftawy, A., and Cartwright, K., 1981, Evaluating the Saturated and Unsaturated Hydraulic Conductivity of Soils, *in* Permeability and Groundwater Contaminant Transport, ASTM International100 Barr Harbor Drive, PO Box C700, West Conshohocken, PA 19428-2959, p. 168–181, doi:10.1520/STP28323S.

Eng, K., Wolock, D.M., and Dettinger, M.D., 2016, Sensitivity of Intermittent Streams to Climate Variations in the USA: River Research and Applications, v. 32, p. 885–895, doi:10.1002/rra.2939.

Fakir, Y., Bouimouass, H., and Constantz, J., 2021, Seasonality in Intermittent Streamflow Losses Beneath a Semiarid Mediterranean Wadi: Water Resources Research, v. 57, doi:10.1029/2021WR029743.

Freeze, R.A., and Cherry, J.A., 1979, Groundwater: Prentice-Hall, v. 63.

Gaur, M., and Squires, V., 2018, Geographic Extent and Characteristics of the World's Arid Zones and Their Peoples, *in* Climate Variability Impacts on Land Use and Livelihoods in Drylands, p. 3–20, doi:10.1007/978-3-319-56681-8_1.

Hssaisoune, M., Bouchaou, L., Matsumoto, T., Araguas, L., Kraml, M., and Aggarwal, P., 2019, New evidences on groundwater dynamics from the Souss-Massa system (Morocco): Insights gained from dissolved noble gases: Applied Geochemistry, v. 109, p. 104395, doi:10.1016/j.apgeochem.2019.104395.

Hssaisoune, M., Boutaleb, S., Benssaou, M., Bouaakkaz, B., Bouchaou, L., 2016b. Physical geography, geology, and water resource availability of the souss-massa River Basin, in: Choukr-Allah et al. (Ed.), Handbook of Environmental Chemistry. Springer International Publishing Switzerland 2016, pp. 1–12. https://doi.org/DOI 10.1007/ 698_2016_68

Hssaisoune, M.; Bouchaou, L.; N'Da, B.; Malki, M.; Abahous, H.; Fryar, A.E., 2017. Isotopes to assess sustainability of overexploited groundwater in the Souss–Massa system (Morocco): *Isot. Environ. Health Stud, v. 53*, p. 298–312. https://doi.org/10.1080/10256016.2016.1254208

Hssaisoune, M., Boutaleb, S., Tagma, T., Benssaou, M., Beraaouz, M., Karaoui, I., and Bouchaou, L., 2021, Geophysical data revealing the control of geological structures in the El Gouna springs in Souss river valley in Morocco: Groundwater for Sustainable Development, v. 15, p. 100669, doi:10.1016/j.gsd.2021.100669.

Jadoon, K.Z., Al-Mashharawi, S., Hanafy, S.M., and Schuster, G.T., 2016, Anthropogenic-Induced Changes in the Mechanism of Drylands Ephemeral Stream Recharge, Western Saudi Arabia: Water, v. 8, p. 136, doi:https://doi.org/10.3390/w8040136.

Jaeger, K., Sando, R., McShane, R.R., Dunham, J.B., Hockman-Wert, D., Kaiser, K., Hafen, K., Risley, J.C., and Blasch, K., 2018, Probability of Streamflow Permanence Model (PROSPER): A spatially continuous model of annual streamflow permanence throughout the Pacific Northwest: Journal of Hydrology X, v. 2, p. 100005, doi:10.1016/j.hydroa.2018.100005.

Jarlan, L. et al., 2015, Remote Sensing of Water Resources in Semi-Arid Mediterranean Areas: the joint international laboratory TREMA: International Journal of Remote Sensing, v. 36, p. 4879–4917, doi:10.1080/01431161.2015.1093198.

Kozeny, J., 1927, Über kapillare Leitung des Wassers im Boden: Sitzungsberichte der Akademie der Wissenschaften in Wien, v. 136, p. 271.

Lever, J., Krzywinski, M., and Altman, N., 2017, Principal component analysis: Nature Methods, v. 14, p. 641–642, doi:10.1038/nmeth.4346.

Markovich, K.H., Manning, A.H., Condon, L.E., and McIntosh, J.C., 2019, Mountain-Block Recharge: A Review of Current Understanding: Water Resources Research, v. 55, p. 8278–8304, doi:10.1029/2019WR025676.

Modeste, M., Abdellatif, K., Nadia, M., and Zhang, H., 2016, Impact of Land Use and Vegetation Cover on Risks of Erosion in the Ourika Watershed (Morocco): American Journal of Engineering Research.

Ouassanouan, Y., Fakir, Y., Simmonneaux, V., and Kharrou, H., 2022, Multi-decadal analysis of water resources and agricultural change in a Mediterranean semiarid irrigated piedmont

under water scarcity and human interaction: The Science of The Total Environment, v. 834, doi:10.1016/j.scitotenv.2022.155328.

Partington, D., Shanafield, M., and Turnadge, C., 2021, A Comparison of Time-Frequency Signal Processing Methods for Identifying Non-Perennial Streamflow Events From Streambed Surface Temperature Time Series: Water Resources Research, v. 57, p. e2020WR028670, doi:10.1029/2020WR028670.

Pascon P., 1978. Le Haouz de Marrakech: Revue française de sociologie, v. 19-4, p. 620-623.

Portoghese, I., Brigida, S., Masciale, R., and Passarella, G., 2022, Assessing Transmission Losses through Ephemeral Streams: A Methodological Approach Based on the Infiltration of Treated Effluents Released into Streams: Water, v. 14, p. 3758, doi:10.3390/w14223758.

Rawls, W.J., Gimenez, D., and Grossman, R., 1998, use of soil texture, bulk density, and slope of the water retention curve to predict saturated hydraulic conductivity: v. 41, p. 983–988, doi:10.13031/2013.17270.

Rhoujjati, N., Hanich, L., Bouchaou, L., Patris, N., N'da, A.B., and Chehbouni, A., 2021, Isotopic tracers to assess the snowmelt contribution to the groundwater recharge: a case from the Moroccan High and Middle Atlas Mountains: Arabian Journal of Geosciences, v. 14, p. 2611, doi:10.1007/s12517-021-08737-1.

Richards, D.F., and Milewski, A., 2022, Coastal Dryland Subsidence Detection Using Interferometric Synthetic Aperture Radar (InSAR): v. 2022, p. G42D-0247.

Saouabe, T., El Khalki, E.M., Saidi, M.E.M., Najmi, A., Hadri, A., Rachidi, S., Jadoud, M., and Tramblay, Y., 2020, Evaluation of the GPM-IMERG Precipitation Product for Flood Modeling in a Semi-Arid Mountainous Basin in Morocco: Water, v. 12, p. 2516, doi:10.3390/w12092516.

Shanafield, M., and Cook, P.G., 2014, Transmission losses, infiltration and groundwater recharge through ephemeral and intermittent streambeds: A review of applied methods: Journal of Hydrology, v. 511, p. 518–529, doi:10.1016/j.jhydrol.2014.01.068.

Shawky, M., Moussa, A., Hassan, Q.K., and El-Sheimy, N., 2019, Performance Assessment of Sub-Daily and Daily Precipitation Estimates Derived from GPM and GSMaP Products over an Arid Environment: Remote Sensing, v. 11, p. 2840, doi:10.3390/rs11232840.

Taheri, S., Ghomeshi, S., and Kantzas, A., 2017, Permeability calculations in unconsolidated homogeneous sands: Powder Technology, v. 321, p. 380–389, doi:10.1016/j.powtec.2017.08.014.

Zhou, Z.-G., and Tang, P., 2016, Continuous anomaly detection in satellite image time series based on Z-scores of Season-Trend model Residuals, *in* 2016 IEEE International Geoscience and Remote Sensing Symposium (IGARSS), p. 3410–3413, doi:10.1109/IGARSS.2016.7729881.

CHAPTER 5

CONCLUSIONS

Broadly, flow intermittency is expanding into previously perennial channels, and becoming more extreme in presently ephemeral systems. This is primarily thought to be driven by climate shifts to overall reduced total precipitation and increasingly sporadic events in arid environments. Dryland systems historically have strongly been defined by seasonality of precipitation, but such shifts are eroding these boundaries. This work broadly underscores the role of wet season moisture and its timing in controlling stream intermittency. The wet season, commonly October– April in arid regions, was identified at both the continental and basin scale as having a significant contribution to intermittent flow and associated infiltration. Across CONUS, precipitation which occurred at the onset or cessation of the wet season was observed to exert the largest control on developing intermittency throughout the year. In representative basins in Morocco, wet season precipitation was further identified as driving the majority of potential recharge events in both mountain front and plains recharge zones. Despite an observed expansion of intermittency at the continental, basin, and field scale, maintenance of flow events during the wet season indicates the potential for sustained patterns of groundwater recharge. This underscores the need for future work to further prioritize the characterization of wet season phenomena and local climate patterns. Advancements in flow identification through the application of DFA and remote sensing show promise for surface flow characterization in data scarce systems, but further breakthroughs are necessary to quantify precipitation total, intensity, and temporal and spatial distribution in systems which lack gaging.

Across all scales, intermittent channels present challenges to characterization. Flow intermittency can be heterogenous both spatially and temporally, with channels displaying a combination of both localized flow and dry sections. As a result, observations of flow intermittency can be spatially dependent. Within gaged systems, the characterization of intermittency relies on the alignment of channel dry sections with gage locations. This was particularly relevant to work at the continental scale, which prioritized broad characterizations of flow to understand dominant regional trends. Within ungaged systems at both the basin and field scale, lack of gage data presented a challenge to validation of localized surface conditions and limited finer resolution distinctions in intermittency.

Future work focused on the details of flow seasonality, particularly the variability of wet and dry season onset and duration, will further clarify our understanding of temporal and spatial flow variability, and sustained groundwater recharge. Paired with improved satellite imagery and recharge estimates, research outcomes have the potential to refine management decision making, particularly in water-limited environments faced with an uncertain climate future.

APPENDICES

APPENDIX, CHAPTER TWO

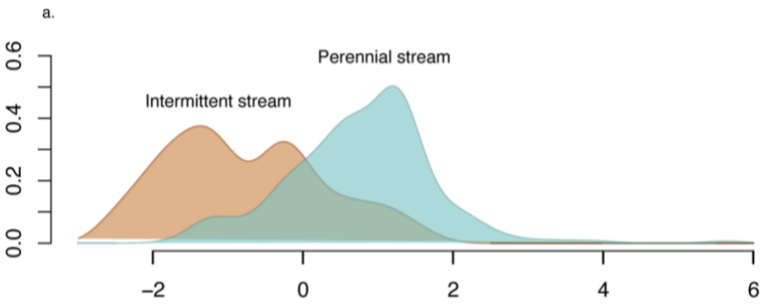

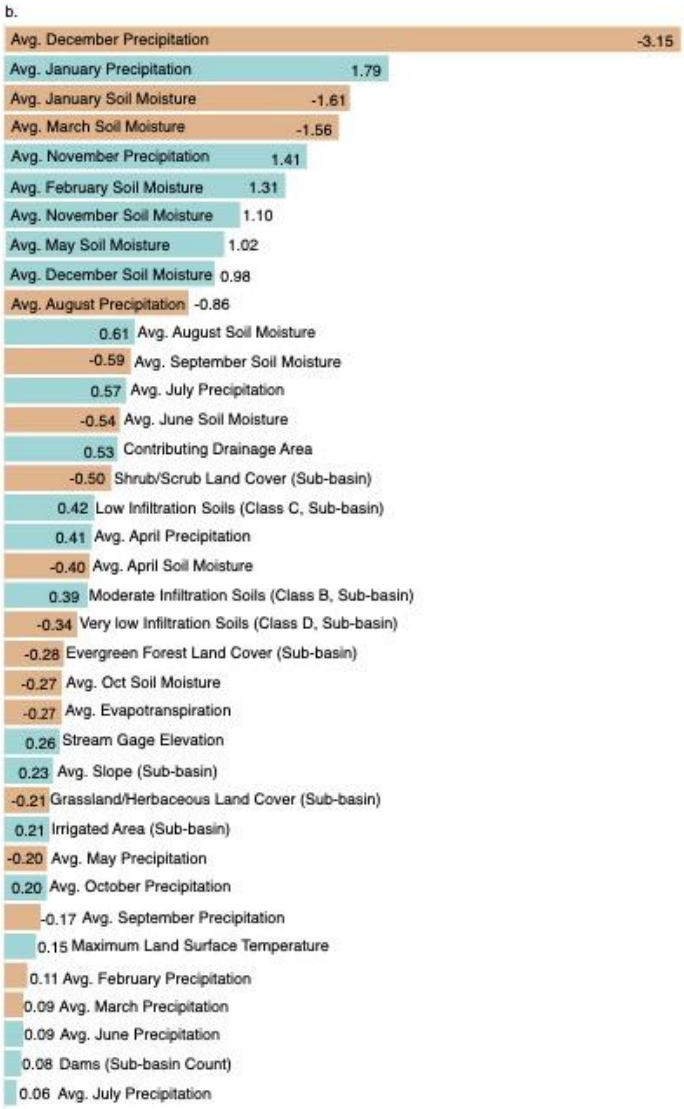

Appendix Chapter 2, Figure 1. DFA Analysis. (a) Graphical distribution of DFA analysis for intermittent vs. perennial streams. Distinct groupings and tight within-group distribution indicates effective group separation by the linear function. (b) DFA loadings for 33 variables. Largest values indicate greatest contribution and variable color marks group correlation.

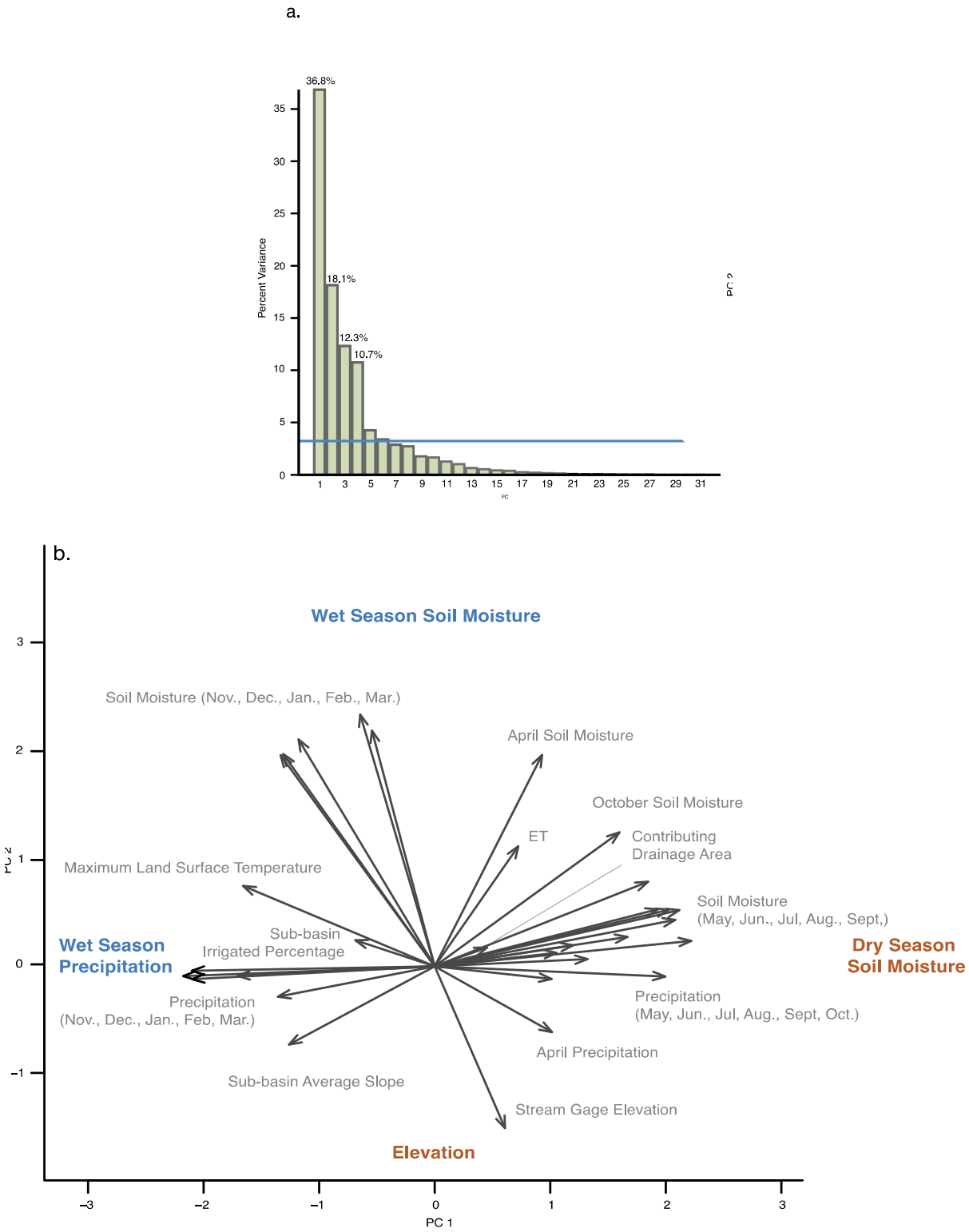

Appendix Chapter 2, Figure 2. PCA Analysis. (a) Principal components explain 78.1% of data variance, and (b) relationships between variables demonstrate distinct seasonal groupings.

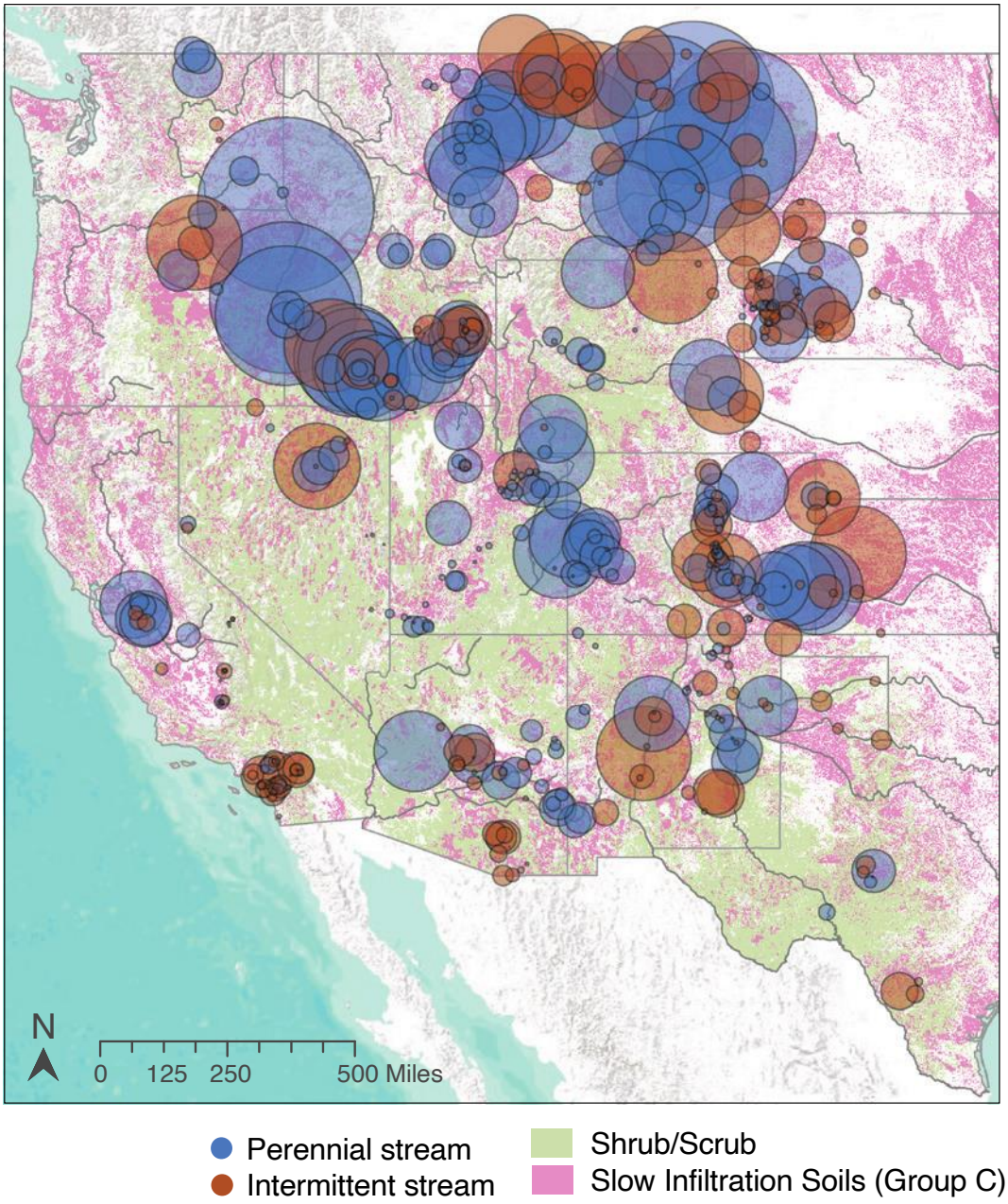

Appendix Chapter 2, Figure 3. Non-climate variables exert minor controls on stream intermittency. Contributing basin drainage area (displayed as gage size), and sub-basins dominated by shrub/scrub and slow infiltration soils display subtle correlation to group distinction. Intuitively, perennially streams are observed to correlate to greater contributing drainage areas than intermittent systems.

APPENDIX, CHAPTER THREE

Appendix Chapter 3, Table 1. Pixel comparison across training and test imagery.

Training DFA	3200 Pixels (1600 Water, 1600 Non-Water)
Upstream section	23,741 pixels
Midstream section	137,056 pixels
Downstream section	45,598 pixels

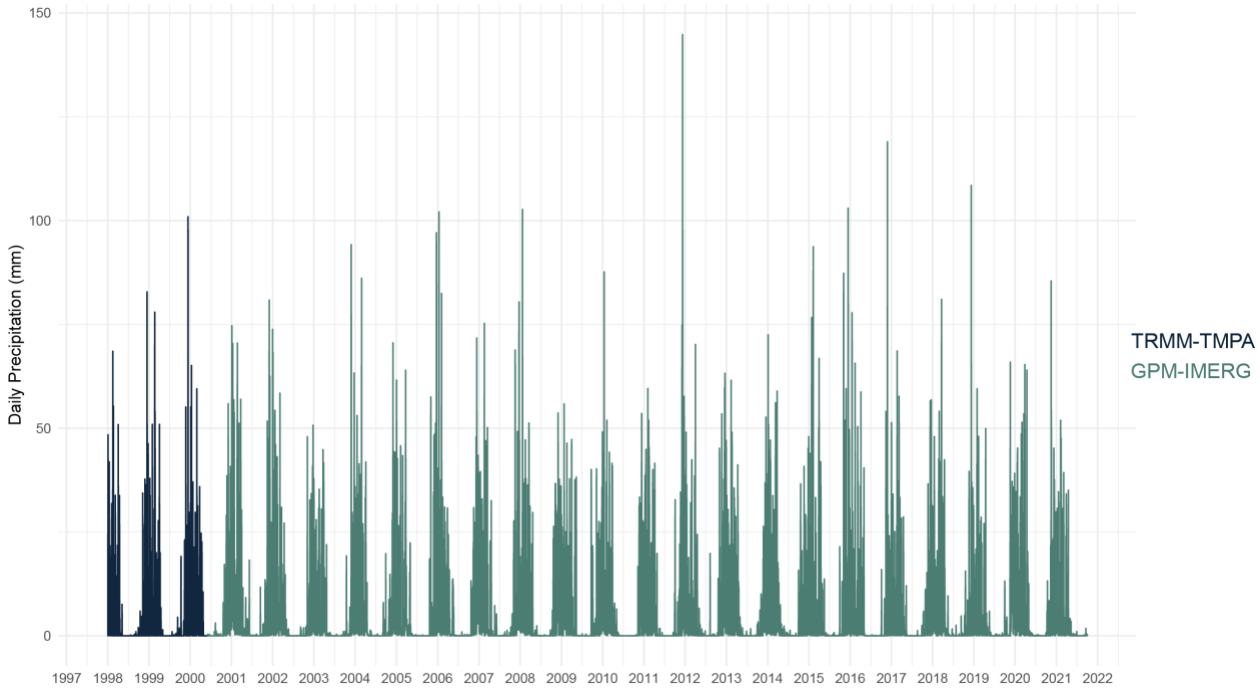

Appendix Chapter 3, Figure 1. Average daily precipitation as estimated by the TRMM and GPM satellites, across the upstream section of the Souss channel. Due to its improved estimation capabilities, GPM-IMERG data were prioritized over TRMM-TMPA data, beginning in 2000.

APPENDIX, CHAPTER 4

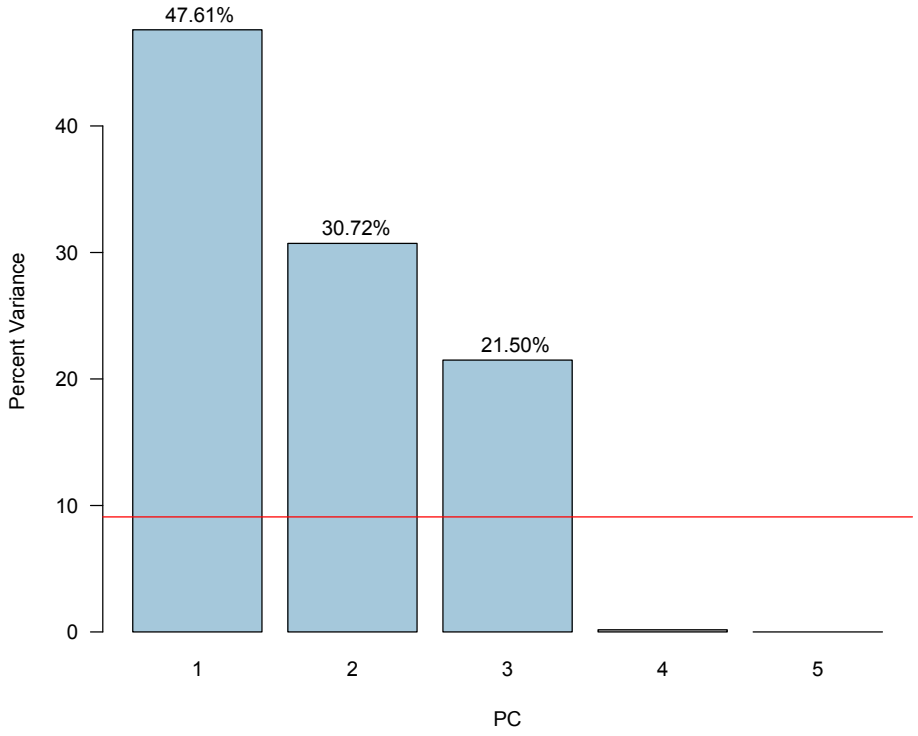

Appendix Chapter 4, Figure 1. PCA Analysis scree plot, principal components explain 99.82% of data variance.

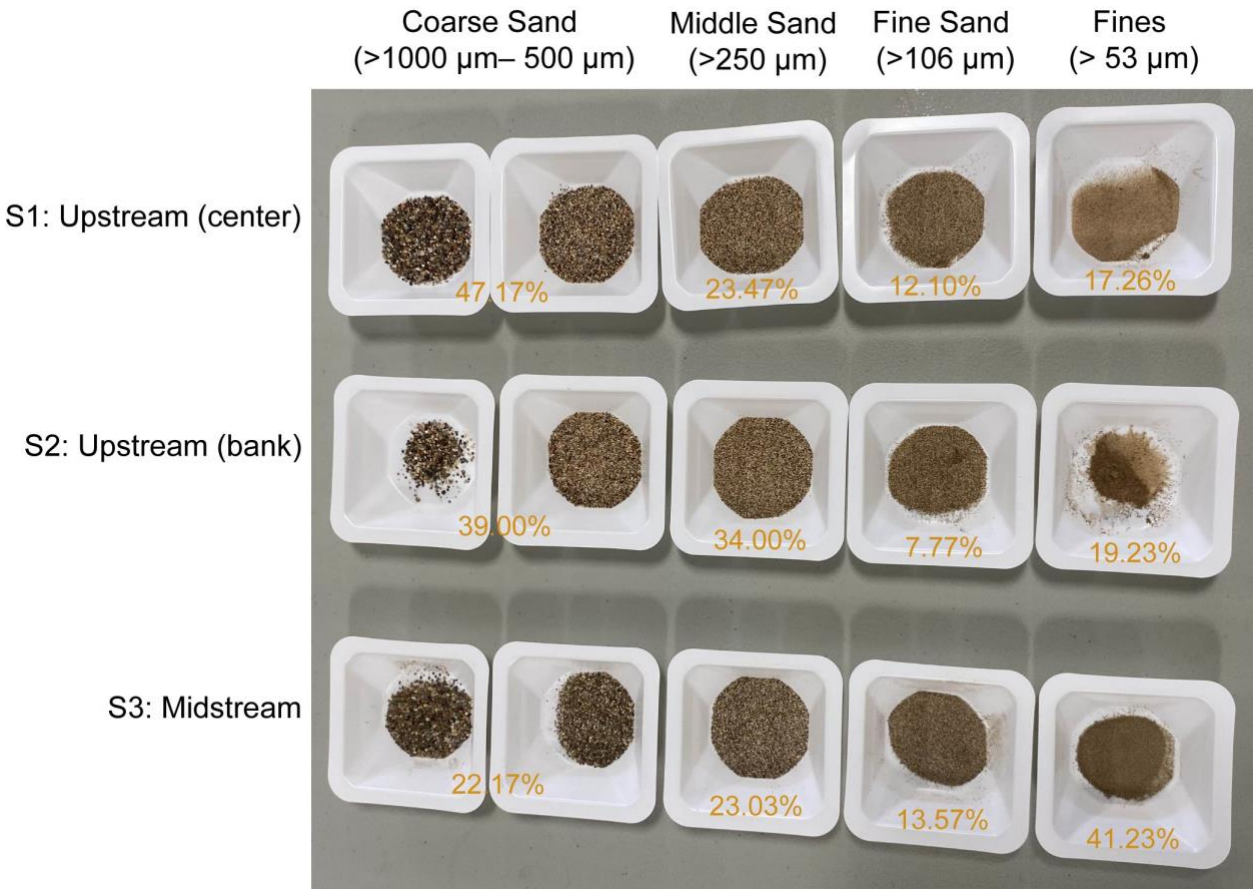

Appendix Chapter 4, Figure 2. Sieved sediment samples from transect locations within the Souss basin. Percentage of sediment grain size within each sample is noted in orange.